FLASH Conceptual Design Report

FLASH Collaboration

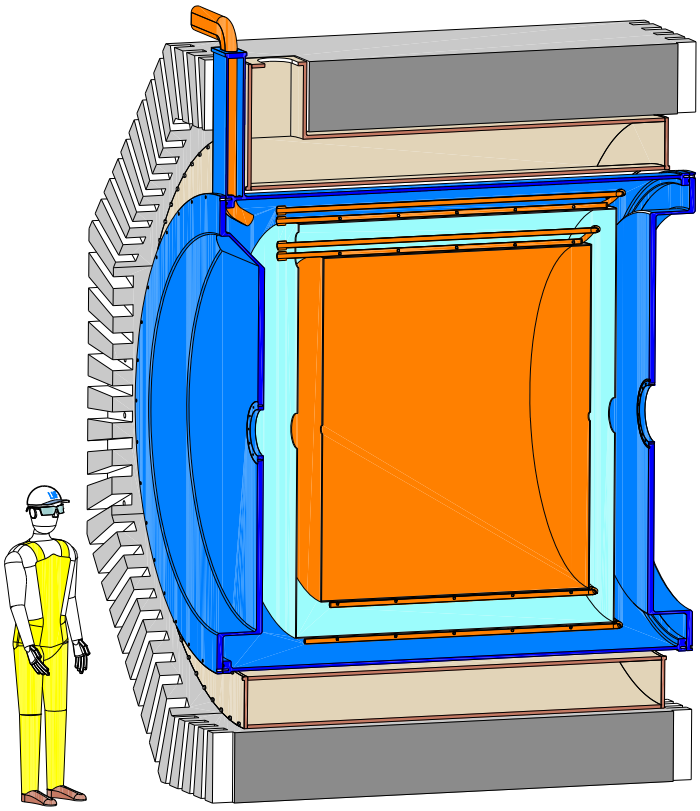

October 30, 2024

FLASH Conceptual Design Report

FLASH Collaboration

Contents

1 Introduction

The evidences for the existence of Dark Matter (DM) is overwhelming, with observations spanning from the rotation of galaxies [1], the gravitational lensing of light [2], and the large-scale structure of the Universe [3, 4] which all point to the presence of a vast amount of invisible matter. Despite these considerations, a non-gravitational probe of the cosmic DM is yet to be obtained, due to its feeble interaction with the Standard Model (SM) degrees of freedom which makes its detection very challenging.

A possible DM candidate is the QCD axion [5, 6], a light pseudoscalar particle arising within the solution to the strong CP puzzle proposed by Peccei and Quinn (PQ) [7, 8]. The puzzle emerges as a naturalness problem in the following way. The QCD sector possess a continuum of vacua characterised by a CP-violating angle θ [9, 10]. However, the physical measurable quantity is $\overline{\theta} = \theta + \arg\det M$, with M being the mass matrix of quarks. The above quantity induces an electric dipole moment in the neutron [11, 12], and is severely constrained $\overline{\theta} \lesssim 10^{-10}$ [13].

CP-violating contributions to the electric dipole moment of the neutron are also induced by the SM electroweak interaction. However, these effects are significantly smaller [14–16] than the current phenomenological reach. Nevertheless, it is somewhat puzzling that two separate unrelated contributions produce such a minuscule quantity.

The axion makes the angle $\overline{\theta}$ dynamical and relaxes the vacuum structure to the CP-invariant sector. The mechanism relies on a $U(1)$ global symmetry broken by the QCD anomaly. Any other source of explicit breaking would reintroduce CP violation, therefore posing a challenge for the mechanism which, in order to explain a tiny number, requires the exactness of its global symmetry. This is even more evident when considering gravity. In fact, any global $U(1)$ symmetry is expected to be explicitly broken by quantum gravity effects [17]. This leads to the so-called axion-quality problem [18–20]. Several mechanisms have been proposed to protect the symmetry from this sort of explicit breaking, see e.g. Refs. [21, 22].[1]

Although the original QCD axion model proposed in Refs. [5, 6] has been long excluded, other models in which the axion feebly couples to the SM degrees of freedom have been proposed, such as the Kim-Shifman-Vainshtein-Zakharov (KSVZ) model [25, 26] and the Dine-Fischler-Srednicki-Zhitnitsky (DFSZ) model [27, 28]. These benchmark models belong to a larger class which is referred to as the "invisible" axion models. A rich experimental program will probe the existence of the QCD axion in the next decade [29–31]. Among the experiments, ADMX [32–39],

[1] Recently it has also been argued that consistency with quantum gravity forces the axion mechanism to be exact, see [23, 24].

HAYSTAC [40–44], ORGAN [45–47], BabyIAXO [48], the facilities at IBS-CAPP [49–54], CAST-CAPP [55], RADES [56–59], QUAX [60–68], DMRadio/ABRACADABRA [69–71], CADEx [72], GrAHal [73] and TASEH [74] will use a haloscope, i.e. a detector composed of a resonant cavity immersed in a strong magnetic field [75–78].

In this document we propose the realization of the FINUDA (FIsica NUcleare at DAΦNE) magnet for Light Axion SearcH (FLASH) experiment a new haloscope to be built and operated at the Frascati National Laboratories of INFN (INFN-LNF), which will probe the existence of cosmic axions of masses around 10^{-6} eV. This window is currently unexplored and lies in between the mass range that is actively scanned in present and near-future searches by ADMX [38], BabyIAXO [48] and DMRadio [71, 79] collaborations. In this view, FLASH will close the mass gap in the range of the μeV where the QCD axion is expected to provide the DM budget. As indicated by the name, the realization of the haloscope is based on the reuse of the 3 m diameter superconducting magnet of the FINUDA experiment that took data at DAΦNE until 2007.

FLASH will also be able to constrain cosmological scenarios in which exotic particles other than the QCD axion play a role. One such example includes axion-like particles (ALPs) [80–82], see also the various reviews on the subject [83–90]. Alternative scenarios predict that the DM is composed of scalar rather than pseudoscalar particles. In this work, we assess the reach of the FLASH instrumentation when exploring models of the dilaton [91, 92] and the chameleon [93, 94], two scalar fields. Another avenue that motivates the FLASH experiment is related to hidden photon (HP) DM [95–97], see also Ref. [98]. In fact, haloscope experiments can efficiently constrain the mixing parameter describing the coupling between the SM photon and the cosmic HP in the viable phenomenological window.

Finally, it has been recently realized that resonant cavities could also serve the purpose of detecting gravitational waves (GWs) signals within the band ranges falling in the MHz-GHz region [99]. High-frequency GWs in the kHz range from coalescent compact objects or making up a stochastic background have been sought for in past experiments Explorer [100] at CERN and Nautilus [101] at INFN-LNF. Here, we show that the FLASH experiment can probe the GW bandwidth $\sim (100 - 300)$ MHz. As discussed below, exploring this frequency range may provide insights on the abundance of primordial black holes (PBHs).

The document is organized in three parts. The first two parts, "Physics Case" I and "Conceptual Project" II, are published in Ref. [102].

The first part, "Physics Case" I, deals with the physics reach of the experiment. In Sec. 2 we summarize the design and the forecast reach of the FLASH haloscope. In Sec. 3 we review the cosmology of the axion and we report the potential results for the search of QCD axions with FLASH. The forecast results for other models such as an axion-like particle, the hidden photon, chameleons, and GW signals are discussed in Sec. 4. In Sec. 5, we discuss how to further broaden the discovery potential achievable within the FLASH collaboration, both during the data-taking phase of FLASH and after its conclusion.

The second part, "Conceptual Project" II, deals with the design of the haloscope detector. The details of the design and tuning for the radio frequency cavity are given in Sec. 6, while the cryogenics is discussed in Sec. 7. The methods developed for the acquisition and analysis of the data are reported in Sec. 8 and Sec. 9, respectively.

The third part, "Project Organization" III, deals with the aspects necessary to write the Technical Design Report. In Sec. 10 we describe the tests, developments or R&D's needed to reach the desired Technology Readiness Levels between TRL6 and TRL9. In Sec. 11 we lists the points to be addressed in term of safety and radio-protection in the TDR. In Sec. 12 we describe the WP organization of the FLASH-TDR project and the participants role, while the estimated costs for the TDR phase, and a preliminary estimate of the experiment cost, are discussed in Sec. 13. Finally, our conclusions are drawn in Sec. 14.

We work in natural units $\hbar = c = k_B = \varepsilon_0 = 1$ unless otherwise specified.

2 Summary of the FLASH haloscope forecast reach

The FLASH experiment is expected to investigate the existence of the axion in the mass region between $m_a = 0.49\,\mu$eV and $m_a = 1.49\,\mu$eV by using resonant cavity techniques. Such a haloscope apparatus foresees a copper resonant cavity with an inner volume of approximately $4.15\,\mathrm{m}^3$ in the first stage of the search. The material and the properties of the cavity walls affect the cavity's efficiency in storing energy, which is quantified by the *unloaded* quality factor Q_0. The *loaded* quality factor $Q_L = Q_0/(1+\beta)$ accounts for the additional coupling between the cavity and the receiver by a quantity β. Coordinates and orientation of the detector are shown in Tab. 1.

Table 1: Position and magnetic-field direction of FLASH experiment

Latitude	41° 49′ 26″
Longitude	12° 40′ 13″
Elevation	100 m
B field direction	East−northeast

The axion converts in the presence of the strong magnetic field provided by the FINUDA magnet [103, 104], an iron shielded solenoid coil of 1.4 m in radius and 2.2 m in length, made from an aluminium-stabilised niobium titanium superconductor. The magnet can provide a homogeneous axial field of strength up to $B_0 = 1.1\,\mathrm{T}$. The field homogeinity, $\delta B_Z/B_0 < 5\%$ and $\delta B_X/B_0 < 1\%$, is provided by the two iron end-caps that close the magnet yoke. See Fig. 1 for additional details.

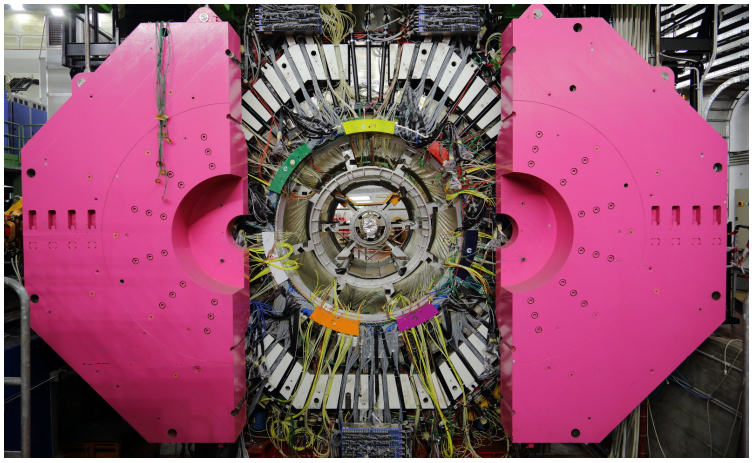

Figure 1: The FINUDA apparatus.

The expected power P_{sig} for a QCD axion converting inside a cavity resonating at the frequency ν_c can be as low as $10^{-22}\,\mathrm{W}$, see Eq. (11) below. Therefore the cavity has to be cooled to cryogenic temperatures to efficiently detect the signal. For this, ultra-low noise cryogenic-amplifiers are needed for the first stage amplification, with the cryostat apparatus cooled down to 4.5 K being inserted inside the bore of the FINUDA magnet. The scheme of the FLASH detector is shown in Fig. 2.

According to the Dicke radiometer equation [105], the signal to noise ratio (SNR) is

$$\mathrm{SNR} = \frac{P_{\mathrm{sig}}}{T_{\mathrm{sys}}}\sqrt{\frac{\tau}{\Delta\nu_I}}\,, \tag{1}$$

where T_{sys} is the combination of the amplifier and the thermal noises, τ is the integration time and $\Delta\nu_I$ is the intrinsic signal bandwidth. For galactic axions, the latter corresponds to $\Delta\nu_I = \nu_c/Q_a$, where the astrophysical factor $Q_a \simeq 10^6$ accounts for the DM velocity dispersion. The integration time for each value of the scanning resonant frequency and for a given SNR can be determined from inverting Eq. (1),

$$\tau = (\mathrm{SNR})^2 \frac{\nu_c}{Q_a}\left(\frac{T_{\mathrm{sys}}}{P_{\mathrm{sig}}}\right)^2 . \tag{2}$$

If the loaded quality factor of the cavity is smaller than Q_a, the number of signal bandwidths that can be scanned simultaneously by a cavity is $\sim Q_a/Q_L$. The scan rate is obtained as the ratio of the frequency step $\Delta\nu = \nu_c/Q_L$ and the scan time in Eq. (2) to obtain (see also Refs. [40, 106])

$$\frac{\mathrm{d}\nu}{\mathrm{d}t} \approx \frac{Q_a}{Q_L}\left(\frac{P_{\mathrm{sig}}}{\mathrm{SNR}\,T_{\mathrm{sys}}}\right)^2 . \tag{3}$$

As discussed in Ref. [106], the scan rate refers to the minimum target for the axion coupling and thus provides a measure of the sensitivity of the experiment.

Once the signal has originated in the cavity it has to be amplified and picked up efficiently. A Microstrip SQUID Amplifier (MSA) [107, 108] operating at 300 mK is an optimal solution, in terms of low noise, frequency band and gain, for the first stage of signal amplification. In the 4 K region a cryogenic heterojunction field-effect transistor (HFET) amplifier is employed. A summary of amplification steps and the equivalent temperature noise is shown in Table 2, with a discussion of the amplification stage being given in Sec. 8.1.

Table 2: Summary of amplification steps and equivalent noise temperature.

Device	Gain	Noise Temperature	operating temperature
MSA	20 dB	0.04 K	0.3 K
HFET	15 dB	5 K	4.5 K
Secondary Amplification	60 dB	150 K	300 K

This represents the base configuration for the FLASH haloscope. During the TDR phase we will consider other solutions to increase the detector sensitivity such as cooling the cavity down to 1.9 K, or below, and using superconducting cavities. The need of cooling the SQUID to 0.3 K to reduce its added noise may turn out to be unnecessary since the linear dependence with temperature of the added noise could saturate well before reaching that of the cryostat. This will be verified during the R&D phase. The choice of the cavity frequency ranges may also change after the final design of the FLASH cryostat will be available.

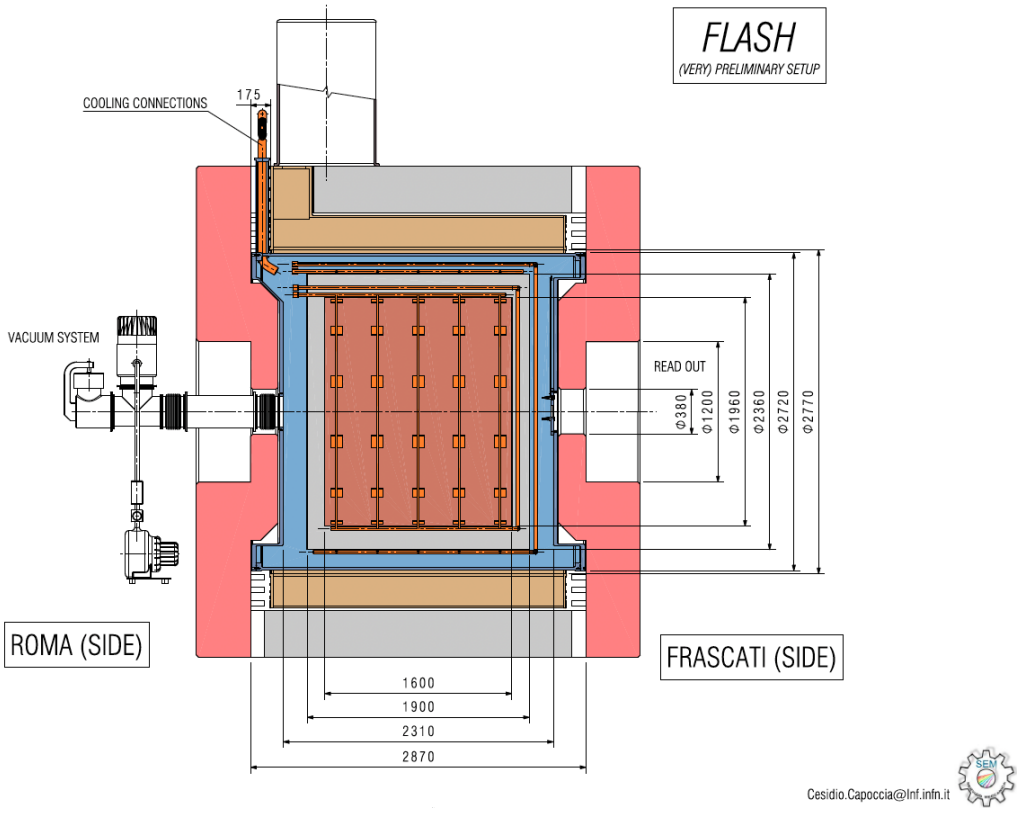

Figure 2: Scheme of the FLASH detector (C. Capoccia - LNF).

Part I
Physics Case

3 Models of the QCD axion in the range of FLASH

3.1 Basic concepts

In the following three sections, we discuss the physical scenarios accessible to FLASH. We begin with the QCD axion, arguably one of the most motivated and studied new-physics candidate. At energies below the PQ and the electroweak symmetry breaking scales, the dynamics of the axion field a is described by an effective Lagrangian

$$\mathcal{L} = \frac{1}{2}(\partial^\mu a)(\partial_\mu a) + \frac{\alpha_s}{8\pi}\frac{a}{f_a}\tilde{G}^{\mu\nu}G_{\mu\nu} + \frac{1}{4}g^0_{a\gamma\gamma}a\tilde{F}^{\mu\nu}F_{\mu\nu} + \frac{1}{2f_a}(\partial_\mu a)j^\mu_{a,0}\,, \tag{4}$$

where α_s is the strong force coupling strength, f_a is the QCD axion decay constant, $F^{\mu\nu}$, $G^{\mu\nu}$ are the electromagnetic (EM) and gluon field strengths respectively, and a tilde indicates the dual of the field strengths. The coupling of the axion to the photons is described by the coupling constant

$$g^0_{a\gamma\gamma} = \frac{\alpha_{\rm EM}}{2\pi f_a}\frac{E}{N}\,, \tag{5}$$

where $\alpha_{\rm EM}$ is the fine-structure constant and E/N is the ratio of the EM and the color anomalies. Different QCD axion models predict different values of the ratio E/N. The last term in Eq. (4) describes any model-dependent coupling of the axion with the SM fermions, with fermionic current $j^{\mu}_{a,0}$.

The QCD axion mass originates from non-perturbative effects during the QCD phase transition [5]. After a rotation of the quark fields, the interaction of the axion field with the chiral condensate implies a potential for the QCD axion of the form [109, 110]

$$V(a) = -m_\pi^2 f_\pi^2 \sqrt{1 - \frac{4 m_u m_d}{(m_u + m_d)^2} \sin^2\left(\frac{a}{2 f_a}\right)}\,, \tag{6}$$

where m_π and f_π are the mass and the decay constant of the pion and m_u, m_d are the masses of the up and down quarks, respectively. The axion mass at zero temperature from the mixing with the neutral pion is then [5]

$$m_a = \frac{\sqrt{m_u m_d}}{m_u + m_d} \frac{m_\pi f_\pi}{f_a} \equiv \frac{\Lambda^2}{f_a}, \tag{7}$$

where $\Lambda \approx 75.5\,\text{MeV}$ is an energy scale related to the QCD phase transition.

In the new quark field basis, the axion-photon coupling is redefined as

$$g_{a\gamma\gamma} = \frac{\alpha_{\rm EM}}{2\pi f_a}\left(\frac{E}{N} - \frac{2}{3}\frac{4m_d + m_u}{m_d + m_u}\right) \equiv \frac{\alpha_{\rm EM}}{\pi f_a}\, g_\gamma\,, \tag{8}$$

$$g_\gamma \equiv \frac{1}{2}\left(\frac{E}{N} - \frac{2}{3}\frac{4m_d + m_u}{m_d + m_u}\right), \tag{9}$$

where the model dependent parameter is $g_\gamma = -0.97$ ($g_\gamma = 0.36$) in the KSVZ (DFSZ) axion model [25–28]. The properties of the QCD axion today are determined by the behavior of its potential with temperature, which controls both the dynamics of the axion field in the early Universe as well as the production of topological defects [111, 112].

At temperatures higher than that of the QCD phase transition, the effects of instantons become severely suppressed. This reflects onto the value of the axion mass, whose dependence on the temperature is fixed in terms of the QCD topological susceptibility. The axion mass decreases quickly with an increasing value of the temperature of the plasma above the confinement temperature T_C [113]. Generally, the QCD axion mass is expressed in terms of the QCD topological susceptibility $\chi(T)$ as

$$m_a^2(T) = \frac{m_a^2}{\Lambda^4}\,\chi(T)\,, \tag{10}$$

where $\chi(T)$ is normalised such that $\chi(T=0) = \Lambda^4$. Estimating the temperature dependence of the topological susceptibility is one of the goals of QCD lattice simulations that capture the dynamics of the quark-gluon plasma around T_C [114–117].

3.2 Detecting cosmic axions with FLASH

The axion-photon coupling sparks hope to detect cosmic axions that make up the DM in the Galaxy by means of resonant cavities on Earth. FLASH is expected to operate within the EM resonant frequency of $(117-360)\,\text{MHz}$, corresponding to an axion in the mass range $m_a \simeq (0.49-1.49)\,\mu\text{eV}$. The search is divided into a low-frequency (LF) region within $(117-206)\,\text{MHz}$ and a high-frequency (HF) region within $(206-360)\,\text{MHz}$, with the corresponding mass ranges within $(0.49-0.85)\,\mu\text{eV}$ and $(0.85-1.49)\,\mu\text{eV}$, respectively. When the resonant frequency of the cavity ν_c is tuned to the

corresponding axion mass $m_a/(2\pi)$, the expected power deposited by DM axions is [40, 41]

$$P_{\rm sig} = \left(g_\gamma^2 \frac{\alpha_{\rm EM}^2}{\pi^2} \frac{\rho_a}{\Lambda^4} \right) \times \left(\omega_c Q_L \frac{\beta}{1+\beta} B_0^2 V C_{mnl} \right) . \tag{11}$$

Here, ρ_a is the local axion density, and the second set of parentheses contains the magnetic field strength B_0, the cavity volume V, the angular frequency $\omega_c = 2\pi\nu_c$, and a geometrical factor $C_{mnl} \simeq O(1)$ that depends on the cavity mode.

The discovery potential in the coupling-mass plane calculated through Eqs. (1) and (11) is shown in Fig. 3. The FLASH sensitivity can reach the band predicted for QCD axions down to the KSVZ model line. It is assumed here that axions make up the totality of the dark matter, with the local DM energy density fixed to the reference value $\rho_{\rm DM} = 0.45\,{\rm GeV\,cm^{-3}}$ [118–120]. We

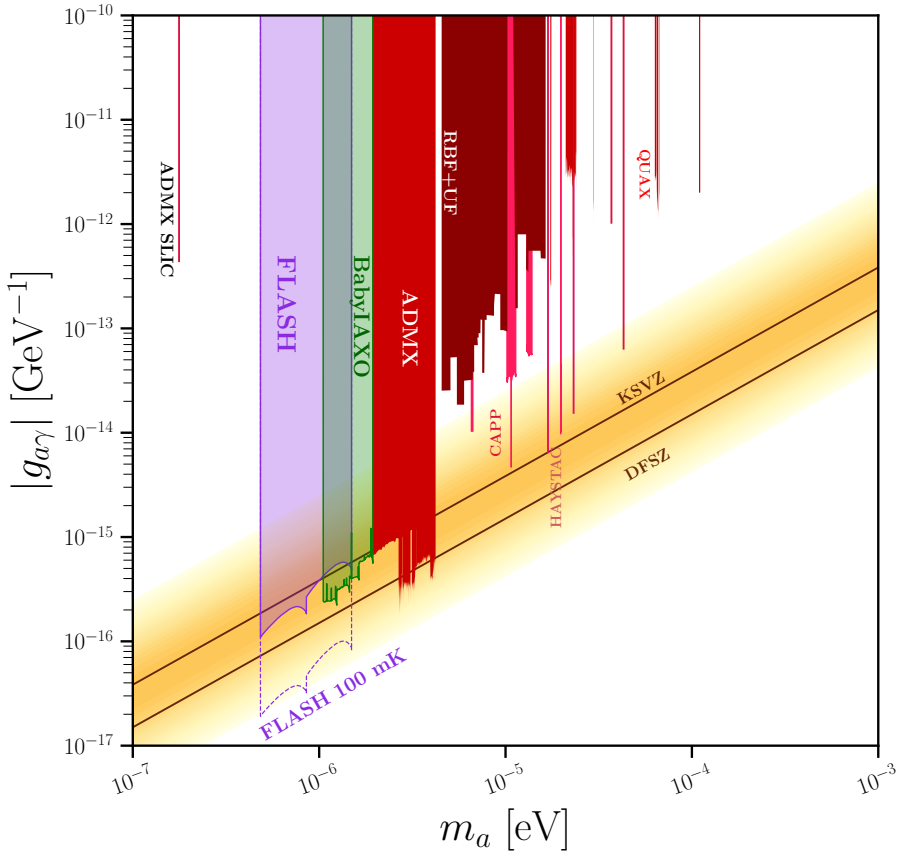

Figure 3: The FLASH discovery potential (90% confidence level or c.l.) compared to existing experimental limits. The brown lines with yellow error-band show the theoretical predictions for the KSVZ and DFSZ axions [25–28]. The forecast reach of FLASH is compared with experimental limits from other haloscopes [32, 33, 40, 41, 45, 46, 121–123] as well as a projection from [48] labled 'babyIAXO' in green, which is expected to be realized somewhat later than FLASH. Image realized with [124].

considered an integration time of 5 minutes for a single measurement with the large cavity and 10

minutes for measurements for the small cavity. Here, we conservativelly considered MSA SQUID at the cryostat temperature of 4.5 K, leading to a total noise system of about 5 K. In Table 3 we take as an example the search in the larger volume setup for the frequency $\nu_c = 150\,\mathrm{MHz}$, corresponding to a KSVZ axion of mass $m_a = 0.62\,\mu\mathrm{eV}$ and coupling $g_{a\gamma\gamma}^{\mathrm{KSVZ}} = 2.45 \times 10^{-16}\,\mathrm{GeV}^{-1}$. The parameters used in Eq. (11) are given in the table, with the scan rate obtained from Eq. (3). According to the estimated number of frequency steps shown in Table 5 the total integrated time will be about 2 years. We also show the potential reach with a cryogenic system upgraded to operate at a lower temperature $T_{\mathrm{sys}} = 100\,\mathrm{mK}$ pointing to the possibility of probing the DSFZ-axion model. Further solutions will be considered during the TDR phase. Cooling down to 1.9 K the cryostat would push the sensitivity close to the central value expected for DFSZ axions. Furthermore, using a superconducting cavity, such as NbTi [125] or ReBCO, would increase the quality factor and allow a sensitivity beyond DFSZ axions.

Table 3: The FLASH discovery potential for KSVZ axions. The choice of the parameters corresponds to the search at the peak frequency $\nu_c = 150\,\mathrm{MHz}$ in the large volume cavity and for a period $\tau = 5\,\mathrm{min}$. The coupling $\beta = 2$ is chosen to optimize the scan rate [40, 41].

Parameter	Value
$\nu_c\,[\mathrm{MHz}]$	150
$m_a\,[\mu\mathrm{eV}]$	0.62
$g_{a\gamma\gamma}^{\mathrm{KSVZ}}\ [\mathrm{GeV}^{-1}]$	2.45×10^{-16}
Q_L	1.4×10^5
C_{010}	0.53
$B_{\mathrm{max}}\ [\mathrm{T}]$	1.1
β	2
$\tau\ [\mathrm{min}]$	5
$T_{\mathrm{sys}}\ [\mathrm{K}]$	4.9
$P_{\mathrm{sig}}\ [\mathrm{W}]$	0.9×10^{-22}
Scan rate $[\mathrm{Hz\,s}^{-1}]$	8
$m_a\,[\mu\mathrm{eV}]$	0.49 - 1.49
$g_{a\gamma\gamma}$ 90% c.l. $[\mathrm{GeV}^{-1}]$	$(1.25 - 6.06) \times 10^{-16}$

3.3 Production of cold axions in the early universe

Cold axions are produced in the early universe through various mechanisms, which include the vacuum realignment mechanism (VRM) [126–128] and the decay of topological defects. Both these mechanisms have to be studied jointly, nominally by means of numerical simulations.

The present energy density stored in the coherent oscillations of the field can be obtained by solving the equation of motion for the axion field in an expanding universe,

$$\ddot{a} - \nabla^2 a + 3H\dot{a} + \frac{\mathrm{d}V(a)}{\mathrm{d}a} = 0\,, \tag{12}$$

where a dot means a derivative with respect to cosmic time t.

At very high temperatures, the axion potential can be safely neglected, so that the axion field is frozen on super-horizon scales. The axion potential becomes a relevant term in Eq. (12) when the Universe has sufficiently cooled off so that the Hubble rate $H(T)$ at temperature T is of the same order of the axion mass,

$$3H(T_{\rm osc}) \approx m_a(T_{\rm osc})\,, \tag{13}$$

where $T_{\rm osc}$ is the temperature at which the coherent oscillations in the axion field begin. If the transition takes place in the standard cosmological scenario, the number of axions in a comoving volume is preserved to present time, so that the present abundance of axions is expressed as

$$\Omega_a = \frac{m_a(0)}{m_a(T_{\rm osc})}\frac{\rho_a(T_{\rm osc})}{\rho_{\rm crit}}\frac{s(T_0)}{s(T_{\rm osc})}\,. \tag{14}$$

Here, T_0 is the present temperature of the CMB photons, $s(T)$ is the entropy density at temperature T, and $\rho_{\rm crit} = 3H_0^2 M_{\rm Pl}^2$ is the present critical density in terms of the Hubble constant H_0 and the reduced Planck mass $M_{\rm Pl}$. The axion energy density at the onset of field oscillations $\rho_a(T_{\rm osc})$ is obtained upon solving Eq. (12). Thus, it depends on the choice of the potential and of the initial conditions for the axion field a_i which are set at the time of the PQ phase transition. We parametrize this by introducing the initial axion angle $\theta_i \equiv a_i/f_a$, whose variance in the distribution across the observable Universe $\langle\theta_i^2\rangle$ reveals information about the state of the early Universe when $T \simeq f_a$.

3.3.1 Pre-inflation axions

We first discuss the scenario in which the PQ symmetry breaking happens before or during inflation and it is never restored afterwards. In this scenario, topological defects are inflated away and do not contribute to the QCD axion energy density. One single patch within which the initial axion angle θ_i has a homogeneous value inflates outside of the scale of the observable Universe, so that the present energy density in axions is found by solving Eq. (12) on super-horizon scales to give (see e.g. Ref. [129])

$$m_a \approx 5\,\mu{\rm eV}\,\theta_i^{12/7}\,. \tag{15}$$

3.3.2 Post-inflation axions

If the PQ symmetry breaking happens after the end of inflation, topological defects such as axionic strings and domain walls form, with properties that greatly depend on the specific model for the QCD axion considered. In this scenario, which is generally referred to as *post-inflationary scenario*, $\langle\theta_i^2\rangle$ is the average of the initial VRM angle squared over the circle, assuming that θ_i is drawn from a uniform distribution. For a quadratic potential one has $\langle\theta_i^2\rangle = \pi^2/3$, however, in the periodic potential that defines the QCD axion, this result is modified due to the presence of non-harmonic terms [130].

The expression in Eq. (15) with $\theta_i = \pi/\sqrt{3}$ yields to the naïve estimate for the QCD axion mass in this scenario $m_a \approx 20\,\mu$eV, which is about one order of magnitude above the reach of FLASH. Including the sub-horizon dynamics and the contributions from topological defects generally leads to a higher value of the axion mass, in the range $m_a = [20 - 500]\,\mu$eV, according to recent simulations [131–140], pushing the window further away from the FLASH sensitivity.

Nevertheless, various uncertainties in the standard cosmological model and the particle content beyond the SM can greatly affect the above picture and modify the expected window of DM axion masses. In this sense, an axion discovery by FLASH would provide insights on the particle content of the early universe.

In the following we briefly discuss possible mechanisms that lower the expected mass window of the QCD axion to the range accessible to FLASH, leaving further details to the literature cited.

3.4 Scenarios of axion cosmology within the reach of FLASH

3.4.1 Initial misalignment angle

In the standard cosmological scenario, the QCD axion is the DM particle with the mass expressed in Eq. (15), when the PQ symmetry is spontaneously broken during inflation. In this scenario, the range of mass sensitivity in FLASH corresponds to the range $|\theta_i| \in (0.2 - 0.4)$. For a uniform probability of $\theta_i \in [-\pi, \pi]$, the probability that θ_i is drawn with the desired value is about 6%. Details for the probability distribution derived from the Fokker-Planck equation can be found in Refs. [141, 142] and lead to a somewhat lower probability.

Recently, Ref. [143] used a Bayesian analysis technique, based on the code GAMBIT [144] and its module DarkBit [145], to present a global fit to explore the parameter space of the QCD axion (both the KSVZ and the DFSZ models). In particular, it is considered the scenario in which the Peccei-Quinn symmetry breaks during a period of inflation, while taking into account results from various observations and experiments in the likelihood including the light-shining-through-wall experiments, helioscopes, cavity searches, distortions of gamma-ray spectra, supernovae, horizontal branch stars and the hint from the cooling of white dwarfs. The marginalised posterior distribution obtained in Ref. [144] when demanding that the totality of DM is in axions gives the range $0.12\,\mu\text{eV} \leq m_a \leq 0.15\,\text{meV}$ at the 95% equal-tailed confidence interval. We stress that a portion of the range inferred by this analysis is well within the reach of the FLASH experiment.

Small initial values of θ_i might also occur naturally, i.e. without any fine tuning, in low-scale inflation models in which inflation lasts sufficiently long [141, 142]. If $H_I \lesssim \Lambda_{\text{QCD}}$ (see e.g. Ref. [146]), the axion acquires a mass already during inflation, the θ_i-distribution flows towards the CP conserving minimum and, for a long duration of the inflation period, stabilises around sufficiently small θ_i values. As a result the QCD axion can naturally give the DM abundance for axion masses well below the classical window, down to $10^{-12}\,\text{eV}$ [141].

3.4.2 Entropy generation

If a new species is present in the early universe and if it decays into thermalized products prior to Big Bang Nucleosynthesis (BBN), the entropy density in a comoving volume is not conserved. If a relevant amount of entropy is generated after the axions are produced, for example by the decay of a massive scalar field, the axion density in Eq. (14) would be diluted by a factor Δ [127, 129, 147–152], which would in turn lower the value for the DM axion mass. When $\rho_A^{\text{tot}} \to \rho_A^{\text{tot}}/\Delta$, the axion mass is

$$m_a \approx \frac{(5-50)\ \mu\text{eV}}{\Delta^{7/6}}. \tag{16}$$

The range explored by FLASH is reached if the contribution from the dilution factor is of order $\Delta \approx (10 - 100)$. The value of the quantity Δ depends on the details of the modified cosmological model and, ultimately, on the reheating temperature. A detailed derivation has been given in Refs. [151–159].

3.4.3 Modifying the relation between the axion mass and decay constant

A different approach to modify the relation between the temperature and the mass of the axion in Eq. (10) is through the addition of particle content, without changing the cosmological evolution. This approach has the advantage of ensuring the preservation of well-tested cosmological predictions, in particular BBN. It is indeed possible to make the axion *lighter* than expected. A particle physics model that realises this scenario has been proposed in Ref. [160]. The model relies on a Z_N symmetry under which $a \to a + \frac{2\pi f_a}{N}$, and furthermore the axion interacts with N copies of QCD whose fermions transform under Z_N as $\psi_k \to \psi_{k+1}$. Surprisingly, adding up the contributions

of all the sectors one finds that cancellations occur in the axion potential with a high degree of accuracy, and as a result, for even N the axion mass gets exponentially suppressed:

$$m_a \to \frac{4\, m_a}{2^{N/2}}\,, \tag{17}$$

while, if N is odd, the axion potential retains the minimum in $\bar{\theta} = 0$. The mass range accessible to FLASH corresponds to $9 \lesssim N \lesssim 13$. This scenario has been further explored in Refs. [161, 162]. A different possibility to generate DM axions with a mass below the canonical window can be engineered within the framework of the *mirror world* [163–165] extended to include the axion, see Ref. [166].

4 Additional models that will be probed with FLASH

4.1 Axion-like particles

Along with the QCD axion, other axion-like particles or ALPs can arise in theories of grand unification or quantum gravity [167–169] and share a phenomenology similar to what discussed so far. Here, an ALP is defined by a negligible axion-gluon coupling in Eq. (4) so that the instantons appearing during the QCD phase transitions do not affect the axion potential and the mass of the particle is independent of the temperature. Viable scenarios explored in the literature include axions from closed strings [170, 171] or from heterotic string models [172]. From a theoretical viewpoint, the embedment of the QCD axion within an UV-completed theory such as string theory is desired as the QCD axion potential has to be protected against corrections that would otherwise raise the axion mass and spoil the PQ solution. More generally, the ALP dark matter mass predicted from string theory generally takes the form [167, 173]

$$m_a \propto e^{-S/2}\, \frac{M_{\rm Pl}^2}{f}\,, \tag{18}$$

where S is the string instanton action. Testing this formula against cosmological data reveals a preference for light "fuzzy" axion dark matter [174, 175]. Another effect resulting from string theory is to provide additional massive "moduli" fields whose decay reheats the Universe leading to the dilution discussed in Sec. 3.4.2. Given these uncertainties, it is not possible to give a generic statement on the predictability of FLASH in targeting fundamental parameters, although specific string axion models already exist in the literature for which the viable mass range overlaps with this laboratory search.

The ALP potential $V(a)$ is usually modeled as a quadratic form to incorporate the explicit breaking origin of the mass term, so that the Lagrangian describing this particle is

$$\mathcal{L} \supset -\frac{1}{4} F_{\mu\nu}\, F^{\mu\nu} + \frac{1}{2}(\partial^\mu a)(\partial_\mu a) - \frac{1}{2} m_a^2 a^2 - \frac{1}{4}\, g_{a\gamma\gamma}\, a \tilde{F}_{\mu\nu}\, F^{\mu\nu}\,. \tag{19}$$

Here, an explicit dependence on temperature is not included due to the absence of a strong coupling with the QCD sector. The ALP-photon coupling is also generally expressed in terms of the coupling $g_{a\gamma\gamma}$, similarly to what given in Eq. (5) and for some particle content that justifies the appearance of the E/N ratio.

The same physical scenario described in Sec. 3.3 for the cosmological production of QCD axions holds equally well for an ALP, with the important difference that the potential does not depend on temperature, and the axion abundance in Eq. (14) when compared to the present DM abundance yields (see e.g. Ref. [96, 152])

$$m_a \approx 5\, \mu\text{eV} \left(\frac{10^{13}\,\text{GeV}}{f_a}\right)^4 \theta_i^{-4}\,. \tag{20}$$

When $\theta_i = \mathcal{O}(1)$, the ALP is generally lighter than the QCD axion for a given decay constant. In fact, for $\langle\theta_i\rangle^2 = \pi^2/3$, the ALP mass is in the range of FLASH for $f_a \sim 10^{13}\,\text{GeV}$.

4.2 Scalar dark matter

So far we have investigated the case in which DM is composed of pseudoscalar particles. The FLASH setup can be used to explore other types of DM candidates such as scalar particles [176], which are motivated in theories of dilaton models [91, 92]. Scalar DM can be produced in the early Universe through similar mechanisms as axionic DM, the most prominent for the range of masses of interest for FLASH being VRM.

We consider a system comprising a scalar field ϕ of mass m_ϕ interacting with the EM field strength with a coupling $g_{\phi\gamma\gamma}$, as described by the Lagrangian

$$\mathcal{L} \supset -\frac{1}{4}F_{\mu\nu}\,F^{\mu\nu} + \frac{1}{2}(\partial^\mu\phi)(\partial_\mu\phi) - \frac{1}{2}m_\phi^2\phi^2 - \frac{1}{4}\,g_{\phi\gamma\gamma}\,\phi F_{\mu\nu}\,F^{\mu\nu}\,, \tag{21}$$

where the last term is the scalar-photon interaction that can be interpreted as the scalar counterpart of the axion-photon interaction in Eq. (4). The conversion of ϕ in the cavity leads to a signal whose power is analogous to the axion case in Eq. (11) upon the replacement $g_{a\gamma\gamma} \to g_{\phi\gamma\gamma}$ and $m_a \to m_\phi$ [177]. Due to the different structure between the axion-photon and the scalar-photon couplings, the coupling to the cavity is given by [177]

$$C_\alpha = \frac{1}{B_0^2 V}\,\frac{|\int_V \mathrm{d}^3\mathbf{x}\,e^{i\mathbf{k}\cdot\mathbf{x}}\,\mathbf{B}_0\cdot\mathbf{B}_\alpha|^2}{\int_V \mathrm{d}^3x\,\mathbf{B}_\alpha\cdot\mathbf{B}_\alpha}\,, \tag{22}$$

where $\mathbf{B}_\alpha$ is the magnetic field associated with the resonant mode α. Since all of the TM modes as well as the TE_{010} mode possess a vanishing magnetic field along the z-direction, we consider here the modes TE_{011} and TE_{111}, see Table 6. The mode TE_{011} is described by the component of the magnetic field along the z direction

$$B_z = B_0\,J_0(v_0 r/R)\,\sin(\pi z/L)\,, \tag{23}$$

where $v_0 \approx 3.832$, while the mode TE_{111} is described by

$$B_z = B_0\,J_1(v_1 r/R)\,\sin(\pi z/L)\cos\theta\,, \tag{24}$$

with $v_1 \approx 1.8412$. In A, we compute the coupling in Eq. (22) for the two modes TE_{011} and TE_{111} interacting with the magnetic field of the cavity assuming an isotropic DM distribution for the bosonic wave number $k = mv$ with speed $v \approx 200\,\text{km/s}$. Because of the different angular distribution of B_z, the two couplings scale differently with the bosonic DM momentum, leading to different estimates as already noted previously [177]. In fact, we obtain $C_{011} \approx 5\times10^{-13}$ and $C_{111} \approx 3\times10^{-7}$, so that only the bound obtained by considering the TE_{111} mode is consistently competitive with the existing bounds.

Figure 4 shows the forecast on the constraint for the scalar field coupling with the photon, once the coupling obtained for the axion field has been rescaled by a factor $\sqrt{C_{111}/C_{010}} \approx 10^{-3}$. This is merely an estimate based on the simulations for the axion reach, since the TE_{111} mode has a different quality factor and frequency range (see Table 6). A proper analysis that considers the coupling of the mode to the cavity is required and will be carried out along with the data analysis.

The bound has been expressed in terms of the dimensionless quantity $|d_e| \equiv \sqrt{2}M_{\text{Pl}}g_{\phi\gamma\gamma}$ that is relevant for scalar field models [178, 179]. Also shown are the current bounds placed by laboratory searches for $|d_e|$ and reported in Ref. [124]. Future experiments involving a mechanical resonator made of a single crystal can lead to competitive bounds in the mass range of interest for FLASH [180] Note, that fifth-force and equivalence principle searches are generally stronger than laboratory constraints [181–183]. For an update of the the bounds and forecasts on the coupling of scalar particles in various mass ranges see the recent review in Ref. [31].

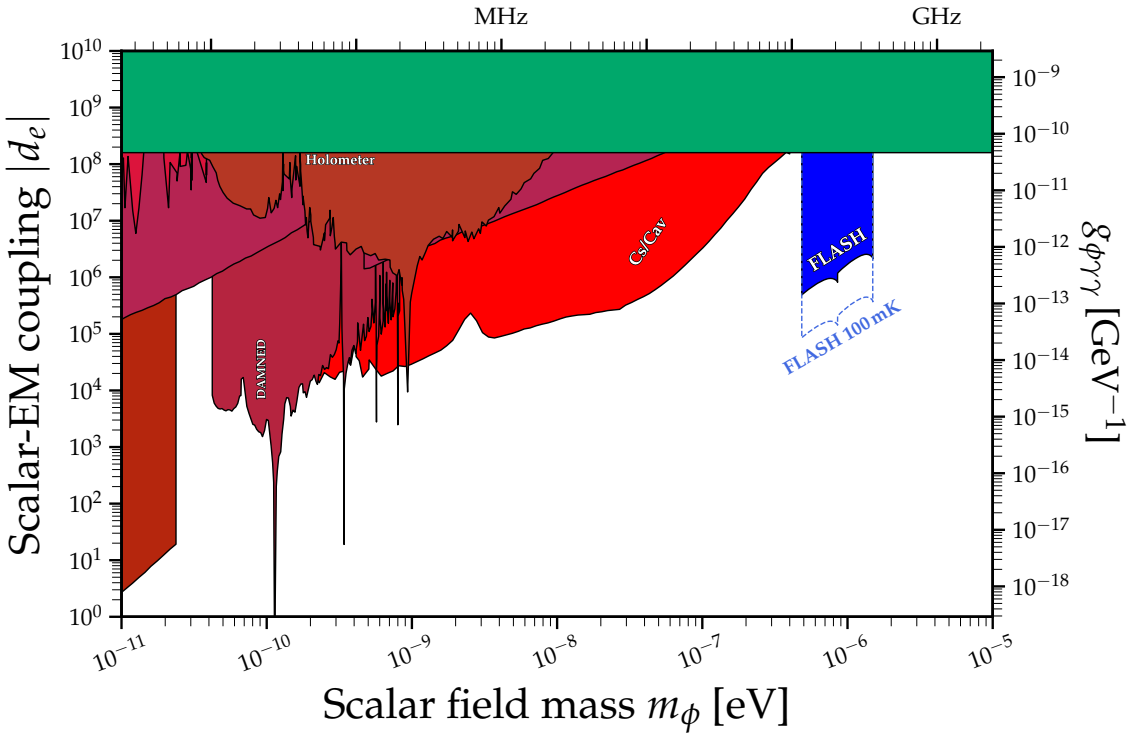

Figure 4: The predicted sensitivity in FLASH for the coupling between a scalar particle and the photon $|d_e|$ as expressed in Eq. (21), for the setup adopted for the first stage (filled blue area) and once the cryogenic has been improved to reach $T_{\rm sys} = 100\,\mathrm{mK}$ (dashed blue line). Also shown are current laboratory bounds, see Ref. [124] for details.

4.3 Chameleons

The "chameleon" was first introduced to potentially explain the present accelerating expansion of the Universe through a variable effective mass that depends on the ambient energy density.[2] The chameleon field ϕ is generally characterized by an effective interaction whose strength is a function of the local environment [93], with a "screening" potential modeled as [94, 185]

$$V_{\rm eff}(\phi) = V(\phi) + \exp\left(\frac{\beta_m \phi}{M_{\rm Pl}}\right)\rho_m + \frac{1}{4}\exp\left(\frac{\beta_\gamma \phi}{M_{\rm Pl}}\right) F^{\mu\nu}F_{\mu\nu}\,. \tag{25}$$

Here, β_m and β_γ are couplings to the density in matter ρ_m and photons, respectively, and $V(\phi) \propto \phi^{-n}$ is the self-interacting potential of the chameleon in the absence of other couplings, which depends on the index $n \geq 0$. See Refs. [186, 187] for reviews of the chameleon model.

The effective mass associated with the potential in Eq. (25) depends on the couplings and on the relative energy content in matter and radiation. Inside the walls of the cavity, the magnetic field $B_{\rm wall}$ can be neglected and for $\beta_m \rho_m > \beta_\gamma B^2_{\rm wall}$, the effective mass squared of the chameleon

[2] However, see Ref. [184] for a no-go theorem related to self-acceleration and for possible caveats.

is

$$m^2_{\rm eff,wall} = n(1+n)\frac{\Lambda^4}{M^2_{\rm Pl}}\left(\frac{\beta_m \rho_m}{n\Lambda^4}\right)^{\frac{2+n}{1+n}}\,, \tag{26}$$

where Λ is the energy scale of the self-interacting potential. In the empty space within the cavity, we assume that the effective mass $m_{\rm eff}$ is mostly provided by the interaction of the chameleon with the magnetic field, with $m_{\rm eff} \ll m_{\rm eff,wall}$. It is therefore possible that the chameleon mass in the walls of the cavity is higher than the mass inside the cavity itself, effectively trapping the field along with the magnetic field [188–190]. In the interspace within the cavity walls, the chameleon field follows the Klein-Gordon equation [190]

$$\left(\frac{{\rm d}^2}{{\rm d}t^2} - \nabla^2 + m^2_{\rm eff}\right)\phi = \frac{\beta_\gamma}{M_{\rm Pl}}\,\mathbf{B}\cdot(\nabla\times\mathbf{A})\,, \tag{27}$$

where $\mathbf{A}$ is the potential of the propagating photon. Once the chameleon field is trapped inside the resonant cavity, it experiences a delayed decay through the so-called afterglow effect [190, 191]. To reconstruct the signal produced inside the cavity, we derive the field equations from Eq. (25) as [190]

$$\Box A = \frac{\beta_\gamma}{M_{\rm Pl}}\,\nabla\phi\times\mathbf{B}\,, \tag{28}$$

with the condition that we observe a standing wave instead of a moving wave as in the DM case.

We estimate the potential reach of FLASH for the coupling of the chameleon with the photon β_γ, following the procedure outlined in Ref. [192] in which the $\rm TE_{011}$ cavity mode is excited by an external source of power $P_{\rm in} = 0.5\,{\rm mW}$ for a period $t_0 = 10\,{\rm min}$, with a sweeping time $\tau = 10\,{\rm min}$ in Eq. (1) and a noise temperature $T_{\rm sys} = 4.5\,{\rm K}$. The natural frequency of the $\rm TE_{011}$ mode resonating in the large cavity setup is $f_{\rm res} \approx 214.5\,{\rm MHz}$, with a quality factor $Q \approx 1.3\times10^6$ (see Table 6). The result will be independent on the chameleon mass for $m_{\rm eff} < \omega_d = 2\pi f_{\rm res} \approx 1.3\,{\rm GHz}$, where we have assumed that the external driving source operates with the pulsation ω_d. The results derived below are then valid in the region $0.38\,\mu{\rm eV} < m_{\rm eff} < 0.9\,\mu{\rm eV}$, where the upper bound corresponds to ω_d in eV and the lower bound on the chameleon mass is obtained by requiring that the field relaxes to its ground state inside the cavity, or $m_{\rm eff} \sim 2/R \approx 0.38\,\mu{\rm eV}$ for $R = 1050\,{\rm mm}$. Since the chameleon mass heavily depends on the underlying model and on the details of the self-interaction [93, 94], we do not explicitly specify the expression for $m_{\rm eff}$ in terms of model parameters here.

Following the computation related to the expression in Eq. (22), we fix the coupling of the cavity $C_{011} \approx 0.005$ as shown in A. This leads to the forecasts at one sigma level:

$$3\times10^9 \lesssim \beta_\gamma \lesssim 8\times10^{14}\,, \tag{29}$$

which overlaps with previous searches that already exclude the coupling for cosmic chameleons in some ranges, including GammeV [193], GammeV-CHASE (here CHASE) [194, 195], ADMX [192], and CAST [196]. These results have been summarized in Fig. 5. Recently, a model describing an axion with chameleon-like properties has been considered [197], although it seems that the favored region is well outside the target in current haloscopes.

4.4 Hidden photon dark matter

This subsection is devoted to the simplest case of *hidden photon* (HP) [198–200] dark matter.[3] Although several extensions are possible and have been proposed in the literature the advantage of the realization discussed here is that the experimentally constrained signal is determined by two

[3]These particles have also been dubbed "dark photons" or "paraphotons".

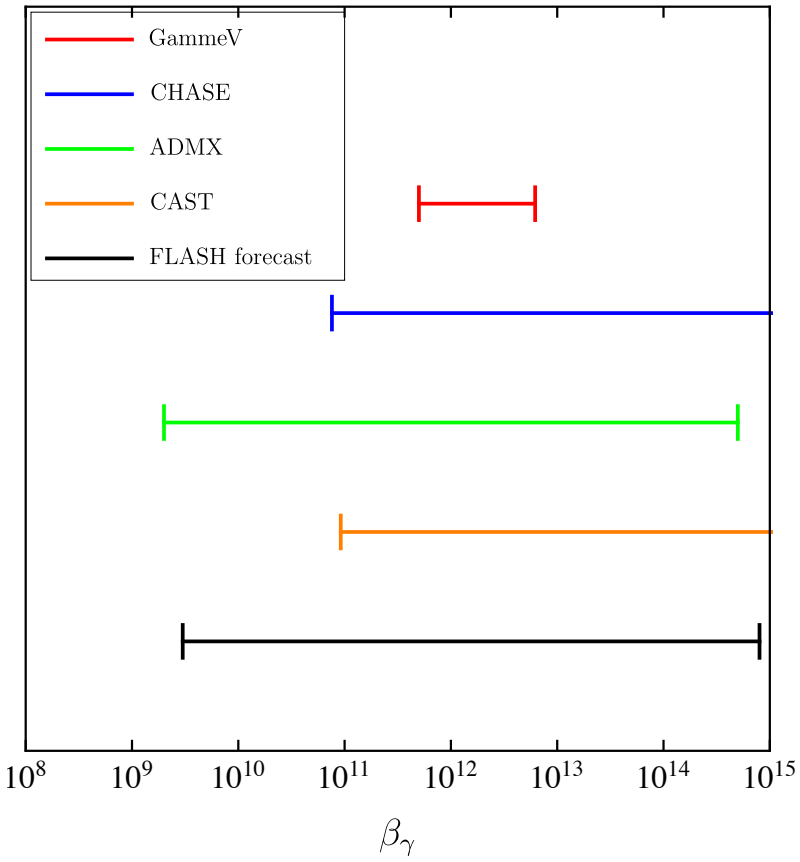

Figure 5: Forecast reach for the search of the chameleon-photon coupling with FLASH, for the setup described in the text (black line). Also shown are the results obtained by GammeV [193] (red line), CHASE [194, 195] (blue line), ADMX [192] (green line), and CAST [196] (orange line).

parameters [96]: the kinetic mixing term χ and the mass of the HP itself $m_{\gamma\prime}$. The dimensionless mixing parameter χ can be probed experimentally as a function of $m_{\gamma\prime}$, and is generally expected to be $\chi \ll 1$. For this reason, we work in this limit hereafter.

Before delving into the discussion it should be mentioned that $\mathcal{O}(1)$ fraction of DM can be obtained from inflationary fluctuations in the form of hidden photon for [97]

$$m_{\gamma\prime} \simeq 10^{-5}\,\mathrm{eV}\,\left(10^{14}\,\mathrm{GeV}/H_I\right)^4\,, \tag{30}$$

depending on the scale of inflation H_I. As mentioned before, FLASH will be able to constrain the mass scales of hypothetical particles in the range around $\sim 10^{-6}\,\mathrm{eV}$, therefore close to values expected in Eq. (30) for a narrow range of H_I. To our knowledge there is no consensus on a formation model leading to the production of the right abundance of dark matter. Therefore, in the following we will simply assume this to be the case and we remain agnostic on the exact mechanism of production (see Ref. [98] for a review).

The HP field X_μ describes a hidden $U(1)$ symmetry group that mixes with the photon through

a Lagrangian density of the form [95]

$$\mathcal{L} \supset -\frac{1}{4} F_{\mu\nu} F^{\mu\nu} - \frac{1}{4} X_{\mu\nu} X^{\mu\nu} + \frac{\chi}{2} X_{\mu\nu} F^{\mu\nu} + \frac{1}{2} m_{\gamma'}^2 X_\nu X^\nu - j^\mu_{\rm em} A_\mu \,, \tag{31}$$

where X_μ is the field describing the HP with field strength tensor $X_{\mu\nu}$ and $j^\mu_{\rm em}$ is the electromagnetic current. The Lagrangian in Eq. (31) leads to a possible decay channel of the HP into three photons [201]. Demanding that the HP is a stable relic on cosmological timescales leads to the bound

$$m_{\gamma'} (\chi^2 \alpha_{\rm EM})^{1/9} \lesssim 1\,{\rm keV} \,, \tag{32}$$

which is clearly satisfied for the range of masses of interest in FLASH, see Fig. 6. This motivates the search for the HP as the cosmic DM.

Note, that the microwave resonant cavity experiments searching for axion can also be used to probe the photon-HP mixing when operated without the magnetic field [96], which is unnecessary in this case. The equation of motion for the photon field A^μ

$$\partial_\mu \partial^\mu A^\nu = \chi\, m_{\gamma'}^2 X^\nu \,, \tag{33}$$

implies that HP could source ordinary photon. In particular, the power emission of the cavity is related to the energy stored and the quality factor of the cavity, and it is given by [96, 202]

$$P_{\rm sig} = \left(\chi^2 \rho_{\gamma'} \cos^2\theta\right) \times \left(\omega_c Q_L \frac{\beta}{1+\beta} V C_{nml}\right) \,, \tag{34}$$

where Q_L is the quality factor, V the volume of the cavity and θ the direction between the hidden photon field and the magnetic field as defined in Table 1.

Assuming the energy density of the HP to be equal to the DM density, the same quality factor used for the axion search, and the volume of the cavity equal to $V_{\rm Large}$ for the large phase of the experiment or $V_{\rm Small}$ for the small phase, Eq. (34) gives the expected power in the cavity that enters the SNR in Eq. (1). This leads to a constraint of the HP as the DM with the FLASH microwave cavity. The large dimensions of the cavity significantly enhance the sensitivity for HP. The predicted sensitivity for FLASH is computed inserting in Eq. (1) the $P_{\rm sig}$ obtained from Eq. (34). Two scenarios are possible, depending on the relative orientation of the cavity with respect to an a priori unknown direction of the HP field. This is represented by the factor $\cos^2\theta$ in Eq. (34). Assuming that all directions in space are equally likely and demanding that the real value is bigger with 95% probability leads to the value $\cos^2\theta = 0.0025$ [98, 202],[4] while an average over all possible directions gives $\cos^2\theta = 1/3$.

Fig. 6 shows the predicted HP detection sensitivity of the FLASH experiment for the setup discussed above and for $\cos^2\theta = 0.0025$ (shaded dark purple area) or $\cos^2\theta = 1/3$ (shaded light purple area), the latter being a more optimistic forecast. Also shown are the sensitivities expected in an upgrade setup of FLASH with an improved cryogenics able to reach the noise temperature $T_{\rm sys} = 100\,{\rm mK}$ (dashed lines). Finally, we also show a compilation of current constraints on and sensitivities of planned experiments to photon-HP mixing in the $m_{\gamma'} - \chi$ plane [124]. Even in the most conservative scenario and with the planned setup, FLASH will be able to probe the HP coupling orders of magnitude below.

[4] Here we use the value 0.0025 for comparison with previous experiments. A truly 90% C.L. can only constraint the product $\chi \cos\theta$.

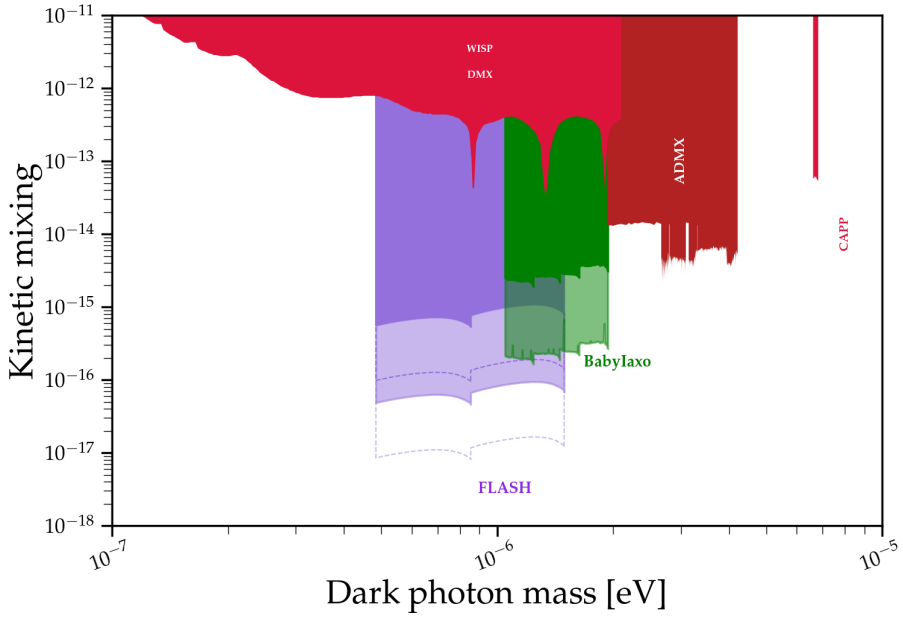

Figure 6: Compilation of current constraints and projected sensitivities to photon-HP mixing of current and planned experiments in the $m_{\gamma'} - \chi$ plane. The predicted sensitivity for FLASH is reported with full lines of different purple shades. The shaded dark purple region, represents the predicted FLASH sensitivity in the scenario of highly directional HP field ($\cos^2\theta = 0.0025$). The shaded light purple region reports the predicted FLASH sensitivity in the scenario of the isotropic distribution of the HP field ($\cos^2\theta = 1/3$). The projections from [48] labelled 'babyIAXO' in green follow the same color-scheme. The dashed lines represent the FLASH forecast sensitivities when operating the haloscope at a temperature of 100 mK. Dashed dark purple line: highly directional HP field; Dashed light purple line: isotropic distribution of the HP field. Image realized with the code in Ref. [124].

4.5 Detection of gravitational waves

The direct detection of gravitational waves (GWs) stands out as one of the most groundbreaking achievements in 21st-century physics. These GWs have frequencies in the Hz to kHz range and are produced during merger events of black holes or neutron stars. Furthermore, the detection of high frequency gravitational waves (HFGW) in the MHz-GHz range has recently attracted interest with many proposals currently under development, moved by the theoretical considerations that predict various exotic sources to emit at such high frequencies [99]. One highly promising route to search for HFGWs is through their expected signals in electromagnetic cavities exposed to high electromagnetic (EM) fields. These signals result from two distinct effects: first, the modification of the stationary modes of a cavity distorted by the passage of a GW; second, the generation of an effective current by GWs in the presence of a background EM configuration, a phenomenon known as the inverse Gertsenshtein effect. The ability to generate very strong stationary magnetic fields and the similarity to searches for axionic dark matter motivate the consideration of a setup with a stationary magnetic field.

Potential sources of HFGWs are generally divided into two categories, namely sources of cosmological origin produced before recombination and sources of astrophysical origin. A cosmo-

logical background of stochastic HFGWs is expected from various sources, including the primordial thermal plasma [203, 204] or a first order phase transition in the dark sector [205]. When of cosmological origin, the HFGW strain h_0 as a function of the HFGW frequency ν_c is constrained by BBN considerations and CMB data to be [206–208]

$$h_0 \lesssim 10^{-29}\ (100\,\mathrm{MHz}/\nu_c)\ \Delta N_{\rm eff}^{1/2}\,, \tag{35}$$

several orders of magnitudes below the expected reach of cavity searches [209]. For this, in the following we consider astrophysical sources in the late Universe at such high frequencies, whose origin likely requires new physics.

4.5.1 Gravitational waves from compact objects

Besides compact objects of astrophysical origin such as black holes (BH) and neutron stars, exotic configurations in the form of primordial BHs or boson stars formed in the earliest stages of the Universe could also be present today. As an example, primordial BHs (PBH) are too light to be explained by known stellar dynamics and hence, if detected, their origin would require new physics. A possibility is that they are formed in the early Universe, hence the name primordial (see Ref. [210] for a recent review). The exact details of the formation scenario is currently unknown. Historically, they have been conjectured to follow from inflationary overdensities [211–213]. However, these scenarios require significant tuning in order to produce a sizeable amount of dark matter, see e.g. Ref. [214] for a recent discussion. Over the past years, mechanisms that avoid such issues have been proposed. For example, PBHs could form due to the preheating dynamics [215], or from the confinement of heavy quarks [216]. Regardless of the specific formation scenario, PBHs could constitute a substantial fraction of dark matter for masses of the order of $\left(10^{-15}-10^{-11}\right)\,M_\odot$. Heavier PBHs as the main DM constituents are excluded by severe lensing constrains, although a small contribution is still allowed [217].

The GWs emitted by binary configurations of compact objects could possess the frequency range and the strain required to be detectable with present or near-future technologies. Consider two compact objects of similar mass M and size R, each of compactness $\mathrm{C} \equiv GM/R$, forming a system of total mass $M_{\rm tot} \approx 2M$. The frequency of the emitted GW spectrum at the end of the inspiral phase when the innermost stable circular orbit (ISCO) is occupied is $\nu_{\rm ISCO}$. For the case of two coalescing PBHs, the GW frequency at the ISCO is [218]

$$\nu_{\rm ISCO} = \frac{\mathrm{C}^{3/2}}{3\sqrt{3}\pi G M_{\rm tot}}\,, \tag{36}$$

so that a signal in the bandwidth $\mathcal{O}(100\,\mathrm{MHz})$ and for the compactness of a BH, $\mathrm{C} = 0.5$, is expected for PBHs in the mass range $M_{\rm PBH} \sim 10^{-5}\,M_\odot$. The GW strain sourced by a merging event of total PBH mass $M_{\rm tot}$ is [219]

$$h_0 \simeq 9.77\times 10^{-28}\left(\frac{\mathrm{kpc}}{d}\right)\left(\frac{M_{\rm tot}}{10^{-8}M_\odot}\right)^{\frac{5}{3}}\left(\frac{\nu}{100\,\mathrm{MHz}}\right)^{\frac{2}{3}}\,, \tag{37}$$

where the distance d between the Earth and the source is found by demanding that at least one merger event per year occurs within d [220]. The rate of merger events is obtained following the analyses in Refs. [207, 221].

4.5.2 *Gravitational waves from Chern-Simons couplings*

Along with the axion-photon interaction, an axion-gravity coupling can be introduced through a Chern-Simons term of the form [222, 223]

$$\mathcal{L}_{\rm CS} = \frac{M_{\rm Pl}}{8}\,\ell_{\rm CS}^2\,a\,\tilde{R}R\,, \tag{38}$$

where the product $\tilde{R}R = (1/2)\epsilon^{\mu\nu\sigma\rho}R_{\mu\nu\alpha\beta}R^{\alpha\beta}_{\sigma\rho}$ in terms of the Riemann tensor $R^{\mu}_{\nu\alpha\beta}$ and the Levi-Civita tensor $\epsilon^{\mu\nu\sigma\rho}$. The coupling is parametrized in terms of the length scale $\ell_{\rm CS}$ [224], which is bound from the induced reduction of frame-dragging effects [225] and from the search for secondary GWs associated with the coalescence of compact object binaries [226, 227].

An additional technique that leads to the constraint of the Chern-Simons coupling is the resonant enhancement of the GW signal from binary systems [228, 229], which would take place assuming that the cosmic DM is in the form of an axion-like particle of mass m_a and with the coupling in Eq. (38). An incoming GW of frequency $\omega_{\rm GW} = m_a/2$ would stimulate the decay of an axion into a coherent wave of gravitons. For $m_a \sim 10^{-13}$ eV, the effect enhances a chirping GW signal at the frequencies that are discernible at the LIGO-Virgo-KAGRA array of detectors, while the stimulated decay would be visible at FLASH if the dark matter axion falls in the mass range $m_a \approx$ (1-3) μeV.

4.5.3 *FLASH forecast reach for gravitational wave detection*

A resonant cavity designed to probe the conversion of axions into photons can also be used to detect gravitational waves through a graviton-photon conversion via the inverse Gertsenshtein effect [230] (see also Refs. [231, 232]). In its simplest formulation, the coupling of the photon with gravity is described by the Maxwell-Einstein action,

$$S = \int \mathrm{d}^4x\sqrt{-g}\left(-\frac{1}{4}g_{\mu\alpha}g_{\nu\beta}F^{\mu\nu}F^{\alpha\beta}\right)\,, \tag{39}$$

where $g_{\mu\nu}$ is the space-time metric with determinant g. The expansion of the metric to first order around a flat background as $g^{\mu\nu} = \eta^{\mu\nu} + h^{\mu\nu}$, with $|h^{\mu\nu}| \ll 1$, leads to a coupling between a GW of strain h_0 and frequency ω_g in an external magnetic field B_0 as $\propto h_0 E B_0$, where E is the electric field. Including the effects of the source requires adding a Breit-Wigner distribution of the form [233, 234]

$$F(\omega) = \frac{1}{(\omega-\omega_c)^2 + \frac{1}{4\tau^2}}\,, \tag{40}$$

where the relaxation time is defined as the time spent by the binary system within the frequency range $\Delta\nu$,[5]

$$\tau = \frac{\Delta\nu}{\dot{\nu}_c} = \frac{2\pi N_{\rm cycle}}{\omega_c}\,. \tag{41}$$

A quality factor describing the coherence of the source can then be defined as $Q_S = 2\pi N_{\rm cycle}$, analogously to the quantity Q_a introduced earlier for the axion. An electric signal of the same frequency is then produced in the cavity with the signal power [209]

$$P_{\rm sig} = \frac{1}{2}Q_{\rm eff}\,\omega_c^3\,V^{5/3}\,(\eta h_0 B_0)^2\,, \tag{42}$$

[5]Note, that this definition differs from other work in the literature [220], where $N_{\rm cycle}$ is defined in terms of the frequency range $\Delta\nu \sim \nu_c$.

where $Q_{\rm eff} = \min(Q_L, Q_S)$.

In the limit of an infinitely coherent source, the sensitivity of the cavity search to GW detection estimated through Eq. (1) leads to [235]

$$h_0 \gtrsim 9\times10^{-22}\left(\frac{200\,\mathrm{MHz}}{\omega_g/2\pi}\right)^{\frac{3}{2}}\left(\frac{0.1}{\eta}\frac{\mathrm{T}}{B_0}\right)\left(\frac{4\,\mathrm{m}^3}{V}\right)^{\frac{5}{6}}\left(\frac{2\times10^5}{Q_L}\frac{T_{\rm sys}}{5\,\mathrm{K}}\right)^{\frac{1}{2}}\left(\frac{\Delta\nu}{1\,\mathrm{kHz}}\frac{2\,\mathrm{min}}{t_{\rm int}}\right)^{\frac{1}{4}}, \tag{43}$$

where the expression accounts for an experimental setup similar to that of FLASH, corresponding to the FINUDA magnet with a nominal magnetic field $B_0 = 1.1\,\mathrm{T}$ and a cavity volume $V_{\rm Large} = 4.15\,\mathrm{m}^3$. We have also set the measurement integration time $t_{\rm int} = 2\,\mathrm{min}$ with the signal bandwidth (BW) equal to the cavity bandwidth $\Delta\nu = 1\,\mathrm{kHz}$ and the cavity-GW coupling coefficient $\eta = 0.14$ for the mode TM_{012}. The quality factor for the mode is expected to be $Q_0 \simeq 7\times10^5$. For comparison, the sensitivity of ADMX could be in the range $h_0 \sim 10^{-22}$, where the difference comes from the fact that although the FINUDA magnet has a smaller magnetic field, it has a much larger effective volume than the ADMX magnet. In a realistic setup where the coherence of the source is limited by Q_S, Eq. (43) holds when replacing $Q_L \to Q_{\rm eff}$ and $t_{\rm int} \to \min(t_{\rm int}, \tau)$; moreover, we demand that the source satisfies $N_{\rm cycle} \gtrsim 1$. For $N_{\rm cyc} \gtrsim Q_L$ matched filtering with a table of expected waveforms could also be implemented allowing to substitute $\Delta\nu \sim 1/t_{\rm int}$, so that the sensitivity in Eq. (43) would scale differently [235]:

$$h_0 \gtrsim 5\times10^{-23}\left(\frac{200\,\mathrm{MHz}}{\omega_g/2\pi}\right)^{\frac{3}{2}}\left(\frac{0.1}{\eta}\frac{\mathrm{T}}{B_0}\right)\left(\frac{4\,\mathrm{m}^3}{V}\right)^{\frac{5}{6}}\times\left(\frac{2\times10^5}{Q_L}\frac{T_{\rm sys}}{5\,\mathrm{K}}\right)^{\frac{1}{2}}\left(\frac{2\,\mathrm{min}}{t_{\rm int}}\right)^{\frac{1}{2}}. \tag{44}$$

By comparing the theoretical expectation in Eq. (37) with the reach in Eq. (43), it could be expected that an event originating within a distance $d \lesssim 1\,\mathrm{kpc}$ would fall within the reach of FLASH. However, the in-spiraling binary that sources the GW signal is not as coherent as DM axions are. This results in an effective limitation of the source resonating with the detector. Similarly, the bandwidth also depends on how fast the system spans a given frequency range. It follows that $\Delta\nu \equiv \nu_c/Q_{\rm eff}$ [220].

Fig. 7 shows the reach of the GW strain in Eq. (43) as a function of the binary mass $M_{\rm tot}$ for the planned FLASH setup (red solid line) and for an upgraded cryogenic system to $T_{\rm sys} = 0.15\,\mathrm{K}$ (red dashed line). Also shown is the signal generated by a merger event as in Eq. (37) for $f_{\rm PBH} = 1$, assuming that at least one event per year is observed [207, 220]. For simplicity, a monochromatic spectrum has been assumed at each value of $M_{\rm tot}$. The rate of mergers in the range of interest is also enhanced by the galactic overdensity [236]. Theoretical uncertainty arises from several unknowns in the early Universe. For example, as shown in [220], the presence of non-Gaussianity in the inflationary density perturbation can lead to a significant increase of the rate up to roughly two orders of magnitude.

In Fig. 7 the frequency is fixed at 200 MHz, which is relevant for the FLASH setup. Mergers with black holes heavier than about $10^{-7}M_\odot$ produce a signal resonating within the cavity for less than one cycle therefore requiring a different search strategy. For lighter black holes, the lack of signal coherence - in the limit where $N_{\rm cycles} \ll Q_L$ - causes a significant decrease of the sensitivity reach, down to masses of order $10^{-11}M_\odot$. At a first glance, the reach of FLASH might seem much worse than the estimates proposed in Refs. [207, 220, 235]. However, previous results follow from the assumption of a sufficiently coherent source within the frequency bandwidth, which is not the

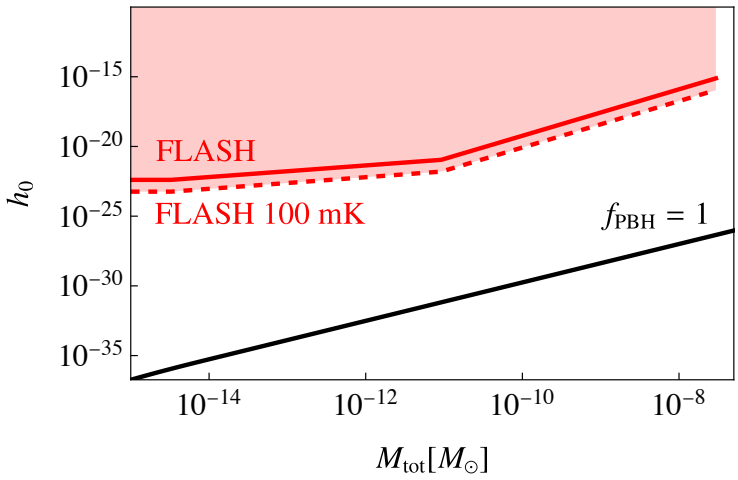

Figure 7: Comparison of FLASH reach for different PBH masses. The red line correspond to the reach of FLASH according to the values described below Eq. (43). The dashed red line corresponds to the reach with improved cryogenics. The black line correspond to the expected gravitational wave signal in case of a monochromatic spectrum at $f_{\rm PBH} = 1$. The frequency of the signal is fixed to $\nu_c = 200\,\text{MHz}$.

case for merging PBHs as already discussed above. Finally, for black holes heavier than about $10^{-14} M_\odot$ a drop in the sensitivity is also caused by the fact that the duration of the signal in the relevant bandwidth is shorter than the chosen integration time of order minute. Slightly different values, but of comparable order are obtained within the frequency range of FLASH experiment.

For a deepened technical discussion of these findings, and a more general overview comparing FLASH experiment with the reach of other resonant cavities, see the recent publication by some of us [237].

4.6 GravNET: a global network of multiple cavity experiments

A key difference of HFGW detection from axion-like particle searches is rooted in the observation that gravitational waves originating from distant sources yield a coherent signal across the Earth. Instead of constructing a single dedicated cavity-based experiment, a global network of multiple cavity experiments can combine their measurements coherently, significantly boosting sensitivity. This idea was recently proposed as the GravNet proposal [238]. It is therefore foreseen to integrate the FLASH haloscope as major site in the GravNet initiative. For this, the recorded signal will be associated to GPS signals, hence allowing to a subsequent data-analysis of all cavity measurements within GravNet. Including the FLASH haloscope into GravNet will allow to probe a completely new parameter space of HFGW sources. It should be noted, that this does not impact the search for axion like particles at all and will be conducted in parallel.

5 Broadening the discovery potential

In this section we discuss how to broaden the discovery potential achievable within the FLASH collaboration, both during the data-taking phase of FLASH and after its conclusion. In Sec. 5.1, we discuss the case of Bulk Acoustic Wave resonators (BAW). These resonators have been proposed to search for axion [239] and scalar [180, 240] dark matter as well as for HFGWs [241] in a frequency range from a few hundred kHz to a few hundred MHz. The proposed experiments have much in common with those with RF cavities and FLASH in particular: the cryogenic environment, including the presence of a strong magnetic field; the SQUID amplifiers; the multi-mode digitization and data acquisition; the data analysis. BAWs with modes at 100 MHz will be used in the FLASH R&D to test and validate the amplification and acquisition chain as discussed in Sec. 10.

In Sec. 5.2 we propose possible uses of the FLASH cryostat for future experiments after the FLASH data-taking is concluded.

5.1 Bulk Acoustic Wave Resonators

The piezoelectric effect is a property of certain materials where mechanical stress can generate an electric charge. Conversely, these materials can deform mechanically when subjected to an electric field. This effect is rooted in the non-centrosymmetric crystal structures of piezoelectric materials, which lack a center of symmetry. When such a crystal is deformed, the symmetry-breaking leads to a polarization within the material, creating an electric field and vice versa.

Key materials exhibiting piezoelectric properties include quartz, lead zirconate titanate, and certain ceramics. These materials are widely used in sensors, actuators, and resonators because they can efficiently convert between mechanical and electrical forms of energy.

The piezoelectric effect is utilized by Bulk Acoustic Wave (BAW) Resonators to generate and sustain acoustic waves that propagates through the bulk of a crystal [242]. BAW resonators have very high quality factors, meaning they can sustain oscillations for a long duration with minimal energy loss. This property enhances the sensitivity of the device to weak interactions, making it easier to detect low-amplitude signals that might be indicative of DM or gravitational waves.

While FLASH is highly effective for detecting axions and other weakly interacting particles in the 10^{-1} GHz frequency range, Quartz BAW devices offer a complementary approach for exploring lower frequencies, particularly around the MHz range. This is crucial for accessing a different region of the potential axion and scalar field mass spectrum and for investigating new GWs windows.

In the context of axion detection, BAW resonators operate on the principle that axion DM can induce oscillatory forces within the crystal via the *piezoaxionic* effect. These forces are resonantly amplified when their frequency matches the resonant frequency of the BAW device. The piezoelectric properties of the BAW material convert these mechanical vibrations into electrical signals, which in turn will allow to impose constraints on the QCD axion parameter space [239].

For scalar fields, the interaction can cause periodic variations in the material properties of the crystal, such as its density or elastic constants. These variations allow to constrain the scalar-EM coupling to be $|d_e| \lesssim \mathcal{O}(1)$ around MHz frequencies and $|d_e| \lesssim 10^3$ at 100 MHz [180, 240]. Notice that in both frequency regions, the expected bounds are significantly stronger than the existing ones as it can be inferred from Fig. 4. In particular, in the latter frequency range overlapping with FLASH, the bound from BAW resonator is, at least, one order of magnitude stronger (we remind the reader that a significant loss of sensitivity is caused by the smallness of the quality factor with respect to the TE_{111} mode).

Regarding gravitational wave searches, a bulk acoustic-wave device represents a resonant mass detector whose deformations induced by the passage of GWs could be read through the piezoelectric effect. Some advantages are the access to a large number of sensitive modes (>100) in a single device scattered over the wide frequency range (1–700) MHz or the possibility of scalation

or modifications towards lower frequencies and/or better sensitivities from arrays of detectors. The level of sensitivity of bulk acoustic-wave detectors is estimated at the level of $\sqrt{S_n} \simeq 2 \times 10^{-22}\,\mathrm{Hz}^{-1/2}$ subject to the mode geometry [243]. This level may be improved and the frequency range extended down to hundreds of kHz range.

High-frequency GWs with single bulk acoustic-wave devices and two modes at $\sim 4\,\mathrm{K}$ have been looked for since November 2018. Two strong rare events in the MHz band were reported in these searches [241]. Their origin is still unclear (see e.g. [244]). Among future possibilities, the building of an array of BAWs and multimode read-outs is being pursued by the Bulk Acoustic Wave Sensors for a High-frequency Antenna (BAUSCIA) proposal in Milano Bicocca (MiB) and the Multimode Acoustic Gravitational Wave Experiment (MAGE) in University of Western Australia [245].

Further improvements could come from reaching the quantum ground state of the system [246], counting phonons, performing quantum state tomography or quantum manipulation and characterization of the states of a BAW resonator [247–249]. Finally, [250] recently discussed a theoretical characterization aiming at optimizing the searches of HFGWs with phonons.

5.2 Future applications for the FLASH Instrumentation

Once the current mission of the FLASH experiment's resonant cavity concludes, it holds potential for re-purposing in the pursuit of novel dark matter (DM) models.

One promising direction is the investigation of millicharged DM particles, denoted as $\chi^{\pm}$, which have been the subject of various studies [251–253]. In particular, the study in Ref. [251] proposed to directly detecting light millicharged DM by distorting the local DM flux with time-varying electric fields (deflecting region) and measuring the distortions with shielded resonant detectors (detection region, FLASH cryostat instrument).

These studies can be extended improving experimental setups, dark matter models, production mechanisms, and cosmologies. The Frascati theory group is exploring the viability of these models using coaxial-cylindrical configurations for the deflecting electric field. This field would separate the positive and negative millicharged fluxes, which could then be detected by an apparatus akin to the DMRadio experiment [79], potentially offering improvements over earlier proposals [251].

Additionally, the FLASH cryogenic apparatus could be used to search for solar and halo axions in the higher mass window in the eV range, taking advantage of the strategy outlined in Ref. [254]. Axions from different sources will be converted into photons by the Primakoff effect due to the FINUDA magnetic field inside the apparatus. For a cylindrical-cryogenic structure with a diameter of approximately 2.7 meters and a length of 2.4 metres and magnetic field of about 1.1 T, we estimate the following photon-signals from each sources, using Refs. [22, 90, 255]:

1. For solar axions, we expect about hundred of axion-converted-photon per week for $g_{a\gamma} \simeq 10^{-10}$;

2. For DM halo axions, we expected one photon signal per year.

In comparison to current and forthcoming axion telescopes like CAST and IAXO, utilizing the FINUDA magnet for an experiment would offer the benefit of complete angular coverage of the sky at 4π, which is also perfectly suited for detecting isotropic axion fluxes [256].

For the cryogenic apparatus of FLASH, the experimental instrumentation will need some additional setups, such as mirror configurations, to focus the axion-converted photons to the axis of the cylinder where the electronics are present.

Part II
Conceptual Project

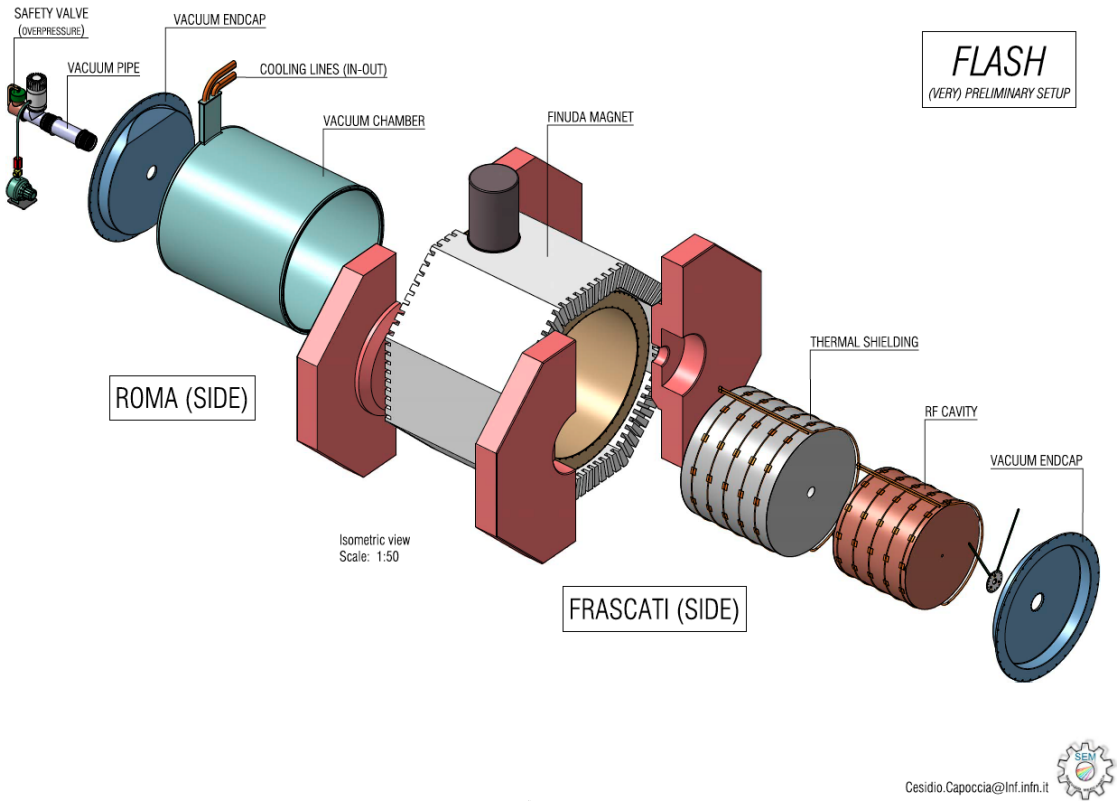

Figure 8: Exploded diagram of the FLASH detector (C. Capoccia - LNF).

6 RF cavity design and tuning

The goal of the FLASH experiment is to cover the range $\nu_c \sim (117 - 360)$ MHz by tuning its resonant frequency that operates on the mode TM_{010} for the axion search. Since this wide range of tuning frequencies cannot be covered in a single setup, two cylindrical resonant cavities of different volumes have been considered, each with its tuning system. The larger cavity has a length of 1200 mm and a radius of 1050 mm for an inner volume $V_{\rm Large} = 4.15\,{\rm m}^3$ and it is expected to operate in the frequency range $\sim$(117 - 206) MHz during the first phase of the operation (FLASH Low Frequency or LF). The second cavity has a length of 1200 mm and a radius of 590 mm for an inner volume $V_{\rm Small} = 1.31\,{\rm m}^3$ and will explore the range $\sim$(206 - 360) MHz during the second phase (FLASH High Frequency or HF). The two setups overlap over a few MHz. The two cavities have different diameter and are schematically represented in Fig. 9.

The resonant cavity will be made of oxygen-free high thermal conductivity copper (OFHC), a type of copper which may show a residual resistance ratio (RRR) that varies between 50 and 700. Assuming RRR = 50, we simulated the quality factor Q and the form factor C_{010} of the

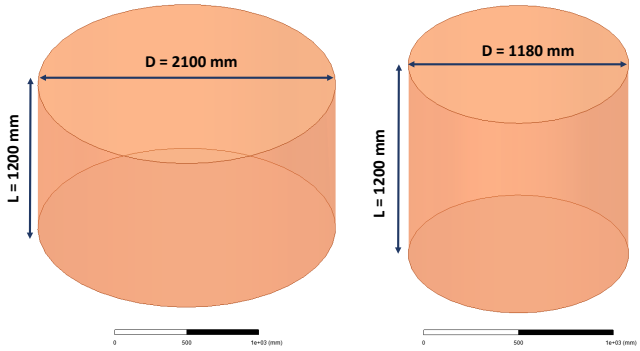

Figure 9: Schematics of the two cavities (without tuning system) proposed to cover the frequency range of resonant frequencies (117 - 360) MHz.

TM_{010} resonant mode of the FLASH resonant cavities with the ANSYS-HFSS code.[6] Simulations predict values for the quality factor that vary from about 3.8×10^5 to 5.7×10^5, while the form factor varies from about 0.63 to 0.75. These results are used to determine the FLASH sensitivity to QCD galactic DM axions and hidden photons.

The tuning system is based on the use of metallic movable rods, similarly to what has been adopted by the ADMX collaboration [32, 33, 106, 257]. After a preliminary investigation in which different possible configurations have been explored in terms of number of rods, dimensions and positions, the optimized case of three rods has been selected as represented schematically in Fig. 10. The final parameters are reported in the Table 4 for both cavities. Each rod of radius $R_{\rm rod}$ rotates by an angle α around a center $C_{\rm rot}$, moving towards the center of the cavity on a circular trajectory of radius $R_{\rm rot}$. The rotation of the rod allows for the tuning of the mode TM_{010} to different frequencies. Although this is equivalent to a rigid rod translation, this latter strategy is harder to realize for a cavity inserted in a cryogenics system.

Parameter	FLASH LF	FLASH HF (S)
R cavity (mm)	1050	590
$R_{\rm rod}$ (mm)	115	60
$R_{\rm rot}$ (mm)	276	160
$C_{\rm rot}$ (mm)	654	367
$L_{\rm rod}$ (mm)	1200	1200
n. tuning rods	3	3
Frequency range (MHz)	117 - 206	206 - 360
$Q/1000$	570 - 450	524 - 380
Form factor	0.63 - 0.73	0.64 - 0.75
BW (Hz) @ $\beta = 1$	410 - 916	786 - 1895

Table 4: Main parameters of the two cavities with frequency tuning system.

[6] https://www.ansys.com/

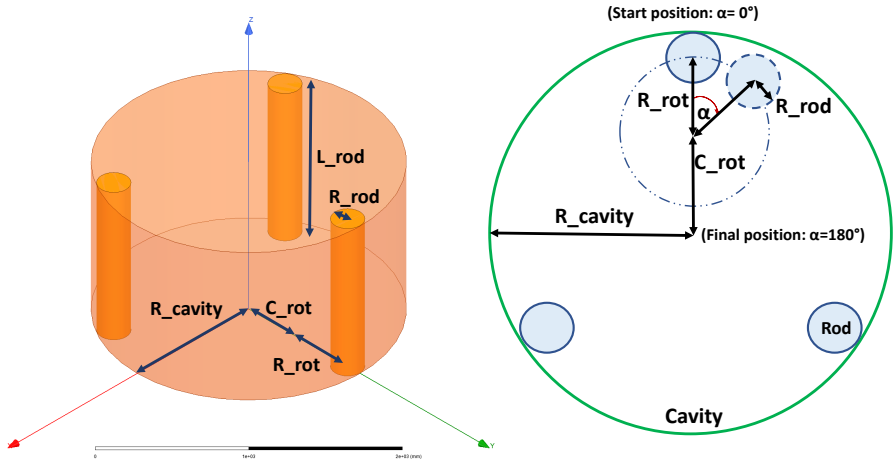

Figure 10: Sketch of the cavity with tuning system.

The contact between the rod and the parallel plates of the cavity must be guaranteed to avoid a deterioration of the quality factor. In fact, a non-perfect contact increases the losses by creating a gap that acts as a capacitor with spurious modes. Simulations show that a gap 1 mm wide leads to a deterioration of the quality factor by less than 5%. This problem was already addressed in Ref. [257]. The different rod-configurations we explored are schematically shown in Fig. 11.

During the preliminary assessment of the schematics, we have considered various configurations consisting of one, two, or three symmetric rods, with different radii, positions, and centres of rotation. Based on the calculation of the frequency range, the quality factor and the form factor of the working mode in all these configurations, a configuration consisting of three rods has been adopted. This choice, along with the size of the rods of radius $R_{\text{Large Rod}} = 115$ mm for the larger cavity and $R_{\text{Small Rod}} = 60$ mm for the smaller cavity, compromise between the complexity and tunability of the system. The frequency range and the number of required frequency steps for the two foreseen runs with the different resonant cavities are summarized in Table 5.

Table 5: Summary of frequency tuning ranges and steps.

Stage	Frequency range	Number of steps
FLASH LF	(117 - 206) MHz	80 600
FLASH HF	(206 - 360) MHz	69 000

In Fig. 12 we show the cavity frequency as a function of the rotation angle α of the TM_{010} and of the other identified modes for the three-rods case. Here, the three rods are moving symmetrically. The rotation angle $\alpha = 0°$ corresponds the rod near the cavity wall. We note that this tuning system does not affect the mode frequencies equally, leading, for some rod positions, to an overlap between different modes. We note, for instance, the overlap of the working mode with TE modes and with the TEM mode generated in the the coaxial line formed by the rod (inner conductor) and the outer cavity wall (outer conductor). These are labelled as "TEM coaxial modes" in the picture. Modes overlap lead to a "mode mixing" that makes the detection of the mode TM_{010} more difficult in the

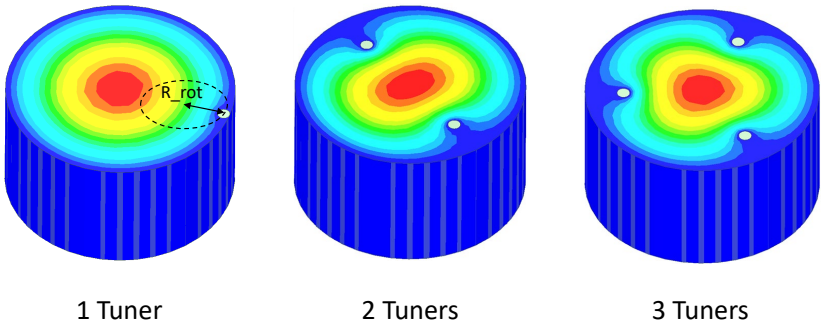

Figure 11: Sketch of the tuning rods configurations analyzed for the setup. Colors code the magnitude of the electric field strength.

crossing region [257].

The signal from the TM_{010} mode is extracted through a coaxial probe inserted in one of the two end-caps of the cavity, parallel to the axis of the cavity itself, as sketched in Fig. 13. The probe coupling β will be varied by changing the penetration depth of the inner conductor (L_{inner}). Simulations show that a change in the penetration depth of a standard-SMA antenna by few tens of cm the coupling β varies in a wide range between 0 and 2. We also verified that the TM_{010} mode is always well identifiable, in particular near the crossing region between TE-TM modes. This is due to the fact that the probe only couples to the longitudinal electric field of the mode, which is equal to zero for ideal TE and TEM modes and leads to a negligible coupling between the TM_{010} mode and TE modes. This test was performed by simulating the transmission coefficient between two coaxial probes coupled to the cavity for different rods positions such that the frequency is in the TM_{010}-TE_{211} mode-mixing region, see Fig. 14. The result was also confirmed by simulations in a smaller frequency range. Residual mode crossings will be resolved by proper rotating the three tuning rods or by the proper insertion of small dielectric tuning rods.

The minimum angle of rotation achievable with the FLASH tuning system must correspond to a frequency variation on the order of the cavity bandwidth reported in the last line of Table 4. The sensitivity of the resonant frequency to the rotation angle is shown in Fig. 15. From this figure, we deduce that the minimum tuning angle of rotation must be less than 12 μrad in the positions range from 80 degrees to 140 degrees. This will be assured by equipping each tuner by a vacuum compliant Hybrid Stepper-Motor (200 step/turn, 150 min^{-1}) with a three-stage epicyclic gear unit (1:200) and a gear couple (1:10). The total angular step will be 9^{-4} degrees ($\sim 2.5\,\mu$rad) (Fig. 16). The whole turn will take around 7 min.

To achieve a more precise tuning a small cylinder of dielectric material (alumina or sapphire) can be inserted as sketched in Fig. 17. With a cylinder of 10 mm of radius, in sapphire, we achieved

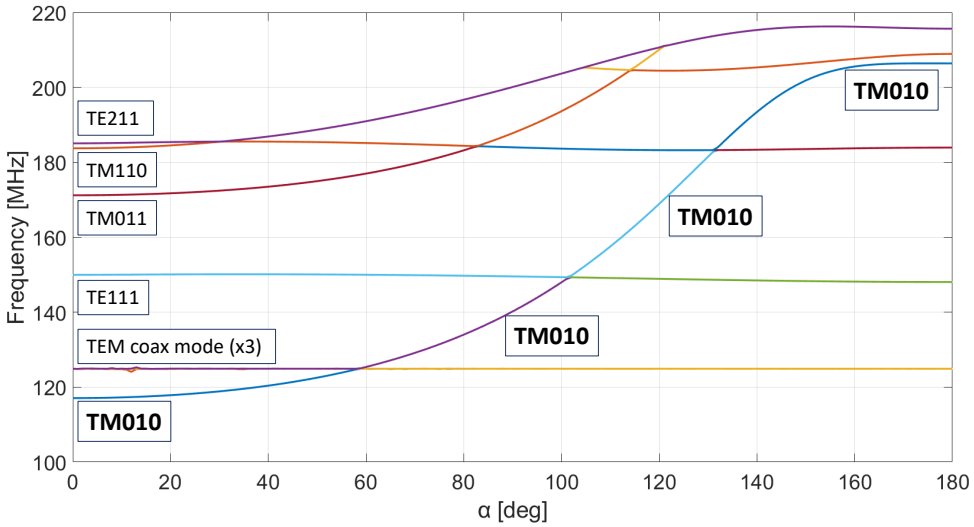

Figure 12: Complete mode mapping in the case of cavity with larger radius (Low Frequency).

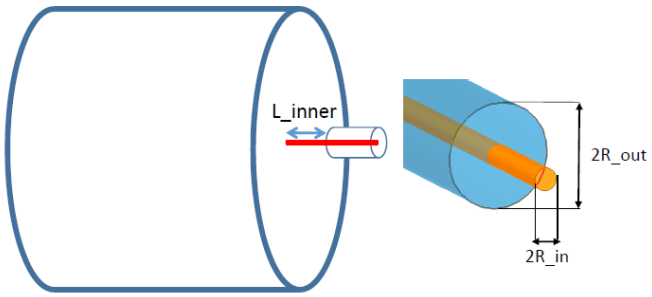

Figure 13: Sketch of the antenna coupled to the cavity modes.

in the simulation a sensitivity of $160\,\mathrm{Hz\,mm^{-1}}$ that can be reduced or increased by decreasing or increasing the diameter of the cylinder itself, or by changing its position on the cavity.

In Fig. 18 we show the quality factor and form factor of the TM_{010} mode as a function of frequency, where we assumed that the rods and the cavity are made of copper with a value of RRR equal to 50 and, as a consequence, with a conductivity at 4 K equal to $\sigma = 2.9 \times 10^9\,\mathrm{S/m}$ [259].

The three tuning rods of the smaller cavity, used to probe the higher frequency range, have radius equal to 60 mm. The cavity with the rods is schematically shown in the left panel of Fig. 19. In the right panel we show the frequency of the TM_{010} mode as a function of the tuner position. The complete mode mapping is given in Fig. 20 while the quality factor and the form factor are shown in Fig. 21.

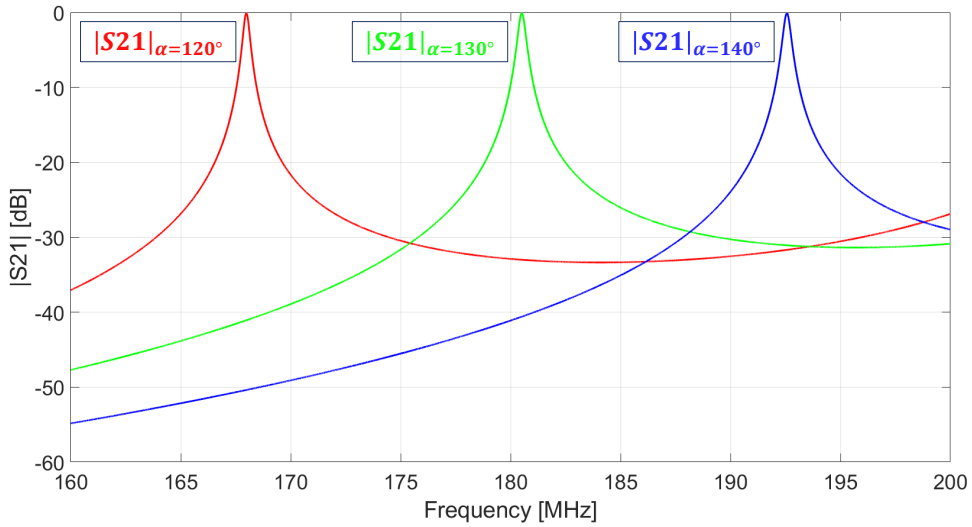

Figure 14: Transmission coefficient between two coaxial probes coupled to the cavity for different tuner positions in the frequency region of the TM_{010} - TE_{211} mode-mixing.

Finally, the sensitivity of the rod tuning-system for the small cavity is reported in Fig. 22.

6.1 Other modes relevant for axion, chameleon and HFGW searches

In order to exploit the full discovery potential of FLASH we must take into account modes higher than the TM_{010}, that couple to the dark-matter axions but also to dilatons, chameleons and high frequency GWs (HFGW). The signal from the TM_{020} mode can be acquired to increase the frequency range of the axion and dark-photon search. For this mode the coupling factor is $C_{020} = 0.13$, about a factor 5 smaller than for the TM_{010} mode. The mode TE_{011} is relevant for chameleons searches as discussed in section 4.3. For HFGW both TE and TM modes are relevant and simultaneous detection of the different modes may be important to increase the signal sensitivity and to exploit the detector directionality [235]. We report frequency and quality factor for some of these modes in Tab. 6 and 7.

Mode	Frequency (MHz)	Q_0 factor (at 4 K)
TE_{111}	150.4	711×10^3
TE_{112}	263.5	871×10^3
TE_{211}	186.9	735×10^3
TE_{212}	285.9	817×10^3
TE_{011}	214.5	1.3×10^6

Table 6: TE Modes for the Large cavity

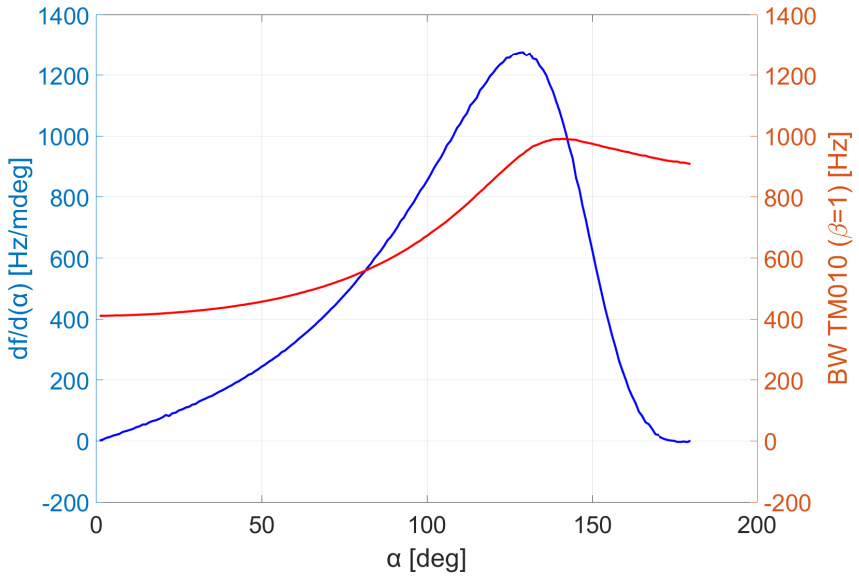

Figure 15: Sensitivity of the resonant frequency and TM_{010} mode bandwidth to the rotation angle.

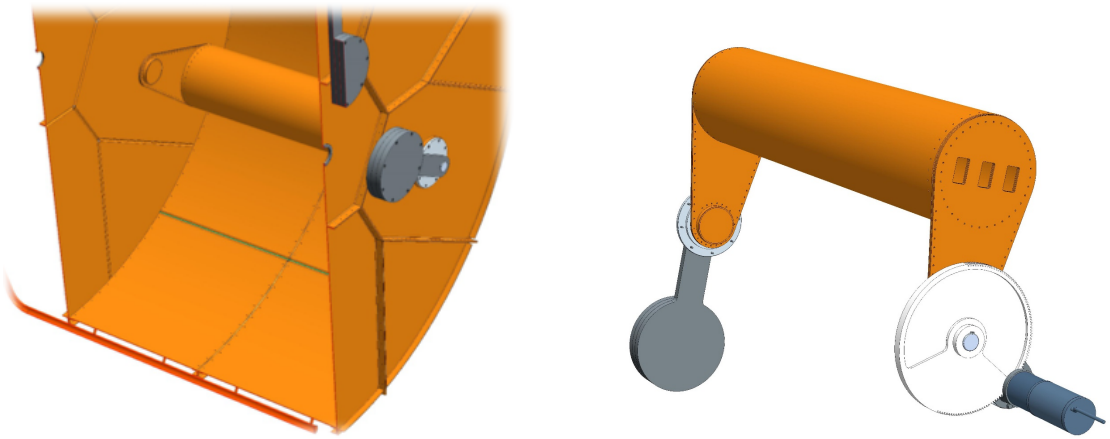

Figure 16: Internal view of the cavity with the tuner (left) [258]; tuner assembly (right).

While the signal from the TM modes can be acquired from the same dipole antenna discussed in the previous section, the TE modes require a different kind of antenna and/or insertion point. In fact, also the TE modes can be acquired by means of a coaxial dipole, placed however in a different insertion point with respect to the TM modes. In general for cylindrical cavities this region is on the lateral surface. This type of signal extraction is called electrical coupling. Signals from TE modes can also be extracted by magnetic coupling created by bending the inner conductor of the

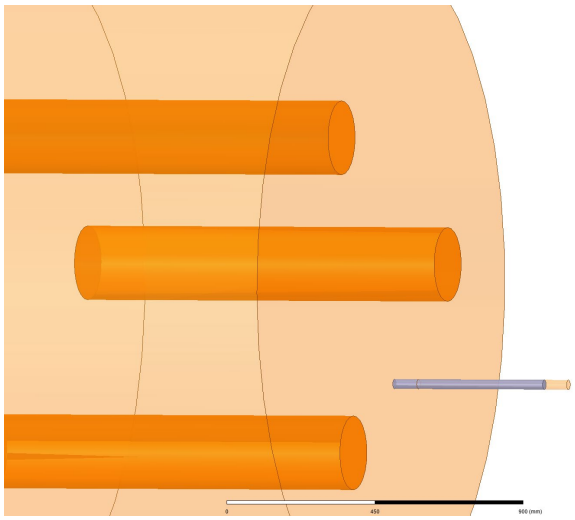

Figure 17: Dielectric tuning system for fine frequency tuning.

Mode	Frequency (MHz)	Q_0 factor (at 4 K)
TM_{010}	109.5	626×10^3
TM_{011}	166.1	526×10^3
TM_{110}	174.4	790×10^3
TM_{020}	251.2	948×10^3
TM_{111}	214.5	598×10^3
TM_{012}	272.3	752×10^3
TM_{112}	304.7	712×10^3
TM_{210}	233.7	915×10^3
TM_{211}	264.9	664×10^3
TM_{212}	342.1	755×10^3

Table 7: TM Modes for the Large cavity

coaxial antenna into a loop. This antenna is placed in an area of the cavity where the magnetic field is maximum and transversal to the surface of the loop. The coupling of the β probe will be varied by changing the angle between the loop surface and the magnetic field, given the loop size. Fig. 23 shows the electric field and magnetic field of TE_{111} mode with an example of electric coupling and magnetic coupling and their insertion point. A further comment is required for TE modes. The resonant cavity will be composed by tiles, realized by cold formed commercial plates of copper OFHC joint by rivets [258]. To minimize eddy current loops, in particular in case of a magnet quench, we planned to insulate the longitudinal joint between tiles by NEMA G10 plates and insulating sleeves. This will however interrupt the currents of TE-modes excitations inhibiting it, requiring a different solution to be used.

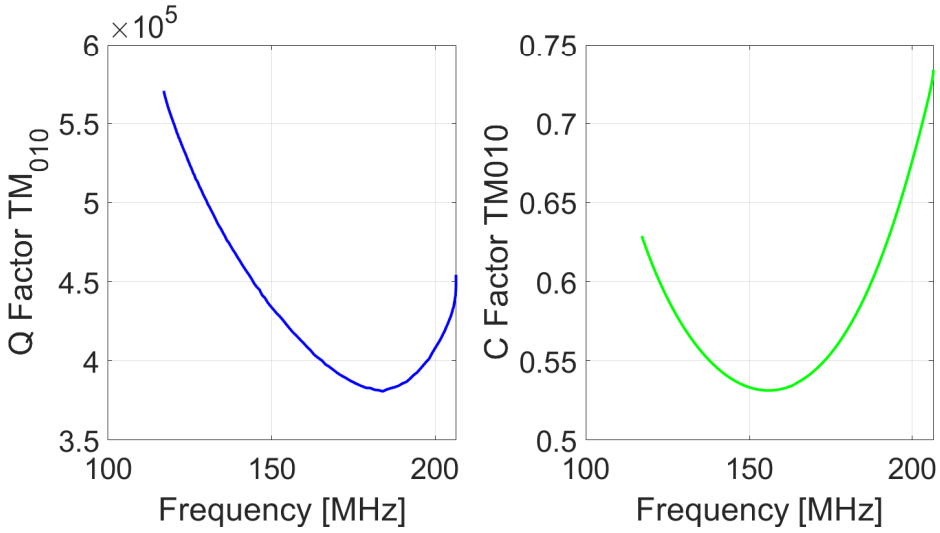

Figure 18: Quality (left) and Form (right) factors of the TM_{010} mode as a function of frequency for Low Frequency cavity.

7 The FLASH cryogenics

The RF cavity for FLASH must be cooled at low temperature to reach the needed sensitivity. To do so, it will be hosted in a dedicated custom cryostat and cooled at 4.5 K or 1.9 K (see later) using liquid helium (LHe). The cryostat will be composed by an external stainless steel vacuum vessel, containing an aluminum-alloy radiation shield kept at about 70 K by cold gaseous helium (GHe) and surrounding the cavity. Both the cavity and the shield are cooled in contact with pipes in which the helium flows.

The FLASH experiment takes advantage of the availability at LNF of two existing apparatuses: the DAΦNE cryogenic plant [260] and the FINUDA magnet. The cryogenic plant is a liquid helium refrigerator/liquefier, which kept cooled the KLOE and FINUDA superconducting magnets during their runs for about twenty years. The plant is capable to be connected and cool both the FINUDA magnet and the FLASH cryostat at the same time.

The general layout of the FLASH cryogenics is shown in Fig. 24. The cryogenic plant, a LINDE TCF50 refrigerator/liquefier, is composed by a Cold Box, in which the gas is cooled down both in supercritical state, (SHe) at 5.2 K/3 bar, and in gaseus state at 70 K/5 bar, and a Valve Box, where the cold helium coming from the Cold Box is distributed to the users. Cold and Valve Boxes are connected via a transfer line (in red in the figure).

The Valve Box has two main send/return connections for the users, formerly used for KLOE

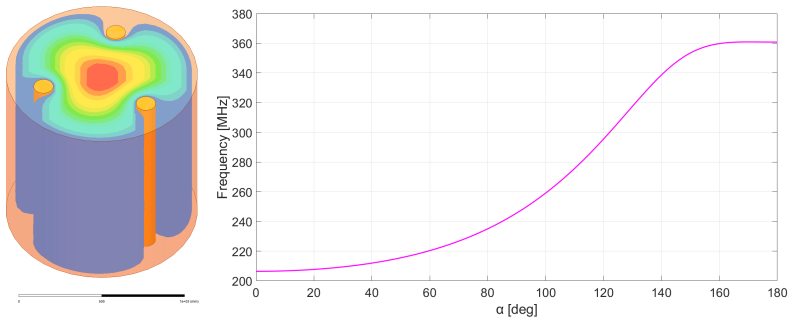

Figure 19: Cavity with smaller radius with tuning system (left); frequency of the TM_{010} mode as a function of the tuner position (right).

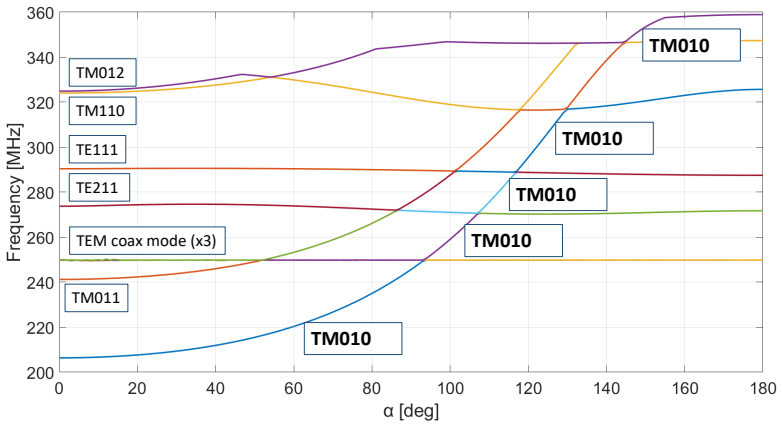

Figure 20: Complete mode mapping in the case of cavity with smaller radius (High Frequency).

and FINUDA. The FLASH cryostat (blue square in the figure) will be connected to the Valve Box in place to the ex-KLOE line.

7.1 The cryogenic plant

The cryogenic plant is based on a LINDE TCF 50 Cold Box and a KAESER ESD442 compressor. As said, the refrigerator can provide both SHe at 5.2 K and GHe at about 70 K, the latter for the radiation shields cooling. Both cryogens are then sent in the Valve Box, where they are split to the users. The Helium liquefaction is carried out directly over the users, in dedicated service turrets equipped with a J-T valve and a buffer volume, for the liquid storage.

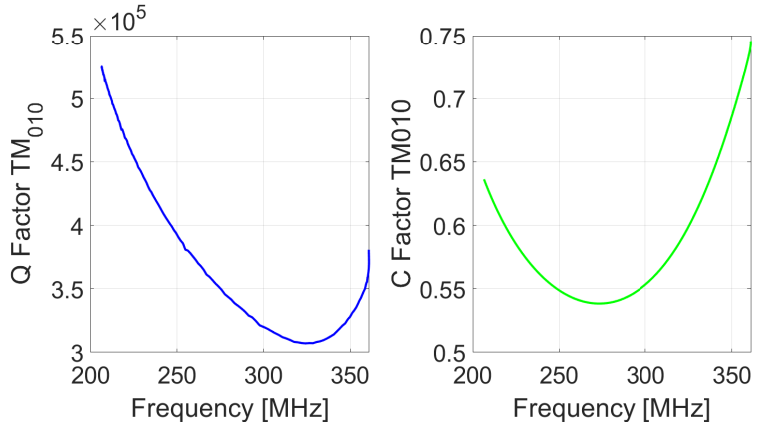

Figure 21: Quality (left) and form (right) factors as a function of frequency.

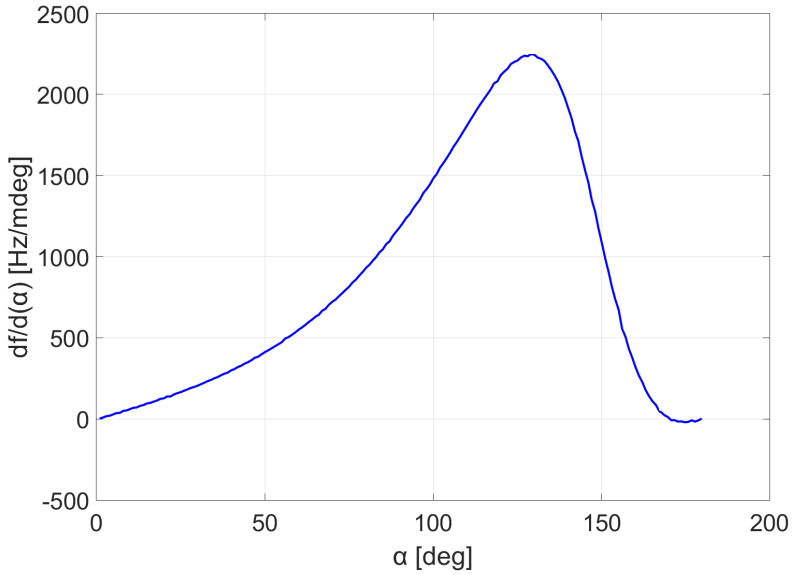

Figure 22: Sensitivity of the tuning system for the cavity with smaller radius.

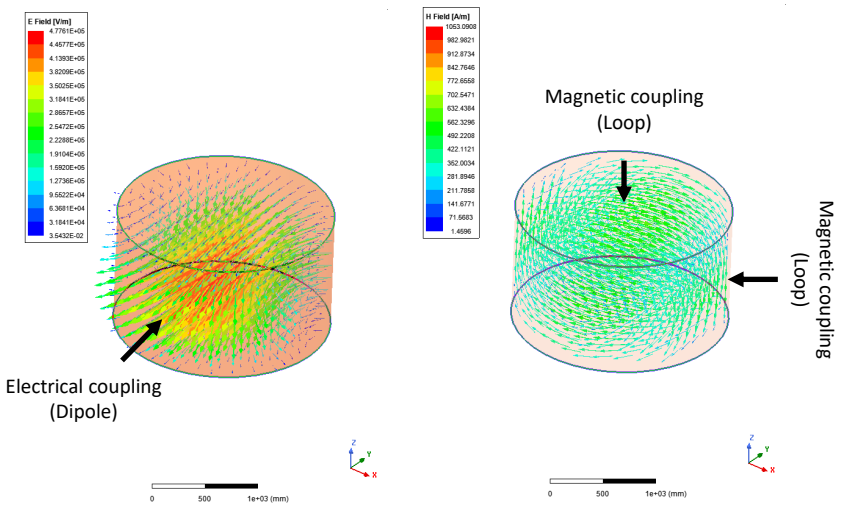

Figure 23: Electric field (left) and magnetic field (right) of TE_{111} mode with a sketch of the insertion points for the two different types of coupling.

The cooling capacity of the plant is as following:

- liquefaction rate = 1.14 g/s;
- Refrigeration capacity at 4.45 K/1.22 bar = 99 W;
- Shield cooling capacity below 80 K = 800 W.

7.2 The FINUDA superconducting magnet

The FINUDA Magnet [103] is an iron shielded superconducting solenoid coil, made by Ansaldo Energia (Italy). The coil is cooled with thermo-siphoning method, and its service turret has a buffer reservoir of about 25 liters. The magnet works in continuous cooling at the temperature of 4.5 K. Its nominal magnetic field is 1.1 T with a current of 2796 A and the stored energy is 10.34 MJ. The magnet bore dimensions consist of a length of 2.4 m and a diameter of 2.7 m. It has operated until 2007 for the FINUDA (FIsica NUcleare at DAΦNE) experiment at INFN-LNF. [7] In Jan 2024, after a 17-years stop, the magnet was reconnected to the cryogenic plant and successfully cooled at 4.4 K and energized at 2700A for one day, using its original cryogenic control system, still in good condition and operating.
For the future, we plan to do a complete refurbishment of the diagnostic hardware and valves control, as well as of the quench detector electronics, as they are very outdated.
The control and monitoring system for the FINUDA magnet must allow for the safe activation of the magnet itself and the reading of all parameters. The previous system consisted of a series of both

[7] http://www.lnf.infn.it/esperimenti/finuda/

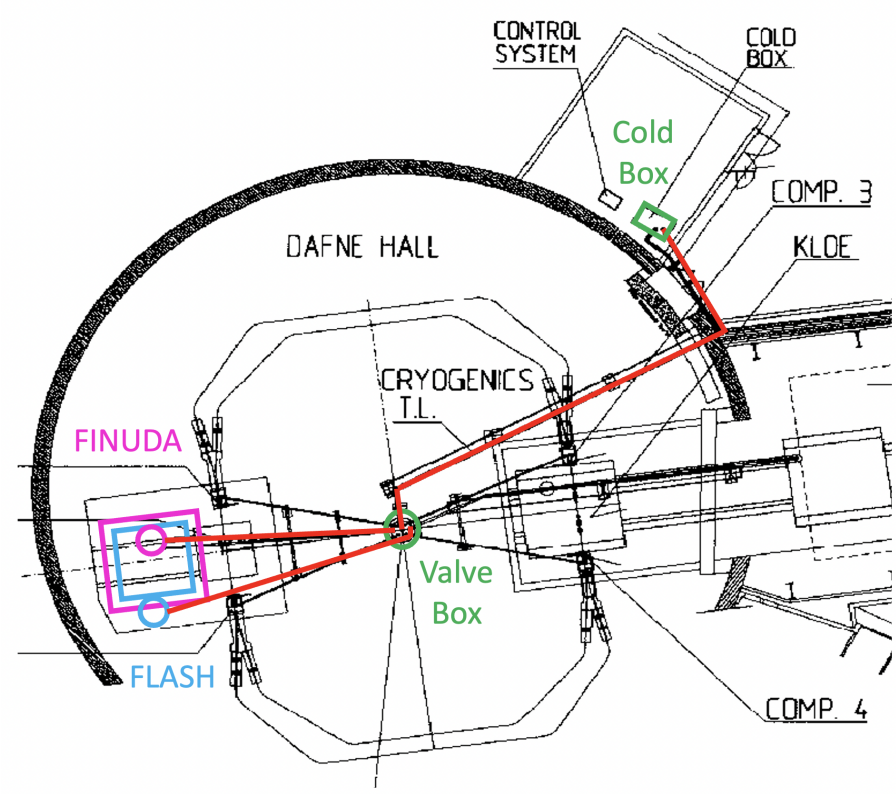

Figure 24: General layout of the FLASH cryogenics

analog and digital elements that enabled its proper functioning. The hardware of the old system, dating back many years, is now obsolete, and some components are out of production. Therefore, it is necessary to design a new system based on more modern technologies. The new system will need to acquire all the temperature and pressure sensors present on the magnet and the pipes of the cryogenic system, read the vacuum status, and read and control the helium transport valves. Additionally, some of these valves will need to be able to manage their opening autonomously based on temperature or pressure values. The magnet power supply will also need to be controlled. The system is planned to be developed using the National Instruments CompactRIO system. The use of this system allows for a real-time processor along with an FPGA system. In this way, we will have the real-time system dedicated to acquiring all slow values, controlling the magnet power supply, and the possibility of creating a server for remote system control, while the necessary PID controllers for the automatic control of the valves will be implemented on the FPGA system.

7.3 The FLASH cryostat

In the base configuration, the FLASH cryostat must keep the RF cavity cold. Two options are under investigation regarding the cavity operating temperature: either using LHe temperature (4.5 K/1.3 bar) or Superfluid He (1.9 K). The general layout of the cryostat is similar in both cases, apart from the turret, which in the first case will host a J-T valve for the last liquid expansion at 1.3 bar, while to get the superfluid Helium a cryogenic pump is needed. Both option are under study

to understand their feasibility. The colder temperature is preferred for the important reduction of the thermal noise, but we have to understand the feasibility of this operating condition in parallel with the 4.5 K FINUDA magnet cooling and also the complication on the FLASH cryostat cold pipes fabrication, mainly to avoid leaks. During the TDR phase we will investigate the feasibility of cooling down the cavity to 1.9 K.
The cryostat must withstand several requirements:

- it should match the available space inside the FINUDA magnet bore, and should be provided by all the mechanical tools for its insertion on the bore.
- it should be supported either by the magnet itself or by the ground, using suitable legs,
- it should be supplied by the cryogenic plant, so it must be equipped with a cryogenic service turret,
- it should contain a 300 mK small-size refrigerator for the low-T amplification device. The need for this last point must be verified during the TDR phase.

Most of the general considerations made for the KLASH cryostat [258] are still valid for FLASH.

7.4 SQUID cooling at 300 mK

In order to minimize the thermal noise generated on the SQUID, we may need to lower its temperature using a compact-size ^{3}He evaporation refrigerator, capable to cool it down to about 300 mK. In fact, the added noise of the SQUID increases linearly for a bath temperature up to a few hundred mK, flattening out afterwards. Therefore, the choice for a 300 mK cooling stage will be decided after the noise saturation value will be measured during the TDR phase.

This kind of refrigerator is commercially available,[8] and can be conveniently inserted inside the FLASH cryostat. It is actually a two-stage refrigerator, where a first stage is a ^{4}He refrigerator, used to pre-cool at about 1 K and allows the condensation of the the ^{3}He present in the second stage. In this way temperatures close to 300 mK can be reached, depending on the thermal input from the SQUID.

The refrigerator requires some dedicated space inside the FLASH cryostat, as the SQUID must be placed in the proximity of the cavity antenna.

8 Signal acquisition

8.1 Cryogenic Amplifiers

A Superconducting QUantum Interference Device (SQUID) is used as a sensitive magnetic flux detector in a variety of applications. It is also used as a low-noise, low-power-dissipation RF and microwave amplifier [261]. At ultracryogenic temperatures, the noise scales with the temperature down to 200 - 300 mK. However, at lower temperatures, the Joule heating of the electrons gas due to the bias current causes the noise to deviate from the linear behavior and saturate [262]. This is due to the fact that the coupling between the electrons in the Josephson junction shunt-resistors R_s (see Fig. 25) and the phonons is very weak.

Nevertheless, at frequencies below 1 GHz, this noise is an order of magnitude lower than the state-of-the-art semiconductor based amplifiers operating at low temperature. Commercially available two-stages dc-SQUID operating at 100 mK demonstrate an energy resolution of $30\hbar$, a factor 30 above the quantum limit, in the radio frequency band. The use of dc-SQUID has

[8] https://www.chasecryogenics.com

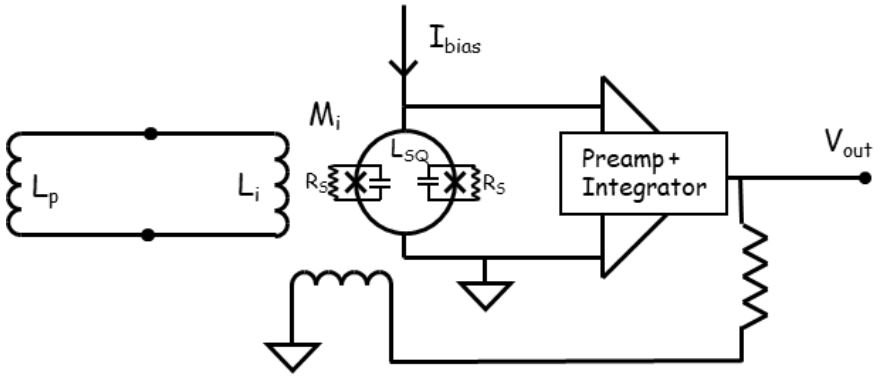

Figure 25: Flux locked DC Squid.

been demonstrated in a flux-locked loop scheme [263], in which the coil is directly inserted in the resonant cavity to pick-up the magnetic field, up to 130 MHz. The operating frequencies of FLASH are slightly higher (from about 117 MHz to about 360 MHz). In addition, micro-vibrations of the apparatus in the presence of an high static field in the cavity, could induce spurious signals in the dc-SQUID. For this reason, a different detection scheme will be used.

A possible solution is the one used by ADMX [36] in which a Microstrip SQUID Amplifier (MSA) [107, 108] is used as first amplifier and a cryogenic heterojunction field-effect transistor (HFET) amplifier is in the 4 K region. The MSA is an effective solution of the problem, allowing to operate with a gain depending on the frequency that is related to the microstrip length, while the bandwidth is defined by the microstrip impedance.

For an operation frequency below 2 GHz, gains are over 20 dB, see Fig. 26 from Ref. [264]. To cover completely the frequency band required by FLASH a varactor diode connected to the input coil can be used. The capacitance is adjusted by changing the reverse bias resulting in an "effective" variation of the microstrip length. In Fig. 27, taken from Ref. [265], the gain is shown as a function of frequency for nine different values of the reverse bias applied to the varactor diode.

The noise temperature T_n of an MSA scales linearly with the operation frequency and the bath temperature [266], saturating at temperatures of a few hundred mK. In Ref. [265] a noise temperature of 170 mK was observed with a bath temperature of 300 mK and an operation frequency of 520 MHz. We scale this value to the FLASH frequencies (ranging from a minimum of 117 MHz for the large cavity, to a maximum of 360 MHz for the small cavity) obtaining a noise temperature ranging from 38 mK to 118 mK (about a factor 7 with respect to the quantum limit in both cases).

Both dc-SQUID and MSA are sensitive to magnetic field, mechanical vibrations and pick up noise. Adequate shielding must be used in order to decrease the static magnetic field in the cavity by 6 or 7 order of magnitude. We studied several possible scheme to shield the SQUID and to guarantee the correct thermalization. A passive approach makes use of both high-permeability and superconducting material to screen effectively both the axial and the radial magnetic field component in a semi-infinite tube [267]. An alternative solution is based on the use of a superconducting magnet in a persistent condition (for example NbTi) cooled in a zero field condition (ZFC). The last solution foresee the use of an active shielding using Helmholtz coils to generate an opposite magnetic field in the region where the SQUID is present. A magnetic filed sensor provides a negative feedback to drive the current in the cancelling coils. All these solutions were detailed in the conceptual design report of the KLASH experiment [258].

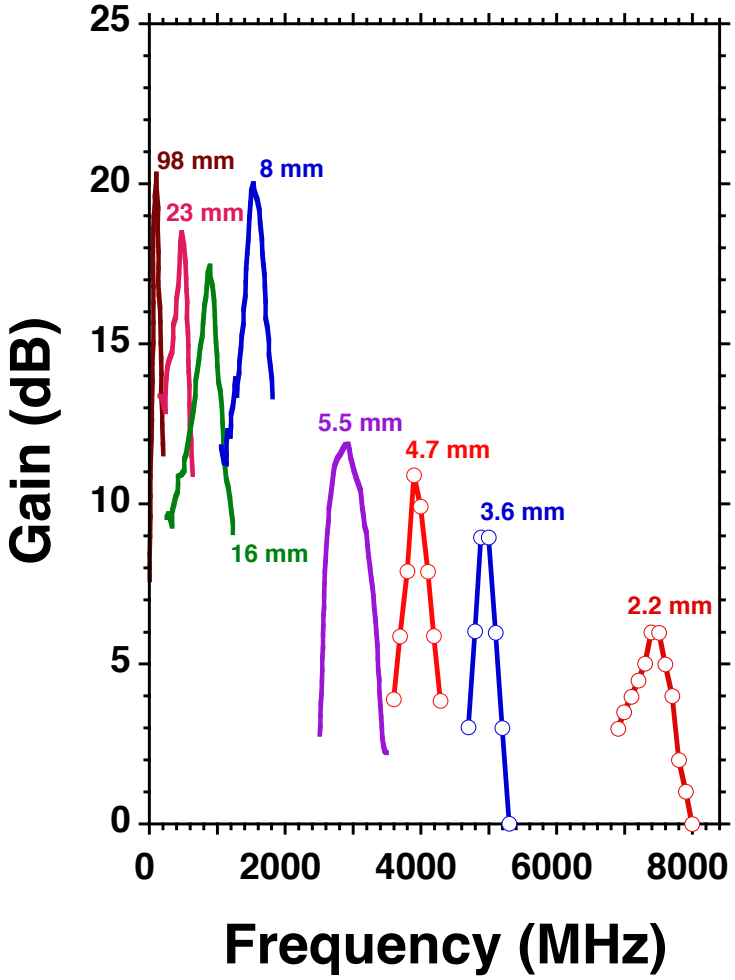

Figure 26: Gain vs frequency for MSA amplifiers. For each curve the length of the microstrip resonator is indicated. Figure from Ref. [264].

8.2 Room temperature amplification and data acquisition

Thanks to the high gain in the cold section of the amplification chain ($>$ 35 dB), the room temperature amplification is not particularly demanding from the noise point of view. After a radio frequency (RF) amplification stage based on commercial low-noise components an intermediate frequency (IF) stage and a audio frequency (AF) mixer stage are foreseen. A power gain of between 30 dB and 60 dB may be required, and two amplification stages may be necessary, in order to match the dynamic range of the following stages.

An equivalent noise temperature up to 150 K is acceptable for the RF amplifier(s). If the power gain of the previous stages is higher than 35 dB, then the contribution of the first RF amplifier to the system noise temperature is lower than 0.05 K and can be considered negligible. Low noise RF commercial amplifiers with a bandwidth of 500 MHz are adequate for this purpose;

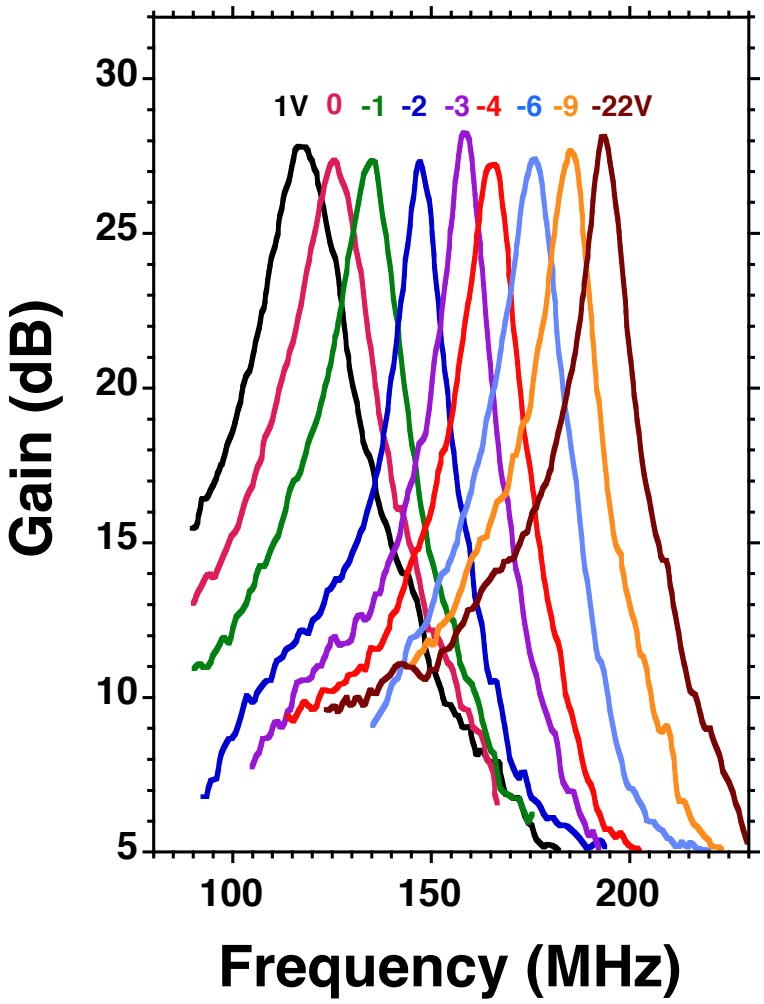

Figure 27: MSA gain vs frequency for different values of bias voltage applied to the varactor diode. Figure from Ref. [265].

for example, the aptmp3-00200005-1627-D9-lN-2 by AmpliTech, Inc. or the CITLF3 by Cosmic Microwave Technology, Inc., although an R&D phase is still needed. The output of the RF stage feeds the IF stage organized with the AF stage in a double heterodyne receiver. A mixer, such as the IRM10-1000 by Sirius Microwave, with an insertion loss of 7 dB and an image rejection better than 25 dB is the first component of this stage. This mixer shifts the RF signal power from the tunable resonant frequencies of the cavity to a fixed intermediate frequency of 10.7 MHz while rejecting image noise power. This image rejection is necessary to avoid mixing off-band RF power into the IF bandwidth, and the chosen value of the intermediate frequency is compatible with commercial devices.

The noise outside the signal bandwidth is reduced using a high selective bandpass filter with a bandwidth around few tens of kHz, compatible with the resonant cavity quality factor. In the AF stage the signal coming from the bandpass filter, after a further amplification stage to increase the

signal to noise ratio, is down-converted to a near audio frequency band with a central frequency of 30 kHz. The reference oscillator is obtained with a low phase noise frequency synthesizer with high frequency stability such the N5171 by Keysight. A commercial fast Fourier transform (FFT) spectrum analyser with a resolution bandwidth of hundreds hertz is used to acquire the power spectrum of the final AF mixer.

9 Data Analysis

9.1 Axions

The signal of axion conversion in haloscopes is detected as an excess in the the measured power spectrum. The analysis procedure relies in the acquisition of data by scanning the resonant frequency with a series of steps that cover a range of possible axion masses. For each value of the frequency scan, the power from axion-to-photon conversion is determined from the data, together with the measurement of experimental parameters that influence the power spectrum.

The expected power produced by the axion-to-photon conversion is very small. Applying Eq. (11) to the FLASH experiment, the expected power released in the cavity is on the order of $P_{\rm sig} \simeq 10^{-22}$ W. The analysis procedure must be designed to identify such a small signal in the presence of significant thermal and amplification-chain noise. A large number of power spectra must be collected for each resonant frequency and combined after subtracting the background contribution using a model of the acquisition chain. Ancillary data will be collected to measure the stability of the system and to characterize the noise components, with the help of a simulation model of the acquisition chain.

The data collection strategy for FLASH is based on the use of two cavities. Three metallic and one dielectric rods are used to tune the resonant frequency of the $\rm TM_{010}$ mode in both cavities. To speed up the scanning rate the antenna will be over-coupled with coupling $\beta = 2$. For each position of the tuning rods the antenna, gain and coupling will be measured and optimized, the resonance frequency and the quality factor of the cavity determined and finally a given number of power spectra acquired. After these measurements the procedure will be repeated with a new value for the resonant frequency obtained by changing the position of the rods.

The importance of measuring the unloaded quality factor Q_0 and coupling β for the TM_{010} mode of the cavity is paramount for determining the expected power of the axions-conversion signal and its relation to the background noise. The Q_0 depends on the geometry of the cavity, requiring it to be measured after each step of the tuning process. To ensure accuracy and stability of the Q_0, which may be affected by mechanical rods stability and the electrical contact between rods and cavity walls, the measurement will be performed before and after each tuning step. A Vector Network Analyser (VNA) will be used to generate an RF sweep around the resonance frequency injected through a first ancillary RF line into the cavity through a weakly coupled calibration port. The Q_0 value will be deduced from the analysis of the transmission and reflection response. The latter will be measured by a signal sent, from a second ancillary RF line, into the readout port through a directional coupler with coupling less than -10 dB. Gain calibration will be possible by combining the transmission coefficients between the ancillary and output lines [66] or by connecting with a switch a 50Ω resistor to the amplifier, and varying its temperature with a heater. Additionally, the stability of the gain of the amplifiers can be checked by injecting a small known signal into the input port of the amplification chain. The measurement of the noise induced by room temperature electronics is less critical. One way to examine the external noise is to detach the cryogenic amplifier from the data collection system and attach it to a suitable termination resistor. The excess power detected in the acquired spectrum is a result of external interference. The speed at which this test can be performed depends on whether noise measurement is possible while the rod is in motion, the presence of external noise on the apparatus (which should

be minimized in any case), and the analysis procedure.

Since the whole data acquisition will last for a rather long time (order of few years) it is important to guarantee periodically the stability of the reference clock with respect to an independent clock lock based on GPS. All the others working parameters (temperatures, pressures, magnetic field, etc.) are constantly measured and added to the data acquired.

We recall the integration time expressed in Eq. (2). As stated in Sec. 3.4, to have the sensitivity required for the measurement an integration time of 5 minutes for each frequency step with the large cavity and 10 minutes for the small cavity is foreseen. According to the number of frequency steps shown in Table 5 for each cavity, this defines the total running time of about two years of data taking. As described before, the power spectrum acquisition is done at the end of the AF stage with a commercial high-speed FFT. Assuming an analysis spectrum of 5 cavity widths, about 5 kHz, each spectrum will be subdivided in 500 bins of 10 Hz each, a factor 10 less than the virialized-axion width. With a typical acquisition time of 10 ms per power spectrum, about 30000 spectra for the large cavity and 60000 spectra for the small cavity, will be acquired for each frequency step. The average of these spectra, for each step, will define the "base spectrum" for the considered frequency.

Starting from the base spectra several steps are applied before the extraction of the final confidence limit as a function of the axion mass:

- definition of bad samples and problematic bins
- normalization of the spectra
- combination of spectra of residuals centered at different frequencies
- test of the null hypothesis
- re-scan of frequency regions that fail the null-hypothesis test
- determination of the exclusion limit for frequency range that pass the null hypothesis test

The acquired spectra may be rejected for a variety of reasons, including fluctuations in resonance frequency, temperature changes, anomalous gain in amplifiers, and transient problems. The experiment slow-control system will be used for detecting and fixing long-standing issues, but will not guarantee that all data will be unaffected by temporary issues. Local and temporary issues such as electromagnetic interference may also lead to some bins of an acquired spectrum being affected. For all these reasons, it will be important to define a strategy to identify and mitigate the contribution of these effects.

A standard approach to extract power spectrum residuals is to use a digital Savitzky-Golay (SG) filter. This filter is a polynomial generalization of a moving average which utilizes two parameters, W and d. It works by fitting a least-squares d-degree polynomial in a W-wide window for each value, x0, of the spectrum. This method is equivalent to a filter with a flat passband and mediocre stop-band attenuation [268]. This works only if the cavity width is much larger than the intrinsic axion width, while for FLASH frequencies we expect large cavity quality-factors, about 5×10^5. We will instead follow the approach described in Ref. [67]. The power spectrum will be first described only by a ratio of first order polynomials or by means of a cavity equivalent-circuit. A null-hypothesis test will be performed at this stage on the χ^2 of the fit. Runs failing this test will be subject to rescan to collect more statistics at specific frequencies, otherwise the fit residuals will be calculated. Given the short duration of data-taking run at different frequencies, 5 or 10 minutes, we do not expect large variations in the operational parameters during the run. The grand spectrum will be built by statistically combining the residuals from different runs in larger frequency-bins of about 100 Hz, corresponding to a virialized axion-width. Frequency bins with fluctuations above

3σ will be subject to re-scan. This corresponds to an expected fraction of the frequency bins of about 0.135% or to a 6% re-scan probability of the run. In case the null-hypothesis test is passed, an upper limit will be calculated. The power spectrum will be now described as the sum of our cavity model and the axion signal, described by the standard halo model for dark matter. The coupling $g_{a\gamma\gamma}(m_a)$ will be determined by a fit to each power spectrum for different of values of the axion mass m_a. The couplings from different spectra fits are combined statistically according to the errors determined from the minimization procedure. Contrary to the S-G method, this fit procedure guarantees an efficiency close to one for the signal extraction.

The large amount of spectra needed to detect a fluctuation larger than the baseline at a specific confidence level necessitates the development of a strategy for data storage and processing. About 150000 frequency steps are foreseen to cover the whole frequency range accessible to FLASH. In each step an average of 45000 spectra will be collected, resulting in a total of about 10^{10} single spectra. The size of a single spectrum is determined by the digitizer. For a spectrum of 5 kHz total width a digitization factor of 10 is necessary in order to identify axions conversion structures. Based on this, a single spectrum would consist of 8 kb assuming that the ADC is 16 bits. The total amount of data will be more than 10 TB. In addition, for each step, ancillary data will be collected. For the FFT calculation there are several solutions available beside a commercial one. One alternative is using a fast dedicated digitizer, as it would provide more information on the spectrum and enable FFT and filters to be applied at software level. An online pre-processing during data acquisition, utilizing the RAM of the computer as a temporary buffer, will compute, the average of the single spectra to obtain the baseline spectrum, needed to trigger the re-scan procedure, and it will include other steps of the proposed analysis, such as an algorithm for identifying problematic bins. If the time required to transition between two steps of the procedure is enough to accommodate the online processing, then this should be feasible. If this is not the case, the process can be parallelized so that the processing of step N-1 can be completed while data is acquired for step N. For more complex processing, such as a Fourier Transform in software, the use of a Graphics Processing Unit (GPU) may be beneficial in order to enable fast, real-time processing without putting back pressure on the digitizer. Another option is to use an FPGA for digitization and online FFT calculation.

9.2 High-frequency gravitational waves

Signals emerging from the conversion of GWs from compact mergers and other coherent sources are expected to have a limited duration in a resonant mode, which means that the integration time for the signal in a resonant mode could not be increased above τ, as defined in Sec. 4.5. Simultaneous data acquisition from different solenoidal normal modes of the cavity, with independent antennas and amplification circuits, would be of great importance for GW detection.

Due to the spin-2 nature of GWs, different normal modes of the cavity have different couplings to the direction of the incoming wave [235], so that multiple normal modes are required to improve the directional sensitivity pattern of the detector, while also allowing some constraints on the location of the source in the sky even with a single cavity [9]. Most importantly, collecting data from multiple normal modes with different frequencies would also help improving the sensitivity and reach of the detector.

In fact, suppose the contribution to the power spectrum of the signal in different normal modes to be about equal and the thermal noise in different amplification circuits to be uncorrelated. Under these premises, the SNR of the detector is expected to scale at least as $\sim \sqrt{M}$ where M is the number of measured modes that effectively couple with the gravitational wave signal. In realistic situations, mode mixing and lower coupling of some modes, especially ones of higher frequencies,

[9] Particularly interesting for directionality would be the use of a cubic cavity [269]

might dampen this scaling. In principle, for signals with $N_{\rm cyc} \gtrsim 1$ a study in terms of Fourier spectrum, wavelets or time series could be implemented (44). A jump in sensitivity of several orders of magnitude will require to exploit the correlations of signals from many modes or cavities, as discussed in Ref. [99] and [270]. The correlations would have to be compared with a model and the likelihood maximized in order to estimate the physical parameters of the source. For related in-depth discussions see Refs. [219, 271, 272]. Note, that the GWs from mergers can couple with different normal modes at different times as the frequency evolves, which means that time discrepancies should be taken into account when exploiting the correlations for sufficiently long signals. The time between the detectable signals in the bandwidth of two different normal modes with $\nu_1 < \nu_2$ could be estimated as [219]

$$t_{\rm tr} \simeq 1.02 \times 10^{-8}\,{\rm s} \left(\frac{\mathcal{M}_{\rm c}}{10^{-5}\,M_\odot}\right)^{-\frac{5}{3}} \left(\frac{\nu_1}{200\ {\rm MHz}}\right)^{-\frac{8}{3}} \left[1 - \left(\frac{\nu_1}{\nu_2}\right)^{\frac{8}{3}}\right] \tag{45}$$

where $\mathcal{M}_{\rm c}$ is the chirp mass. The correlation method could also be applied to the search for stochastic signals, although the expected characteristic strain from a predicted stochastic GWs background would be orders of magnitude lower than the sensitivity of FLASH.

The small power of the induced signal in the cavity and the resulting low SNR make the noise modeling and auxiliary data collection for detector monitoring extremely valuable for either a time series or spectrum analysis or in the correlations method. Multiplexing of more cavities or correlations with other independent detectors could also be implemented in the future to improve both SNR and source localization.

Part III
Project Organization

10 Technology Readiness Level

Table 8: R&D forseen during the FLASH-TDR phase.

R&D	Description	Initial TRL	Final TRL
RF Cavity	500 MHz cavity prototype	TRL4	TRL7
Superconductive Cavity	Feasibility of a FLASH SC cavity	TRL4	TRL5
SQUID Amplifier	MSA at 2 and 4 K and B field	TRL6	TRL9
SQUID Amplifier	Signal Multiplexing	TRL3	TRL7
DAQ	Test of the full amplification and DAQ chain	TRL4	TRL9
Computing	Validation of the Cloud Computing model	TRL7	TRL9

A series of studies will be necessary to bring the technologies described in the previous sections to the level of maturity needed by the experiment. These R&D's are listed in Tab. 8 together with their starting and final TRL [10], and described in the following sections.

10.1 RF Cavity

A scaled prototype of the FLASH cavity is a device that reproduces the geometry and the mechanical system (junction, tuning, probe position) of the cavity in a reduced scale. All main dimensions will be reduced by a factor 5 and the frequency of the operating TM0101 mode and of all other mode will increase by the same factor 5 to about 500 MHz. The prototype will allow to:

- Verify, in scale, the mechanical system including the tuning system and mechanics;
- Check the frequency of the working mode and its quality factor
- Check the range of tunability and the quality factor of the working mode as a function of the tuning position;
- Check eventual cross talk with other modes and degeneration as a function of the tuning position;
- Perform cooling down measurements verifying the working mode quality factor improvement and tunability;
- Verify the RF contact quality at room temperature and at low temperature;
- Verify the antenna coupling to the target modes

[10] TRL1 - basic principles observed; TRL2 - technology concept formulated; TRL3 - experimental proof of concept; TRL4 - technology validated in lab; TRL5 - technology validated in relevant environment (industrially relevant environment in the case of key enabling technologies); TRL6 - technology demonstrated in relevant environment (industrially relevant environment in the case of key enabling technologies); TRL7 - system prototype demonstration in operational environment; TRL8 - system complete and qualified; TRL9 - actual system proven in operational environment (competitive manufacturing in the case of key enabling technologies; or in space).

- Investigate the impact of mechanical vibrations on frequency stability

The cavity prototype will be fabricated in OFHC copper at the University of Bonn and tested in a LHe cryostat at LNF.

The feasibility of using superconducting cavities will be studied in synergy with the INFN project SAMARA/SuperMAD in CSN5. In particular, within the SAMARA project a small 7 GHz Cu cavity was sputtered with NbTi showing a quality factor of about 1×10^6 at 4 K in a 1 T magnetic field [125], corresponding to a surface resistance $R_s = 0.3m\Omega$ that is expected to decrease by more than one order of magnitude at a frequency around 100 MHz since $R_s \sim \omega^2$ for superconductors [273]. With a cryostat temperature at 1.9 K, assuming a conservative unloaded quality factor $Q_0 = 2 \times 10^6$ and increasing the coupling to the cavity to $\beta = 3$ to keep the loaded quality factor $Q_L \sim 500,000$, the sensitivity to the axion-photon coupling would reach $G_{a\gamma\gamma} \sim 4 \times 10^{-7}$ GeV^{-1} at 110 MHz well below the DFSZ level.

10.2 Microstrip SQUID Amplifier

The MSA amplifiers discussed in Sec. 8.1 are commercially available (from ezSQUID, http://www.ez-squid.de/Company.htm) and have been successfully used in the past in the axion experiment ADMX [34]. During this development, MSA amplifiers will be operated and characterized in an operational environment as close as possible to the FLASH one. The study will be finalized to:

- Measure Gain and bandwidth for both narrow and large bandwidth amplifiers.
- Measure noise as a function of bath temperature.
- Verify that MSA Squid can cover the range of frequencies of interest. Determine if more MSA squids are needed to cover the full range. Understand if MSA squid can be used in parallel for signal multiplexing.
- Optimize the squid matching to the resonant cavity
- Test of the shielding of the squid in a 1.1 T magnetic field

Important outputs of this study will be:

- Understanding if the the MSA must be cooled to 300 mK or kept at cryostat temperature
- Understanding how far from the cavity the MSA must be located and the degree of B-shielding needed
- Understanding if any matching circuit is needed to couple the MSA to the cavity

10.2.1 Measure Gain and bandwidth for both narrow and large bandwidth amplifiers; Tunability - TIFPA/Trento

Gain, noise, bandwidth and tunability of different types of MSA will be measured first by the TIFPA/Trento team that has long experience in SQUID devices. The amplifier stability will be investigated when coupled to a high Q resonator, and cold damping network considered for its stabilization [274].

10.2.2 Test of a shielded squid in a 1.1 T magnetic field - UniCam

The UniCam group will do the tests in magnetic field. First, a shield made by different layers of cryogenic high permeability metal, such as CryoPhi, and superconductig material will be designed by consulting the companies that sell these products and purchased. The shielded MSA will then be tested at the University of Camerino in a cryostat reaching 1.5 K and equipped with superconducting magnets generating a tunable magnetic field up to 12 T.

10.2.3 Multiplexing of signal from a single antenna to multiple SQUID; Optimization of squid matching to the resonant cavity; Calibration source - Pisa

The standard data acquisition process of the experiment relies on the detection of the primary TM010 mode for the identification of photons originating from axion conversion. However, it has been observed that for the detection of high-frequency gravitational waves or for other research (such as investigating chameleons), a portion of the information is included within other resonant modes. A critical component for acquiring multiple resonant modes while limiting the number of antennas, thereby avoiding a reduction in signal power within the cavity, is the capability to read a multiplexed signal from the same antenna coupled to the cavity through various narrowband MSA amplifiers. Naturally, the coupling coefficient to different modes for a single antenna optimized for the axion mode will vary, but the optimal geometry and impedance matching between the SQUIDs will be a subject of R&D. Alternatively, the use of a broadband MSA could be considered to simultaneously acquire multiple resonant modes, although it will be necessary to evaluate the noise introduced by this solution.

The Pisa unit will focus on studying the optimal solution for acquiring multiple frequencies without affecting the low-noise reading of the primary mode for axion research. A possible solution is to use multiple MSA amplifiers resonating at different frequencies, in parallel. Something similar has been done for JPA amplifiers for axion searches [275].

In addition, the Pisa unit will define a calibration procedure based on both external sources capable of injecting the required signals into the cavity and broadband/thermal sources (e.g., calibrated black bodies) that directly produce calibrated signals reaching the amplifier. A full test of the calibration, amplification and acquisition of the signal, including multimode acquisition, will be done, at cryogenic temperatures, using a BAW resonators with modes above 100 MHz. This will also allow evaluating the effect of poor thermalizations and reflections on the resonator, as well as the stability of the amplifier and the multiplexing of different modes.

10.3 DAQ

Both commercial solutions (such as commercial fast FFT or a commercial digitizer) and custom made solution based on RFSoc FPGA with high-end digitizer on board, will be considered. This task will be done in synergy with INFN project QubIT/Quartet and QUAX@LNF and the MiB project BAUSCIA.

10.4 Computing model

A computing model analogous to the one foreseen for FLASH is now under testing and development at LNF for the QUAX experiment and it will be ready before the start of the experiment. In the following we give a brief description of it. From the DAQ setup to the Cloud infrastructure the data flow will be quite linear. First of all, data will be directly stored in local disk space (2TB HDD). Then data will be sent to the INFN-Cloud block storage service. Metadata will be collected in a MariaDB DataBase cloud service. Data and metadata will be sent from the local storage to a long term storage solution, the TAPE. These data management operations will be managed via

RUCIO software.
Metadata present inside the MariaDB will be showed and monitored via the Grafana web service. This application will send alert and warnings if some of the parameters do not correspond to the expected configuration. Data will be exposed over the private FLASH Cloud network via a Network File System (NFS) service. This scenario will allow users to analyse data directly from a Jupyter notebook (with its own web interface) configured with the necessary packages (ROOT, python, useful libraries..) deployed in the Cloud.
Furthermore, in order to reconstruct data an HTCondor service accessible via Jupyter notebook will be deployed, together as a Kafka service to perform event streaming and a sentinel process to execute data reconstruction.
All the Cloud services will be deployed through Docker containerization, which allow flexibility, scalability and reliability. On the other hand, due to this implementation method, to manage all the container a Kubernetes cluster will be necessary.
Furthermore, documentation web pages will be created to share experiment documentation from both the point of view of algorithms (GitHub) and meeting notes, updates, "how to" and others general information (INFN Confluence).
With a sampling rate of ∼10 kSample/s, a 4 s sample length, and two 16 bits words for quadratures I and Q, a single file size of about 160 kB is expected per acquired mode. Considering a data acquisition period of ∼6 months/year, this means a throughput of about ∼0.5 TB/year per acquired mode and 5 TB/year assuming 10 modes.

11 Safety and Radioprotection

11.1 Functional requirements

Experience in the construction and operation of the FINUDA experiment shows that residual risks and safety issues related to the operation of the detector are limited. In accordance with experience, the main objective of the FLASH Collaboration is to ensure that all operations are carried out in accordance with regulatory requirements and safety and environmental regulations designed to ensure the health of personnel, respect for the environment, and the integrity and preservation of equipment. To accomplish this goal, we must ensure our ES&H program identifies, addresses, and manages safety, environmental hazards during the design, construction, assembly, commissioning, and operation of the FLASH experiment.

11.2 Risk Analysis

In accordance with best practices in the field of prevention with the TDR we will provide a development of a Risk Analysis (RA) that considers the Health, Safety, and Environmental risks associated with FLASH Experiment. From this risk analysis, the following will be highlighted: – Identification and analysis of incident risks and/or undesired events (Top Events) and prevention methods using internationally recognized Industrial Risk Assessment standards (HazOp, FMEA, Fault Tree Analysis, Event Tree Analysis) through the following steps:

- Detailed description of possible incident scenarios and their likelihood of occurrence
- Evaluation of the extent and severity of the consequences of any identified incidents
- Historical review of FINUDA technical parameters, considering lessons learned
- Description of technical parameters and equipment used to ensure facility safety

– Assessment of environmental risks (if any)
– ElectroMagnetic Fields (EMF) Exposure
– Provisions needed for Pressure Equipment:

- PED Directive 2014/68/EU, (Legislative Decree No. 26/2016), while commissioning and operation of pressure equipment must comply with DM 329/2004.
- Transportable pressure equipment (if any) must comply with the TPED Directive 2010/35/EU (Legislative Decree No. 78/2012).

– Any requirements related to fire prevention

11.3 Decommissioning, Assembly & Commissioning

The disassembly operations will be mirror images of those performed during the construction of the detector, using, where necessary, the same tools used at the time, which have been kept at the LNF (see FINUDA Technical Report LNF-95/024 (IR), in particular Sections 3 and 9). For operations of decommissioning (FINUDA), assembly and at the commissioning of the detector in its various phases the Consolidated Occupational Health and Safety Act Legislative Decree No. 81 of April 9, 2008 (as amended), must be applied. If necessary, the obligations under Title IV for temporary and mobile construction sites will be applied.

11.4 Technical Compliance

An assessment of the regulatory compliance of FINUDA's existing facilities with current legislative requirements will be conducted. In particular, the adequacy and updating of existing facilities, installations, and experimental devices will be checked for worker health and safety and experiment safety. Where necessary, systems will be upgraded.

11.5 Waste Management

The management of waste materials from the decommissioning of FINUDA and the construction of the FLASH detector will take place in accordance with current regulations (Consolidated Environmental Act (Legislative Decree 152/2006 as amended) in particular " Parte IV: Norme in materia di Gestione dei Rifiuti e bonifica dei siti inquinate". Emphasis will be given to management that considers the waste hierarchy, that is, the set of priorities for the efficient use of resources. Waste prevention and reuse are the preferred options, followed by recycling (including composting) and energy recovery, while landfilling of waste should be the last option.

11.6 Radioprotection

LNF in accordance with the Regulations, Legislative Decree 101/2020 (implementing 2013/59/Euratom in Italy), have appointed a Radiation Protection Expert (EQ) to assess individual activities.

For the FLASH experiment, there are no risks related to Radiation Protection.

12 Management

The FLASH-TDR project is organized in 7 work packages (WP) (Fig. 28 and Tab. 9). As discussed in Sec. 10, none of the WP's requires the development of new technologies, but rather the engineering of existing ones.

The objective of WP1 'Physics Reach' is the theoretical computations and the exploration of new physics theories to maximize the potential of the FLASH experiment and its future extensions.

Year	2024	2025				2026	
Quarter	IV	I	II	III	IV	I	II
WP1 - Physics Reach		Modes & Frequencies				TDR Section on Physics Reach	
WP2 - Mechanical Design and Cryogenics	Envelope volume for RF cavity		Define MSA Position in Cryostat and Probe	Prototype Mechanical Design		Cryostat Design	TDR section on Mechanical Design
WP3 - RF Cavity			Cavity RF Design	Prototype RF Design	Fabrication of Cavity Prototype	Cryogenic Test of Cavity Protoype	TDR Section on RF Cavity
WP4 - Amplification and Acquisition		Gain and Noise Characterization of MSA	Test of Shielding in Magnetic Field	DAQ	Multiplexing Prototype Circuit	Full Chain Test with BAW resonator	TDR Section on Amplification & DAQ
WP5 - Data Analysis and Computing					Computing Cloud Model validated	TDR Section on Analysis & Computing	
WP6 - Decommissioning & Commissioning				Tools for FINUDA Decommissioning		TDR Section on Decommissioning &	
WP7 - Management	Periodic Meeting	Periodic Meeting	Periodic Meeting	Periodic Meeting	Periodic Meeting	TDR writing	Technical Design Report

Figure 28: Gantt for the FLASH-TDR preparation.

It sees the participation of several theorists from different institutes (INFN, Pisa University, IFAE-ICREA, TDLI Shangai and University of Saragoza) experts in the field of ALPS and HFGW. They will model the signals, define the modes and frequencies of interest and provide the formula to correctly compute the coupling factors and the sensitivities.

The objective of WP2 'Mechanical Design and Cryogenics' is the design of the FLASH cryostat together with all its components. This will be done by INFN engineers in collaboration with the LNF Service of Mechanical Engineering of the Research Division and with the consultancy of the Cryogenic Group of the Engineering and Mechanical Support Section at CERN.

The objective of WP3 'RF Cavity' is the RF design of the FLASH resonant cavity together with all its components. This will require simulation studies done by LNF, the Universitat de València (UV) and the Universidad Politécnica de Cartagena (UPCT), the fabrication of a 500 MHz cavity prototype, done at the University of Bonn, and the final test in LHe, done at LNF.

The objective of WP4 'Signal Amplification and Acquisition' is to characterize SMA amplifiers in terms of gain, bandwidth and noise down to temperatures of the order of 300 mK and then operate them in conditions similar to those in FLASH as far as concerns operating temperature, ambient magnetic field and resonating input load. It also includes the digitization and acquisition of the signal, and the definition of the calibration procedure. Most of the R&D discussed in Sec. 10 are carried out in this WP that sees the participation of Trento-TIFPA, Pisa University and INFN, University of Camerino and LNF.

The objective of WP5 'Data Analysis and Computing' is to develop a dedicated analysis strategy for axion like particles and High Frequency Gravitational Waves as well as setup and validate an internationally distributed computing infrastructure.

The objective of WP6 'FINUDA Decommissioning and FLASH Commissioning' is to define the tools and procedures, including the safety procedures, for decommissioning the FINUDA detector and commissioning the FLASH experiment, the required certifications and infrastructure services.

12.1 **WP1 Physics Reach**

Participants: LNF, Pisa, Shanghai, Saragoza
Coordinators: Federico Mescia (LNF) and Luca Visinelli (Shanghai)
WP objective: The objective of this WP is either on theoretical computations and the exploration of new physics theories to maximize the potential of the FLASH experiment and its future

Table 9: WPs

WP1	Physics Reach
WP2	Mechanical Design and cryogenics
WP3	RF Cavity
WP4	Signal Amplification and Acquisition
WP5	Data Analysis and Computing
WP6	FINUDA Decommissioning and FLASH Commissioning
WP7	Project Management

extensions. This task would be significant, requiring theoretical, phenomenological and analytical expertise to identify viable probes as well as to find innovative techniques to detect them.
Activity description:
Task 1.1: New Models
Explore new physics models (e.g. the Majoron [276]) and identify modes and frequencies of interest.
Task 1.2: Axion/Scalars/Pseudoscalars/Vector
Compute couplings to cavity modes. Improve sensitivity to scalars (modify magnetic field homogeneity etc.)
Task 1.3: Chameleons
Improve theoretical calculations about their production and detection.
Task 1.4: HFGW
Compute couplings to cavity modes. Calculation of transients. Models for signals. Time domain analysis. Multi-mode analysis. Multi cavity analysis.
Task 1.5: BAW
Review the sensitivity of BAW to scalars, axions and HFGW to extend the FLASH physics case.
Task 1.6: Future applications
Review and improve earlier studies to FLASH physics case and future applications of FLASH infrastructure.

12.2 WP2 Mechanical design and cryogenics

Participants: LNF (with the consultancy of CERN),
Coordinator: Carlo Ligi (LNF)
WP objective: Design the FLASH cryostat together with all its components (cryogenic turret, transfer line, cavity etc.), integrating it with the existing cryogenic plant. The cryostat must fit the FINUDA magnet bore and must be supported by the FINUDA mechanical structure. The cryogenic plant must be refurbished with a new control system and a general maintenance and a re-certification for pressure equipment directive (PED) must be carried out.
Activity description:
Task 2.1: Cryostat Design
The RF cavity cryostat must be designed, taking into account:
- the decision about the cavity working temperature,
- the mechanical constraints due to the fitting inside the FINUDA magnet,
- the available cooling capacity of the cryogenic plant,
- the need for a cryogenic turret, to be placed outside of the magnet bore but close to it as possible,
- the possible insertion of a small 300mK He evaporation cryostat that host the SQUID, if needed,

Task 2.2: Cryogenics control systems
A list of all the signals coming from the FINUDA magnet must be compiled and an upgrade of the actual control system must be done, starting from the present Labview version of the software. Taking in account the signal list, the best solution for a new PLC hardware should be found, one of the best option being a CompactRIO system from NI.
A similar control system must be designed for the cryogenic signals coming from the FLASH cryostat.
A new control system should be considered for the LINDE cryogenic plant, the present one being operating but very old, working from 1996.
Task 2.3: Cryogenic Transfer Line VB-FINUDA
A new transfer line as a connection between the Valve Box and the FLASH cryostat must be designed before being procured. The design must simply replicate the one of the old Valve box-KLOE transfer line.
Task 2.4: FINUDA B field measurement
The magnetic field of the FINUDA magnet must be mapped in all the bore volume. It can either be taken from old measurement from the FINUDA experiment documentation or measured with a dedicated tool and a tri-axial Hall probe.
Task 2.5: Simulation of mechanical resonances on the cavity
The cavity, together with its tuning system, can be subjected to mechanical vibrations due both to external mechanical sources and to the Helium flow inside the pipes. These vibrations can excite resonant modes and become source of instability of its natural frequencies, causing loss of acquired data. A study on the mechanical resonances of the cavity must be performed, in order to found solutions that can minimize this effect.
Task 2.6: preliminary study about a 100mK operating temperature of the cavity
The cavity sensitivity is inversely proportional to its temperature, so we are thinking to a possible upgrade of the cooling system in order to go to sub-Kelvin temperatures. It is actually a challenging scenario in which a (set of) dilution refrigerator(s) can manage the cavity cooling. In this case, some more space for the fridges and for a shield at T about 1K must be considered, so the cavity will be smaller with respect to the present proposal. A detailed study about all the possible thermal inputs to the cavity must be performed, to understand the feasibility of this work and to give an idea about the number of the needed fridges.

12.3 WP3 RF Cavity

Participants: LNF, Universitat de València (UV), Universidad Politécnica de Cartagena (UPCT), University of Bonn
Coordinator: Alejandro Diaz (UPCT), Simone Tocci (LNF) WP objective: The objective of this WP is to do the RF design of the resonant cavity, the tuning and coupling system, considering all the EM modes of interest and the frequency range needed to reach the physics goals defined in WP1, and the estimate/calculation of the cavity expected parameters (Q,V) and couplings for all the physics models of interest.
Task 3.1: Cavity RF design
RF design of a cavity with modes and frequency ranges identified in WP1 "Physics Reach". Study the impact on cavity modes, in particular TE modes, of the solutions found in WP2 "Mechanical Design and cryogenics" to minimize the impact of magnet quenches on the cavity.
Task 3.2: Antenna couplings
Design the pick up antenna needed to couple to the modes identified in WP1 "Physics Reach". The antenna should guarantee overcoupling $\beta \geq 2$ over all the range of frequencies of interest and for all the modes of interest (possibly at the same time). Choose between dipole or loop antenna

based also on the mechanical realization (WP2), the signal amplification (WP4) and considering the effect of vibrations and vibrations inside 1T magnetic field.

Task 3.3: Tuning System

Design a system able to tune the frequency of the modes of interest. The design should be optimized to guarantee the minimum step tunability but at the same time to be insensitive to system vibrations as studied in WP2 "Mechanical Design and cryogenics". The tuning system should also be able to remove the avoid-crossings. We will consider fine tuning mechanisms both for solving vibrations and avoid-crossing problems.

Task 3.4: RF Components at 100 MHz

Identify the RF components commercially available to realize the RF setup. This includes the ancillary lines and component needed for the system calibration studied in WP4 "Signal Amplification and Acquisition"

Task 3.5: Cavity Prototype

Design, fabrication and test at cryogenic temperatures of a smaller cavity prototype resonating at about 500 MHz. The mechanical workshop in Bonn have long lasting expertise on the construction of electromagnetic cavities in the context of the ELSA accelerator. Hence, prototype cavities as well as parts of the final experiments will be constructed there. For the fabrication of the final cavity, given the large surface, the surface polishing methods will need to be investigated.

12.4 WP4 Signal Amplification and Acquisition

Participants: TIFPA/Trento, Pisa, Camerino, LNF, Bonn/Mainz
Coordinator: Paolo Falferi (MSA) (TIFPA/Trento), Gianluca Lamanna (Amplification/DAQ) (Pisa) WP Objective: The objective of this WP is to acquire some complete commercial MSA amplification systems, characterize them in terms of gain, bandwidth and noise down to temperatures of the order of 300 mK and then operate them in conditions similar to those in FLASH as far as concerns operating temperature, ambient magnetic field and resonating input load. It also includes the digitization and acquisition of the signal, and the definition of the calibration procedure.

Activity description

Task 4.1: MSA configurations

Different MSA configurations will be considered and possibly tested: MSA with varactor diode for the tuning of its resonance frequency, MSA with lower resonance Q for a wider bandwidth, two cascaded MSA tuned to different resonant frequencies for a wider bandwidth. Gain, noise and bandwidth measurements will be carried out as a function of the operating temperature down to ultracryogenic temperatures. For a complete characterization of the noise, tests will be conducted with resonant loads at the input of the MSA.

Task 4.2: Stability

High Q loads at the input of the MSA can lead to system instability. Cold damping networks will therefore be considered and possibly applied for the stabilization of the cavity/MSA system.

Task 4.3: Postamplifier

If the MSA gain is not high enough to allow the use of a room temperature amplifier as postamplifier, low noise cryo amps capable of operating at 4K will be identified and tested.

Task 4.4: Magnetic shielding

The MSA should operate in an environment with a low magnetic field (possibly $<<$ Gauss) and low vibrations so that the flux noise collected by the MSA SQUID loop remains $<< \Phi_0$. In FLASH, where the magnetic field reaches 1.1 T, this condition can be satisfied by appropriately shielding the magnetic field around the MSA and/or by moving the MSA sufficiently away. To evaluate whether this is possible, superconductor/cryoperm composite magnetic shields will be realized and

tested and in the design of the FLASH cryostat we will try to identify areas with a low residual magnetic field where the MSA can be safely housed. Tests of the shielded MSA in a 1.1 T magnetic field will be done.

Task 4.5: Multiplexing

The possibility of operating two or more MSAs connected to the same antenna will be evaluated to simultaneously detect higher harmonics of the cavity but avoiding the MSAs interfering with each other.

Task 4.6: Replacement of the MSA

In defining the design of the FLASH cryostat and with prototype tests, the possibility of replacing the MSA without warming up the entire FLASH cryostat to room temperature will be evaluated. In this way it would be possible to cover the entire range of FLASH operating frequencies using some "bayonet design" MSAs optimized to operate on reduced frequency bandwidth.

Task 4.7: Secondary amplification and down conversion chain

The RF amplification at room temperature will depend on the gain obtained in the cold stage and on the requirements of the digitization stage. Considering the non exceedingly high operating frequency (hundreds of MHz), the need for a potential down-conversion stage will be evaluated, based on noise control and acquisition bandwidth considerations.

Task 4.8: Digitization and data acquisition

The Digitization and data acquisition stage will be defined according to the previous stage requirements. In addition both commercial solutions (such as commercial fast FFT or a commercial digitizer) and custom made solution based on RFSoc FPGA with high-end digitizer on board, will be considered. The second solution, although more complex, will offer greater flexibility and the possibility of applying data reduction and control algorithms directly in real-time.

Task 4.9: Full test of amplification chain with a BAW resonator

Test of amplification and DAQ chain with a 100 MHz mode of a BAW in a cryogenic system to simulate the presence of the FLASH cavity. A full calibration procedure as in the real experiment will be implemented by measuring scattering parameters through ancillary lines and by means of calibrated thermal sources.

12.5 WP5 Data Analysis and Computing

Participants: LNF, University of Bonn and Mainz, Pisa

Coordinator: M. Schott (Uni. Bonn) and K. Schmieden (Uni. Mainz) WP objective: The objective of this WP is to develop a dedicated analysis strategy for axion like particles and High Frequency Gravitational Waves as well as setup an internationally distributed computing infrastructure.

Task 5.1: Searching for Axion Like Particles

Beside the baseline analysis described in Sec. 9, a more modern approach of the data analysis will be develop in parallel, employing graph-based or convolutional neural networks. Since the expected signal shape can be simulated to high accuracy and sufficient background data can be easily recorded, the training of a neural network based classifier systems suggests to yield optimal results. To our knowledge, such an analysis approach has not yet been implemented in the context of cavity-based ALPs searches, thus its final performance cannot be reliably estimated at this stage.

Task 5.2: Searching for High Frequency Gravitational Waves

The development of analysis techniques in the context of HFGW is significant more challenging for several reasons: First, the signal characteristics of HFGW sources inhibits strong model dependencies, second the time-dependence of the HFGW frequency needs to be considered, as it yields only relatively short integration times. Thirdly, the expected signal is rather rare, i.e. not more than a few per year. Lastly, the signal search at FLASH needs to be correlated to the recorded

data-sets of other operating cavities at other laboratories within the GravNet initiative. The baseline analysis technique will be based on a similar approach as discussed for the axion-like particle searchers. However, in parallel it is envisioned to implement a HFGW search based transformer neural networks, as they are optimally suited for time-series analysis.
Task 5.3: Computing Infrastructure
The computing model developed for the QUAX experiment will be used for FLASH. Moreover, the data transfered to the INFN computing cloud will be mirrored at the data-center of the University of Bonn, allowing for two redundant analysis facilities.
Task 5.4: Run Automation
Design and requirements for run automation, including calibration and tuning.

12.6 **WP6 FINUDA Decommissioning and FLASH Commissioning**

participants: LNF
Coordinator: Stefano Gazzana (LNF) WP objective: The objective of this WP is to define the tools and procedures, including the safety procedures, for decommissioning the FINUDA detector and commissioning the FLASH experiment, the required certifications and infrastructure services.
Task 6.1:FINUDA decommissioning
Definition of requirements and procedures
Task 6.2:FLASH commissioning
Definition of requirements and procedures
Task 6.3:Infrastructure services
Definition of requirements
Task 6.4:Safety and Radioprotection
This task will be addressed as described in Sec. 11

12.7 Participants

12.7.1 **LNF**

The LNF team, an assembly of physicists and engineers skilled in the design, commissioning, and operation of particle physics experiments at LNF, such as KLOE, FINUDA, PADME, and QUAX@LNF, will spearhead the project under the coordination of Claudio Gatti. The team will oversee WP2 "Mechanical design and Cryogenics" led by C Ligi, and WP6 "FINUDA Decommissioning and FLASH Commissioning" directed by S Gazzana. Their contributions will encompass:
• WP2: Collaborating on mechanical designs with the LNF Service of Mechanical Engineering of the Research Division.
• WP2: Innovating a new magnet control system.
• WP3: Engineering the RF design of the cavity prototype, including tuning and coupling, and selecting the RF components; also conducting tests in an LHe cryostat.
• WP4: Evaluating the amplification and acquisition chain in magnetic field with the Camerino group, determining the optimal magnetic field shield, and developing the FPGA firmware for DAQ.
• WP5: Formulating a data analysis strategy based on QUAX insights and advancing the computing infrastructure within the INFN cloud.
• WP6: Establishing commissioning and decommissioning procedures, including safety protocols, and setting the requirements for infrastructure services.
• WP1: Additionally, researchers associated to the LNF Theory Group, comprising Federico Mescia, Giovanni Grilli di Cortona, Momchil Naydenov, and Enrico Nardi, will contribute to the Physics Reach studies in WP1.

R&D activities will be done at the CryOgenic Laboratory for Detectors (COLD) at LNF (https://coldlab.lnf.infn.it). Here projects on superconducting circuits as well as the QUAX@LNF experiment are ongoing. The COLD group sees the participation of young physicists and engineers (A. Rettaroli, S. Tocci, A. D'Elia, A. Piedju and A.Calanca) now dedicated to projects on external funds (PRIN, PNRR, etc.). S. Tocci, responsible for the RF design of the COLD lab, realized the design of the cavity and tuning system and performed the ANSYS HFSS simulations reported in the KLASH [258] and FLASH [102] papers. A. D'Elia and A. Rettaroli, responsibles for measurements, data taking and analysis of the COLD lab, estimated the sensitivity to axions and dark photons and realized the discovery plots as well as contributed in writing the KLASH [258] and FLASH [102] papers. A. Calanca is working on the COLD computing infrastructures and is responsible for the COLD computing infrastructure for QUAX@LNF. A. Piedju is responsible for superconducting devices design of the COLD lab and supports S. Tocci in the electromagnetic simulations of RF cavities.

Table 10: LNF Team. The people who appear at zero time are currently engaged in external projects (PNRR, H2020 etc.) but have committed to increasing participation as soon as possible. In some cases the activity carried out can be considered synergistic with that of FLASH.

Name		FTE 2025	FTE 2026
Claudio Gatti (RN)	Ric I	30%	50%
Carlo Ligi	Tec II	40%	40%
Stefano Gazzana	Tec II	20%	20%
Giampiero Di Pirro	Tec II	20%	20%
Vannozzi Alessandro	Tec II	10%	10%
Ciambrone Paolo	Tec I	20%	20%
Fabio Bossi	Ric I	40%	40%
Danilo Babusci	Ric II	30%	30%
Paola Gianotti	Ric I	20%	20%
Daniele Di Gioacchino	Ric II	30%	30%
Luca Piersanti	Ric III	0%	20%
Matteo Beretta	Ric II	0%	20%
Giovanni Mazzitelli	Ric II	0%	20%
Sandro Tomassini	Tec II	0%	20%
David Alesini	Tec I	0%	10%

Table 11: LNF Theory Group (FTE not in Preventivi).

Name		FTE 2025	FTE 2026
Federico Mescia	Ric I	30%	30%
Giovanni Grilli di Cortona	AdR	10%	10%
Momchil Naydenov	Ass. Professor	10%	10%
Enrico Nardi	Senior Ass. Scientist	10%	10%

12.7.2 **University of Camerino**

The Unicam Group consists of two researchers, a professor and one phd student contributing to the project. The lab has the possibility to perform the experimental characterization of devices with a closed cycle Helium cryostat. Magnetic response down to liquid nitrogen temperature is available. The group has a long history of precision measurement of low dimensional superconductive systems from theoretical modelling to the pre-designed structure engineering. The group already participates in the design and characterisation of specific SQUID loop for the Lunar Gravitational Wave Detector (LGWD). The group will contribute to FLASH with the characterization of the SQUID in a 1.1 T magnetic field as in the final experimental setup. The SQUID will be appropriately shielded and tested in a cryostat reaching 1.5 K and equipped with superconducting magnets generating tunable magnetic field up to 12 T. We will perform gain and noise temperature measurements of the MSA and measure the scaling of the noise with the operation frequency and temperature.

Table 12: Camerino Team

Name	position	FTE 2025	FTE 2026
Javad Rezvani (RL)	RTDb	40%	40%
Andrea Perali	PA	30%	30%
Nicola Pinto	RU	30%	30%
Benedetta Gianfelici	PhD	30%	0%

12.7.3 **Pisa University and INFN**

The Pisa group consists of theoretical physicists, experimental physicists, and electronic engineers affiliated with the Department of Information Engineering of Pisa. The experimental physicists, in particular, have experience in cryogenic measurements, noise characterization of amplifiers, and multiplexing systems. Some of them have previously worked on experiments dedicated to the search for cosmic axions or the study of cryogenic detectors. The engineers in the group are experts in cryogenic measurements and low-temperature noise studies, 3D and 2D electromagnetic design of microwave circuits and structures, and low-noise acquisition systems based on FPGA. Together, the physicists and engineers will address the problem of using MSA SQUIDs in a multiplexed mode, the potential secondary amplification chain, and the DAQ procedure (WP4 "Signal Amplification and Acquisition"). They will also investigate the use of the same acquisition chain for reading signals from BAW and, potentially, piezoaxionic crystals (WP4).

Theoretical physicists in the unit are interested in contributing to defining the physics reach (WP1), both concerning dark matter models and potential sources of high-frequency gravitational waves (HFGW). The Pisa unit is equipped with a dilution refrigerator (and another one in the acquisition phase), a cryostat capable of reaching a base temperature of 300 mK, a 4K cryogenic probe station, and a facility for fabricating micro- and nano-metric superconducting and semiconductor structures.

12.7.4 **TIFPA Trento**

The TIFPA group, consisting of two experimental physicists from CNR-IFN/FBK, has a long-standing experience in preparation and run of experimental activities down to mK temperatures, high Q mechanical and microwave resonators, electromechanical systems (feedback cooling, parametric squeezing), and cryoelectronics (Josephson Junctions, SQUID, JPA, TWPA). The group

Table 13: Pisa Team

Name	position	FTE 2025	FTE 2026
Gianluca Lamanna (RL)	Prof. Associato	20%	20%
Massimo Macucci	Prof. Ordinario	30%	30%
Paolo Marconcini	Prof. Associato	20%	20%
Andrea Michel	Rtdb	50%	50%
Elena Graverini	Prof. Associato	10%	10%
Paolo Spagnolo	Ric I	10%	10%
Alessandro Pitani	Ric	10%	10%
Claudio Puglia	Ric III	30%	30%
Alessandro Tredicucci	Prof. Ordinario	20%	20%

Table 14: Pisa Theory Group

Name		FTE 2025	FTE 2026
Paolo Panci	Prof. Associato	10%	10%
Giancarlo Cella	Ric II	0%	0%
Angelo Ricciardone	RTDB	0%	0%
Daniele Barducci	RTDA	10%	10%
Michael Zantedeschi	AdR	10%	10%
Giulio Marino	PhD	10%	10%

was and is involved in many national (mainly INFN) and international activities. The local cryogenics laboratory hosts a dilution refrigerator, helium liquefier and dewars, electronics and data acquisition. The group will contribute to WP4 "Signal Amplification and Acquisition" and in particular to the characterization in terms of gain, bandwidth and noise down to ultracriogenic temperatures of MSA amplification systems

Table 15: TIFPA Trento Team

Name	position	FTE 2025	FTE 2026
Paolo Falferi (RL)	FBK/CNR-IFN researcher	30%	30%
Andrea Vinante	CNR-IFN researcher	30%	30%

12.7.5 **University of Bonn and University of Mainz**

The research group of Prof. Matthias Schott [238, 277] is partially based at the University of Mainz as well as the University of Bonn. A full switch to the University of Bonn is expected in the course of the year 2025. From the University of Bonn, one professor, one postdoctoral researcher, one PhD student, two master students as well as one engineer will contribute to the search for axion-like particles, as indicated in the following Table. In addition, members of the local mechanical workshop have long lasting expertise on the construction of electromagnetic cavities in the context of the ELSA accelerator. Hence, prototype cavities as well as parts of the final experiments can be constructed locally.

Apart from the design and construction of prototype cavities, the university of Bonn aims to get involved in the design of DAQ, the subsequent data-analysis and the reinterpretation of the FLASH results in the context of High Frequency Gravitational Waves.

Table 16: Bonn/Mainz Team

Name	position	FTE 2025	FTE 2026
Matthias Schott	Professor	10%	10%
Kristof Schmieden	Senior Scientist	25%	25%
Tim Schneemann	PhD Student	50%	50%
Steffen Krieg + (N.A.)	Research Student (12 months each)	100%	100%
Philip Hänisch (t.b.c.)	Engineer	25%	25%

12.7.6 **Technical University of Cartagena (UPCT)** & **IFIC (CSIC-University of Valencia)** & **IFAE-ICREA**

The UPCT & IFIC team consists of electrical and electronic engineers and experimental physicists with experience in microwave engineering. From its beginning, the UPCT group has been focused on high-frequency high-power electromagnetic systems, with different research lines as the development of numerical methods for electrodynamics, the analysis and design of microwave heating systems, the dielectric characterization at microwave frequencies, or the design of corrugated and multi-cavity microwave filters. From 2015 and together with the IFIC (CSIC-University of Valencia) AITANA team, its main activity is devoted to the development of resonant cavities for DM axion detection, extending them in the last years to the detection of high-frequency gravitational waves. This work has been developed within the RADES group and the CADEx experiment, where the team has been responsible of the cavity and its ancillary systems (coupling, tuning) design.

UPCT counts with a vector network analyzer up to 110 GHz, different coaxial and waveguide calibration kits, different electrical and magnetic characterization devices and home-made software for reverse characterization, as well as a number of licenses of different commercial full-wave electromagnetic simulation software (CST Studio, ANSYS HFSS). IFIC AITANA team has a deep expertise in developing advanced modal techniques (as the BIRME-3D method) for the efficient and accurate calculations of complex microwave and millimeter-wave problems; these techniques have been applied to the analysis of the coupling between DM axion or HFGW and the photons excited in a cavity. From an experimental point of view, IFIC AITANA group has a microwave laboratory operating up to 20 GHz including a four-port vector network analyzer, a spectrum analyzer and other electronic equipments. In other side, IFIC is a research center devoted to research in Nuclear, Particle and Astroparticle Physics and its applications to Medical Physics and to other fields of Science and Technology. IFIC was created in 1985, and recently has been awarded with the 'evero Ochoa' accreditation.

IFAE is a worldclass institute for high energy physics. Since 2021, it counts with Prof. Diego Blas among its staff members. Prof. Blas is an ICREA Professor expert on the phenomenology of gravitational waves in microwave cavities. His work of 2021 set the stage to the first realistic investigation to search for gravitational waves with microwave cavities used for axions searches. In 2023 he expended this work to include the possibility of exploring the mechanical coupling of these signals to the cavity. Since 2022, he has been closely collaborating with the UPCT & IFIC-UV team to implement these theoretical works into realistic studies to eventually build the optimal set-up for this endeavor.

Here is a list of the most relevant papers in the last years [48, 57–59, 209, 269, 278–284].

The contribution of the team will be focused on WP3 "RF Cavity", coordinating it and developing the main tasks related with the cavity design as well as the tuning and re-coupling systems development. The objective will be to maximize the cavity figure of merit ($Q_0V^2C^2$) in the widest frequency (mass) range possible, being able to reach the target coupling (initially β=2) in the whole range. Moreover, the team will work on the use of FLASH cavity for HFGW detection. For that it will be necessary the development of new numerical methods based on BIRME 3D technique, and development of optimal techniques to look for this observable.

Table 17: UPCT, IFIC-UV,IFAE-ICREA team

Name	position	FTE 2025	FTE 2026
Alejandro Díaz-Morcillo (UPCT)	Professor	20%	20%
Juan Monzó-Cabrera (UPCT)	Professor	20%	20%
Antonio Lozano-Guerrero (UPCT)	Assoc. Professor	20%	20%
José Ramón Navarro-Madrid (UPCT)	PhD Student	20%	20%
Benito Gimeno (IFIC-UV)	Professor	20%	20%
José Reina-Valero (IFIC-UV)	PhD Student	20%	20%
Diego Blas (IFAE-ICREA)	Research Professor	20%	20%

12.7.7 **University of Liverpool**

The University of Liverpool group is willing to contribute essentially 10-20% with Paolo Beltrame. Beltrame has experience in particle physics, particularly in the direct search for dark matter, in axions, in both data analysis and Monte Carlo simulations. Further possible contributions can be explored by the University of Liverpool in terms of hardware and quantum sensors R&D.

12.7.8 **Tsung-Dao Lee Institute (TDLI), Shanghai**

At TDLI, current members include Prof. Luca Visinelli and Dr. Michael Zantedeschi. Both members belong to the theory group and plan to contribute with further insight on this behalf, in synergy with the other theoreticians involved in the projects. For this, frequent discussions have already begun with the groups belonging to INFN LNF, INFN Pisa, and the University of Zaragoza. The involvement in the project is expected to average to around 20%, with full-time commitment towards approaching deadlines.

Table 18: Shanghai Team

Name	position	FTE 2025	FTE 2026
Luca Visinelli	Associate Professor	20%	20%
Michael Zantedeschi	Postdoc	20%	20%

12.7.9 **University of Zaragoza**

The Zaragoza team is composed of physicist Maurizio Giannotti, with experience axion and other light feebly interacting particles phenomenology and astrophysics. He will contribute to the FLASH physics case, including the study of the sensitivity potential for axions, axion-like particles, dark photons, chameleons, and gravitational waves.

Table 19: Zaragoza Team

Name	position	FTE 2025	FTE 2026
Maurizio Giannotti	Professor	20%	20%

12.7.10 **Other collaborations**

ezSQUID: ez SQUID is a privately owned company developing and manufacturing superconducting magnetic field sensors (SQUIDs), their readout electronics and selected SQUID applications (http://www.ez-squid.de/Company.htm). In particular, ez SQUID produces the MSA amplifiers proposed for the first stage amplification in FLASH. Michael Mueck (ez SQUID) collaborates in FLASH, for the specification of the amplifiers, since the KLASH proposal [258].

PBC@CERN: The Technology Working Group of the Physics Beyond Collider at CERN has the mandate to explore and evaluate possible technological contributions of CERN primarily to non accelerator related experimental physics initiatives and projects **that may also be hosted elsewhere**. FLASH has been recently inserted in the list of experiments linked to this Working Group [285]. In this context, we are in contact with the Engineering and Mechanical Support Section at CERN, Cryogenics Group, Technology Dept, for technical consultancy for the cryostat design.

12.8 Synergistic projects

- QUAX: QUAX is a CSN2 experiment looking for galactic axions with mass about 40 μeV. One of the two haloscopes of the experiment is located in the COLD laboratory at LNF (https://coldlab.lnf.infn.it).
- BAUSCIA: Project in Milano Bicocca (MiB) with the objective of detecting HFGW with BAWs. Because of the strong synergies with the FLASH physics and involved technologies, the MiB team expressed a strong interest in collaborating with FLASH in the future, for searches at lower frequencies but also extending to the higher frequencies of FLASH.
- PNRR-NQSTI: The objective of the PNRR project NQSTI is the development of quantum technologies, including superconducting quantum devices. The LNF, Trento and Pisa teams are involved in this project.
- PNRR-ICSC: One of the objective of the PNRR project ICSC is to develop the infrastructure for scientific computing. The QUAX cloud computing is developed also within this project.
- Samara/SuperMad: The objective of this project in CSN5 are superconducting materials for axion cavities such as NbTi and Ybco. The LNF team is involved in this project. Solutions for sputtering the FLASH cavity with NbTi will be studied within SuperMAD if approved.
- Qubit/QUARTET: The objective of the project is developing quantum superconducting devices. The LNF, Pisa and Trento teams are involved in this project.
- PRIN-2022bpjl2l (IRONMOON): The objective of the PRIN project IRONMOON is the study of superconducting materials for axion RF cavities. The LNF team is involved in this project.

13 R&D

The funding requested for the R&D and studies discussed in the previous sections is given in Tab. 20. These include, 4 complete sets of MSA amplifiers from ezSQUID with bias electronics and post-amplifiers; Digitizers and signal generators for operating at 100-500 MHz; An FPGA board for multichannel acquisition tests; A thermometer (Cernox type) to operate in strong magnetic field; Material for sample holders and RF components to realize the various R&Ds; cryogenic gases, and in particular LHe for the cavity prototype test at LNF. Travel costs are needed for travel to experimental sites (LNF, Camerino, Bonn) and in particular for travel to CERN to interact with and for training from the Cryogenic Group of the Engineering and Mechanical Support Section at CERN. Each group of the collaboration has a specific role in the project and specific skills and will conduct a well defined work for the R&D or for the detector design as described in sections 10 and 12.

We expect to complete the preparation of the TDR for Summer 2026. The timetable is shown in Fig. 28 where a few milestones have been indicated for each WP. Given the low risk connected to the high starting TRL of the technologies involved, we consider this to be a reasonable timetable.

A preliminary estimate of the cost for the construction of the larger experiment KLASH [258], based on the KLOE magnet, was done in 2019 by Fantini Sud S.p.A.. This included the cryogenic system, the cryostat and cavity and the assembly and was estimated to be about 2.2 Meuro. A new estimate will be provided before Summer 2026. Once approved, we consider additional three years, for fabrication, installation and commissioning, before data taking.

14 Conclusions

The FLASH experiment will be able to probe the existence of dark matter composed by axions predicted by KSVZ and DFSZ models in the galactic halo within the mass range $m_a = (0.49 - 1.49)\,\mu$eV. This window is currently unexplored and lies in between the mass range that will be scanned in near-future searches by BabyIAXO [48] and DMRadio [71, 79] collaborations. Other models for bosonic fields making up the cosmic dark matter such as an axion-like particle, scalar field or hidden photon can also be tested, as well as models of chameleons, which are not necessarily the dark matter, through the "afterglow" effect. Finally, the haloscope can be used to search for high-frequency gravitational waves of astrophysical origin. If the HFGW signal is due to coalescing PBHs, the experiment can probe the existence of mergers in the mass range $M_{\rm PBH} \lesssim 10^{-7}\,M_\odot$, although the expected strain from a single event in the Galaxy is too faint to be observed. We have presented the forecast reach of the FLASH experiment for all of the models above, along with a detailed explanation of the analysis involved. Forecasts have been presented for a detector with and without an improved cryogenic system able to reach temperatures down to $T_{\rm sys} = 100\,$mK. We stress here that in the latter case, the sensitivity of the experiment, even if limited by thermal noise, is still enough to probe KSVZ axions in the 1 μeV region, a result obtainable just by recycling the FINUDA magnet and its cryogenic plant. DFSZ could be partially probed by cooling the cryostat to 1.9 K by pumping on He, while the use of a superconducting NbTi of ReBCO cavity would push the sensitivity beyond this limit. All this combined with the high initial TRL value of the technologies involved and the existing infrastructure at LNFs, makes FLASH a very high-gain/low-risk and relatively low-cost experiment.

Table 20: Funding Requests

Descrizione	Capitolo di Spesa	Sezione INFN	2025	2026
4 complete systems for MSA	Inventario	Trento+Pisa+LNF	25k	0
2 Digitizers >500 MHz	Inventario	Pisa + LNF	15k	0
Multimeter	Inventario	Pisa	6k	0
FPGA for DAQ	Inventario	Pisa	10k	0
Generator 120 MHz	Inventario	LNF-UniCam	6k	0
Thermometer for measurements in B field	Inventario	LNF-UniCam	2k	0
Total	Inventario		64k	0
B field shield	Consumo	LNF-UniCam	3k	0
LHe-cryostat flange	Consumo	LNF	10 k	0
Sample holder for B field setup	Consumo	LNF-UniCam	5k	0
Prototype material	Consumo	LNF	5k	0
RF components	Consumo	LNF	5k	0
RF components	Consumo	Pisa	6k	0
Electronic boards for squid multiplexing	Consumo	Pisa	5k	0
Cryogenic components	Consumo	Pisa	3k	0
BAW	Consumo	Pisa	2k	0
Cryogenic and RF components	Consumo	Trento	5k	1k
Cryo liquids - LN	Consumo	Trento	2k	0
LHe for prototype test	Consumo	LNF	10k	0
Cryo liquids - LN	Consumo	Pisa	2k	0
Total	Consumo		63k	1
Licence	Altro	Pisa	5k	0
Travel to CERN for cryostat design	Missioni	LNF	8+10(SJ)k	2k
Travel UniCam/LNF for test at LNF/UniCam	Missioni	LNF	5 k	1k
Travel for test at Bonn	Missioni	LNF	2 k	0k
Travel for test at LNF	Missioni	Trento	2k	1k
Travel for test at LNF	Missioni	Pisa	3k	2k
Total	Missioni		10+10(SJ)k	6k
Total			152+10(SJ)k	7k

A Computation of the couplings for the cavity modes TE_{011} and TE_{111}

We compute the coupling in Eq. (22) for the cavity mode TE_{011}, whose EM field has components:

$$B_z = B_0\, J_0(v_0 \frac{r}{R})\, \sin(\pi \frac{z}{L})\,, \tag{46}$$

$$B_r = -B_0\, \frac{\pi}{v_0} \frac{R}{L}\, J_1(v_0 \frac{r}{R})\, \cos(\pi \frac{z}{L})\,, \tag{47}$$

$$B_\theta = 0\,, \tag{48}$$

$$E_z = 0\,, \tag{49}$$

$$E_r = 0\,, \tag{50}$$

$$E_\theta = -iB_0\, \omega_0\, J_1(v_0 \frac{r}{R})\, \sin\left(\pi \frac{z}{L}\right)\,, \tag{51}$$

where $v_0 = 3.832$ is the first root of the Bessel function $J_1(x)$ and $\omega_0 = \left(1 + (\pi/v_0)^2 (R/L)^2\right)^{1/2}$, where R and L are the cavity radius and length, respectively. We decompose the phase as $k \cdot x = k_r r \cos\theta + k_z z$, where $\theta \in [0, 2\pi]$ is the angle between the radial direction and the projection of the momentum on the plane perpendicular to the cavity's axis, and we assume $k_z \approx k_r$. With this decomposition, the integral in Eq. (22) reads

$$\begin{aligned} C_{011} &= \frac{1}{\pi^2 L^2 R^2} \frac{\left|\int \mathrm{d}z \int \mathrm{d}\theta \int \mathrm{d}r r\, e^{i\mathbf{k}\cdot\mathbf{x}}\, J_0(v_0 r/R)\, \sin(\pi z/L)\right|^2}{\int \mathrm{d}r r \left[J_0^2(v_0 r/R) + \frac{\pi^2}{v_0^2}\frac{R^2}{L^2}\, J_1^2(v_0 r/R)\right]} = \\ &= \frac{\left|\frac{1+e^{ik_z L}}{\pi^2 - k_z^2 L^2} \int_0^{2\pi} \mathrm{d}\theta \int_0^1 \mathrm{d}x x\, e^{ik_r R x \cos\theta}\, J_0(v_0 x)\right|^2}{\int_0^1 \mathrm{d}x x \left[J_0^2(v_0 x) + \frac{\pi^2}{v_0^2}\frac{R^2}{L^2}\, J_1^2(v_0 x)\right]} . \end{aligned} \tag{52}$$

For the numerical estimate, we consider the large cavity setup with $R = 1050\,\mathrm{mm}$ and $L = 1200\,\mathrm{mm}$. In the case of the chameleon for which the momentum is approximately the inverse Compton length $k_z^{-1} \approx k_r^{-1} \approx 0.2\,\mathrm{m}$, the expression above gives $C_{011} \approx 0.005$. For bosonic DM with a velocity $v = 200\,\mathrm{km/s}$, the momentum scale is set by the inverse de Broglie wavelength so that $k_z \approx mv \approx (200\,\mathrm{m})^{-1}$. In this case, the limits $k_z L \ll 1$ and $k_r R \ll 1$ lead to

$$C_{011} = (mRv)^4 \frac{\left|\frac{1}{\pi}\int_0^1 \mathrm{d}x x^3\, J_0(v_0 x)\right|^2}{\int_0^1 \mathrm{d}x x \left[J_0^2(v_0 x) + \frac{\pi^2}{v_0^2}\frac{R^2}{L^2}\, J_1^2(v_0 x)\right]} \approx 0.003\,(mRv)^4 , \tag{53}$$

which gives $C_{011} \approx 5 \times 10^{-13}$ for the large cavity setup.

We repeat the computation for the cavity mode TE_{111}, whose EM field has components:

$$B_z = B_0\, J_1(v_1 \frac{r}{R})\, \sin\left(\pi \frac{z}{L}\right) \cos\theta , \tag{54}$$

$$B_r = B_0\, \frac{\pi}{2v_1}\frac{R}{L} \left[J_0(v_1 \frac{r}{R}) - J_2(v_1 \frac{r}{R})\right] \cos\left(\pi \frac{z}{L}\right) \cos\theta , \tag{55}$$

$$B_\theta = -B_0\, \frac{\pi}{v_1^2}\frac{R^2}{L\, r}\, J_1(v_1 \frac{r}{R})\, \cos\left(\pi \frac{z}{L}\right) \sin\theta , \tag{56}$$

$$E_z = 0 , \tag{57}$$

$$E_r = iB_0\, \frac{\omega_1}{v_1}\frac{R}{r}\, J_1(v_1 \frac{r}{R})\, \sin\left(\pi \frac{z}{L}\right) \sin\theta , \tag{58}$$

$$E_\theta = \frac{i}{2} B_0\, \omega_1 \left[J_0(v_1 \frac{r}{R}) - J_2(v_1 \frac{r}{R})\right] \sin\left(\pi \frac{z}{L}\right) \cos\theta , \tag{59}$$

where $v_1 \approx 1.8412$ and $\omega_1 = \left(1 + (\pi/v_1)^2 (R/L)^2\right)^{1/2}$. The integral in Eq. (22) for the mode TE_{111} reads

$$C_{111} = \frac{\left|\frac{1+e^{ik_z L}}{\pi^2 - k_z^2 L^2} \int_0^{2\pi} \mathrm{d}\theta \int_0^1 \mathrm{d}x x\, e^{ik_r R x \cos\theta}\, J_1(v_1 x) \cos\theta\right|^2}{\frac{1}{2}\int_0^1 \mathrm{d}x x \left[\left[1 + \left(\frac{\pi R}{v_1^2 L x}\right)^2\right] J_1^2(v_1 x) + \left(\frac{\pi R}{2v_1 L}\right)^2 \left[J_0(v_1 x) - J_2(v_1 x)\right]^2\right]} , \tag{60}$$

which gives $C_{111} \approx 3 \times 10^{-7}$ for the case of the large volume cavity, consistently with other findings [177].

References

[1] V. C. Rubin, W. K. Ford, Jr., Rotation of the Andromeda Nebula from a Spectroscopic Survey of Emission Regions, Astrophys. J. 159 (1970) 379–403. doi:10.1086/150317.

[2] V. Trimble, Existence and Nature of Dark Matter in the Universe, Ann. Rev. Astron. Astrophys. 25 (1987) 425–472. doi:10.1146/annurev.aa.25.090187.002233.

[3] G. Efstathiou, J. R. Bond, S. D. M. White, COBE Background radiation anisotropies and large scale structure in the universe, Mon. Not. Roy. Astron. Soc. 258 (1992) 1–6. doi:10.1093/mnras/258.1.1P.

[4] N. Aghanim, et al., Planck 2018 results. I. Overview and the cosmological legacy of Planck, Astron. Astrophys. 641 (2020) A1. arXiv:1807.06205, doi:10.1051/0004-6361/201833880.

[5] S. Weinberg, A New Light Boson?, Phys. Rev. Lett. 40 (1978) 223–226. doi:10.1103/PhysRevLett.40.223.

[6] F. Wilczek, Problem of Strong P and T Invariance in the Presence of Instantons, Phys. Rev. Lett. 40 (1978) 279–282. doi:10.1103/PhysRevLett.40.279.

[7] R. D. Peccei, H. R. Quinn, Constraints Imposed by CP Conservation in the Presence of Instantons, Phys. Rev. D 16 (1977) 1791–1797. doi:10.1103/PhysRevD.16.1791.

[8] R. D. Peccei, H. R. Quinn, CP Conservation in the Presence of Instantons, Phys. Rev. Lett. 38 (1977) 1440–1443. doi:10.1103/PhysRevLett.38.1440.

[9] C. G. Callan, Jr., R. F. Dashen, D. J. Gross, The Structure of the Gauge Theory Vacuum, Phys. Lett. B 63 (1976) 334–340. doi:10.1016/0370-2693(76)90277-X.

[10] R. Jackiw, C. Rebbi, Vacuum Periodicity in a Yang-Mills Quantum Theory, Phys. Rev. Lett. 37 (1976) 172–175. doi:10.1103/PhysRevLett.37.172.

[11] V. Baluni, CP Violating Effects in QCD, Phys. Rev. D 19 (1979) 2227–2230. doi:10.1103/PhysRevD.19.2227.

[12] R. J. Crewther, P. Di Vecchia, G. Veneziano, E. Witten, Chiral Estimate of the Electric Dipole Moment of the Neutron in Quantum Chromodynamics, Phys. Lett. B 88 (1979) 123, [Erratum: Phys.Lett.B 91, 487 (1980)]. doi:10.1016/0370-2693(79)90128-X.

[13] C. A. Baker, et al., An Improved experimental limit on the electric dipole moment of the neutron, Phys. Rev. Lett. 97 (2006) 131801. arXiv:hep-ex/0602020, doi:10.1103/PhysRevLett.97.131801.

[14] J. R. Ellis, M. K. Gaillard, D. V. Nanopoulos, Lefthanded Currents and CP Violation, Nucl. Phys. B 109 (1976) 213–243. doi:10.1016/0550-3213(76)90203-0.

[15] E. P. Shabalin, The electric dipole moments of baryons in the Kobayashi Maskawa CP-noninvariant theory, Sov. J. Nucl. Phys. 32 (1980) 228.

[16] J. R. Ellis, M. K. Gaillard, Strong and Weak CP Violation, Nucl. Phys. B 150 (1979) 141–162. doi:10.1016/0550-3213(79)90297-9.

[17] R. Kallosh, A. D. Linde, D. A. Linde, L. Susskind, Gravity and global symmetries, Phys. Rev. D 52 (1995) 912–935. arXiv:hep-th/9502069, doi:10.1103/PhysRevD.52.912.

[18] M. Kamionkowski, J. March-Russell, Planck scale physics and the Peccei-Quinn mechanism, Phys. Lett. B 282 (1992) 137–141. arXiv:hep-th/9202003, doi:10.1016/0370-2693(92)90492-M.

[19] S. Ghigna, M. Lusignoli, M. Roncadelli, Instability of the invisible axion, Phys. Lett. B 283 (1992) 278–281. doi:10.1016/0370-2693(92)90019-Z.

[20] S. M. Barr, D. Seckel, Planck scale corrections to axion models, Phys. Rev. D 46 (1992) 539–549. doi:10.1103/PhysRevD.46.539.

[21] A. Hook, TASI Lectures on the Strong CP Problem and Axions, in: TASI 2018 - Theory in an Era of Data, 2018, p. 4. arXiv:1812.02669, doi:10.22323/1.333.0004.

[22] L. Di Luzio, M. Giannotti, E. Nardi, L. Visinelli, The landscape of QCD axion models, Phys. Rept. 870 (2020) 1–117. arXiv:2003.01100, doi:10.1016/j.physrep.2020.06.002.

[23] G. Dvali, C. Gomez, S. Zell, A Proof of the Axion? (2018). arXiv:1811.03079.

[24] G. Dvali, Strong-CP with and without gravity (2022). arXiv:2209.14219.

[25] J. E. Kim, Weak Interaction Singlet and Strong CP Invariance, Phys. Rev. Lett. 43 (1979) 103. doi:10.1103/PhysRevLett.43.103.

[26] M. A. Shifman, A. I. Vainshtein, V. I. Zakharov, Can Confinement Ensure Natural CP Invariance of Strong Interactions?, Nucl. Phys. B 166 (1980) 493–506. doi:10.1016/0550-3213(80)90209-6.

[27] A. R. Zhitnitsky, On Possible Suppression of the Axion Hadron Interactions. (In Russian), Sov. J. Nucl. Phys. 31 (1980) 260.

[28] M. Dine, W. Fischler, M. Srednicki, A Simple Solution to the Strong CP Problem with a Harmless Axion, Phys. Lett. B 104 (1981) 199–202. doi:10.1016/0370-2693(81)90590-6.

[29] C. B. Adams, et al., Axion Dark Matter, in: Snowmass 2021, 2022. arXiv:2203.14923.

[30] M. Baryakhtar, et al., Dark Matter In Extreme Astrophysical Environments, in: Snowmass 2021, 2022. arXiv:2203.07984.

[31] C. Antel, et al., Feebly-interacting particles: FIPs 2022 Workshop Report, Eur. Phys. J. C 83 (12) (2023) 1122. arXiv:2305.01715, doi:10.1140/epjc/s10052-023-12168-5.

[32] S. J. Asztalos, et al., Large scale microwave cavity search for dark matter axions, Phys. Rev. D 64 (2001) 092003. doi:10.1103/PhysRevD.64.092003.

[33] S. J. Asztalos, et al., Experimental constraints on the axion dark matter halo density, Astrophys. J. Lett. 571 (2002) L27–L30. arXiv:astro-ph/0104200, doi:10.1086/341130.

[34] S. J. Asztalos, G. Carosi, C. Hagmann, D. Kinion, K. van Bibber, M. Hotz, L. J. Rosenberg, G. Rybka, J. Hoskins, J. Hwang, P. Sikivie, D. B. Tanner, R. Bradley, J. Clarke, Squid-based microwave cavity search for dark-matter axions, Phys. Rev. Lett. 104 (2010) 041301. doi:10.1103/PhysRevLett.104.041301.
URL https://link.aps.org/doi/10.1103/PhysRevLett.104.041301

[35] C. Boutan, et al., Piezoelectrically Tuned Multimode Cavity Search for Axion Dark Matter, Phys. Rev. Lett. 121 (26) (2018) 261302. arXiv:1901.00920, doi:10.1103/PhysRevLett.121.261302.

[36] N. Du, et al., A Search for Invisible Axion Dark Matter with the Axion Dark Matter Experiment, Phys. Rev. Lett. 120 (15) (2018) 151301. arXiv:1804.05750, doi:10.1103/PhysRevLett.120.151301.

[37] T. Braine, et al., Extended Search for the Invisible Axion with the Axion Dark Matter Experiment, Phys. Rev. Lett. 124 (10) (2020) 101303. arXiv:1910.08638, doi:10.1103/PhysRevLett.124.101303.

[38] C. Bartram, et al., Search for Invisible Axion Dark Matter in the 3.3–4.2 μeV Mass Range, Phys. Rev. Lett. 127 (26) (2021) 261803. arXiv:2110.06096, doi:10.1103/PhysRevLett.127.261803.

[39] C. Boutan, et al., Piezoelectrically Tuned Multimode Cavity Search for Axion Dark Matter, Phys. Rev. Lett. 121 (26) (2018) 261302. arXiv:1901.00920, doi:10.1103/PhysRevLett.121.261302.

[40] S. Al Kenany, et al., Design and operational experience of a microwave cavity axion detector for the 20–100μeV range, Nucl. Instrum. Meth. A 854 (2017) 11–24. arXiv:1611.07123, doi:10.1016/j.nima.2017.02.012.

[41] B. M. Brubaker, et al., First results from a microwave cavity axion search at 24 μeV, Phys. Rev. Lett. 118 (6) (2017) 061302. arXiv:1610.02580, doi:10.1103/PhysRevLett.118.061302.

[42] L. Zhong, et al., Results from phase 1 of the HAYSTAC microwave cavity axion experiment, Phys. Rev. D 97 (9) (2018) 092001. arXiv:1803.03690, doi:10.1103/PhysRevD.97.092001.

[43] K. M. Backes, et al., A quantum-enhanced search for dark matter axions, Nature 590 (7845) (2021) 238–242. arXiv:2008.01853, doi:10.1038/s41586-021-03226-7.

[44] M. J. Jewell, et al., New results from HAYSTAC's phase II operation with a squeezed state receiver, Phys. Rev. D 107 (7) (2023) 072007. arXiv:2301.09721, doi:10.1103/PhysRevD.107.072007.

[45] B. T. McAllister, G. Flower, J. Kruger, E. N. Ivanov, M. Goryachev, J. Bourhill, M. E. Tobar, The ORGAN Experiment: An axion haloscope above 15 GHz, Phys. Dark Univ. 18 (2017) 67–72. arXiv:1706.00209, doi:10.1016/j.dark.2017.09.010.

[46] B. T. McAllister, M. E. Tobar, The ORGAN Experiment, Springer Proc. Phys. 245 (2020) 37–43. doi:10.1007/978-3-030-43761-9_5.

[47] A. Quiskamp, B. T. McAllister, P. Altin, E. N. Ivanov, M. Goryachev, M. E. Tobar, Direct search for dark matter axions excluding alp cogenesis in the 63- to 67-μev range with the organ experiment, Science Advances 8 (27) (2022) eabq3765. doi:10.1126/sciadv.abq3765. URL https://www.science.org/doi/abs/10.1126/sciadv.abq3765

[48] S. Ahyoune, et al., A Proposal for a Low-Frequency Axion Search in the 1-2 μeV Range and Below with the BabyIAXO Magnet, Annalen Phys. 535 (12) (2023) 2300326. arXiv:2306.17243, doi:10.1002/andp.202300326.

[49] S. Lee, S. Ahn, J. Choi, B. R. Ko, Y. K. Semertzidis, Axion Dark Matter Search around 6.7 μeV, Phys. Rev. Lett. 124 (10) (2020) 101802. arXiv:2001.05102, doi:10.1103/PhysRevLett.124.101802.

[50] J. Jeong, S. Youn, S. Bae, J. Kim, T. Seong, J. E. Kim, Y. K. Semertzidis, Search for Invisible Axion Dark Matter with a Multiple-Cell Haloscope, Phys. Rev. Lett. 125 (22) (2020) 221302. arXiv:2008.10141, doi:10.1103/PhysRevLett.125.221302.

[51] O. Kwon, et al., First Results from an Axion Haloscope at CAPP around 10.7 μeV, Phys. Rev. Lett. 126 (19) (2021) 191802. arXiv:2012.10764, doi:10.1103/PhysRevLett.126.191802.

[52] Y. Lee, B. Yang, H. Yoon, M. Ahn, H. Park, B. Min, D. Kim, J. Yoo, Searching for Invisible Axion Dark Matter with an 18 T Magnet Haloscope, Phys. Rev. Lett. 128 (24) (2022) 241805. arXiv:2206.08845, doi:10.1103/PhysRevLett.128.241805.

[53] J. Kim, et al., Near-Quantum-Noise Axion Dark Matter Search at CAPP around 9.5 μeV, Phys. Rev. Lett. 130 (9) (2023) 091602. arXiv:2207.13597, doi:10.1103/PhysRevLett.130.091602.

[54] A. K. Yi, et al., Axion Dark Matter Search around 4.55 μeV with Dine-Fischler-Srednicki-Zhitnitskii Sensitivity, Phys. Rev. Lett. 130 (7) (2023) 071002. arXiv:2210.10961, doi:10.1103/PhysRevLett.130.071002.

[55] C. M. Adair, et al., Search for Dark Matter Axions with CAST-CAPP, Nature Commun. 13 (1) (2022) 6180. arXiv:2211.02902, doi:10.1038/s41467-022-33913-6.

[56] S. Arguedas Cuendis, et al., The 3 Cavity Prototypes of RADES: An Axion Detector Using Microwave Filters at CAST, Springer Proc. Phys. 245 (2020) 45–51. arXiv:1903.04323, doi:10.1007/978-3-030-43761-9_6.

[57] A. A. Melcón, et al., Axion Searches with Microwave Filters: the RADES project, JCAP 05 (2018) 040. arXiv:1803.01243, doi:10.1088/1475-7516/2018/05/040.

[58] A. Álvarez Melcón, et al., Scalable haloscopes for axion dark matter detection in the 30μeV range with RADES, JHEP 07 (2020) 084. arXiv:2002.07639, doi:10.1007/JHEP07(2020)084.

[59] A. A. Melcón, et al., First results of the CAST-RADES haloscope search for axions at 34.67 μeV, JHEP 21 (2020) 075. arXiv:2104.13798, doi:10.1007/JHEP10(2021)075.

[60] R. Barbieri, C. Braggio, G. Carugno, C. S. Gallo, A. Lombardi, A. Ortolan, R. Pengo, G. Ruoso, C. C. Speake, Searching for galactic axions through magnetized media: the QUAX proposal, Phys. Dark Univ. 15 (2017) 135–141. arXiv:1606.02201, doi:10.1016/j.dark.2017.01.003.

[61] N. Crescini, et al., Searching Axions through Coupling with Spin: The QUAX Experiment, Springer Proc. Phys. 211 (2018) 143–150. doi:10.1007/978-3-319-92726-8_17.

[62] D. Alesini, et al., Galactic axions search with a superconducting resonant cavity, Phys. Rev. D 99 (10) (2019) 101101. arXiv:1903.06547, doi:10.1103/PhysRevD.99.101101.

[63] N. Crescini, et al., Operation of a ferromagnetic axion haloscope at $m_a = 58\,\mu$eV, Eur. Phys. J. C 78 (9) (2018) 703, [Erratum: Eur.Phys.J.C 78, 813 (2018)]. arXiv:1806.00310, doi:10.1140/epjc/s10052-018-6163-8.

[64] N. Crescini, et al., Axion search with a quantum-limited ferromagnetic haloscope, Phys. Rev. Lett. 124 (17) (2020) 171801. arXiv:2001.08940, doi:10.1103/PhysRevLett.124.171801.

[65] D. Alesini, et al., Search for invisible axion dark matter of mass $m_a = 43$ μeV with the QUAX–$a\gamma$ experiment, Phys. Rev. D 103 (10) (2021) 102004. arXiv:2012.09498, doi:10.1103/PhysRevD.103.102004.

[66] D. Alesini, et al., Search for Galactic axions with a high-Q dielectric cavity, Phys. Rev. D 106 (5) (2022) 052007. arXiv:2208.12670, doi:10.1103/PhysRevD.106.052007.

[67] R. Di Vora, et al., Search for galactic axions with a traveling wave parametric amplifier, Phys. Rev. D 108 (6) (2023) 062005. arXiv:2304.07505, doi:10.1103/PhysRevD.108.062005.

[68] A. Rettaroli, et al., Search for Axion dark matter with the QUAX-LNF tunable haloscope (2 2024). arXiv:2402.19063.

[69] Y. Kahn, B. R. Safdi, J. Thaler, Broadband and Resonant Approaches to Axion Dark Matter Detection, Phys. Rev. Lett. 117 (14) (2016) 141801. arXiv:1602.01086, doi:10.1103/PhysRevLett.117.141801.

[70] J. W. Foster, N. L. Rodd, B. R. Safdi, Revealing the Dark Matter Halo with Axion Direct Detection, Phys. Rev. D 97 (12) (2018) 123006. arXiv:1711.10489, doi:10.1103/PhysRevD.97.123006.

[71] L. Brouwer, et al., Projected sensitivity of DMRadio-m3: A search for the QCD axion below 1 μeV, Phys. Rev. D 106 (10) (2022) 103008. arXiv:2204.13781, doi:10.1103/PhysRevD.106.103008.

[72] B. Aja, et al., The Canfranc Axion Detection Experiment (CADEx): search for axions at 90 GHz with Kinetic Inductance Detectors, JCAP 11 (2022) 044. arXiv:2206.02980, doi:10.1088/1475-7516/2022/11/044.

[73] T. Grenet, R. Ballou, Q. Basto, K. Martineau, P. Perrier, P. Pugnat, J. Quevillon, N. Roch, C. Smith, The Grenoble Axion Haloscope platform (GrAHal): development plan and first results (2021). arXiv:2110.14406.

[74] H. Chang, et al., First Results from the Taiwan Axion Search Experiment with a Haloscope at 19.6 μeV, Phys. Rev. Lett. 129 (11) (2022) 111802. arXiv:2205.05574, doi:10.1103/PhysRevLett.129.111802.

[75] P. Sikivie, Experimental Tests of the Invisible Axion, Phys. Rev. Lett. 51 (1983) 1415–1417, [Erratum: Phys.Rev.Lett. 52, 695 (1984)]. doi:10.1103/PhysRevLett.51.1415.

[76] P. Sikivie, Detection Rates for 'Invisible' Axion Searches, Phys. Rev. D 32 (1985) 2988, [Erratum: Phys.Rev.D 36, 974 (1987)]. doi:10.1103/PhysRevD.36.974.

[77] L. Krauss, J. Moody, F. Wilczek, D. E. Morris, Calculations for Cosmic Axion Detection, Phys. Rev. Lett. 55 (1985) 1797. doi:10.1103/PhysRevLett.55.1797.

[78] C. Hagmann, P. Sikivie, N. Sullivan, D. B. Tanner, S. I. Cho, Cavity Design for a Cosmic Axion Detector, Rev. Sci. Instrum. 61 (1990) 1076–1085. doi:10.1063/1.1141427.

[79] A. AlShirawi, et al., Electromagnetic modeling and science reach of DMRadio-m^3 (2 2023). arXiv:2302.14084.

[80] L. Di Luzio, F. Mescia, E. Nardi, Redefining the Axion Window, Phys. Rev. Lett. 118 (3) (2017) 031801. arXiv:1610.07593, doi:10.1103/PhysRevLett.118.031801.

[81] L. Di Luzio, F. Mescia, E. Nardi, Window for preferred axion models, Phys. Rev. D 96 (7) (2017) 075003. arXiv:1705.05370, doi:10.1103/PhysRevD.96.075003.

[82] L. Di Luzio, F. Mescia, E. Nardi, P. Panci, R. Ziegler, Astrophobic Axions, Phys. Rev. Lett. 120 (26) (2018) 261803. arXiv:1712.04940, doi:10.1103/PhysRevLett.120.261803.

[83] G. G. Raffelt, Axions in astrophysics and cosmology, in: 30th Rencontres de Moriond: Euroconferences: Dark Matter in Cosmology, Clocks and Tests of Fundamental Laws, 1995, pp. 159–168. arXiv:hep-ph/9502358.

[84] G. G. Raffelt, Axions: Motivation, limits and searches, J. Phys. A 40 (2007) 6607–6620. arXiv:hep-ph/0611118, doi:10.1088/1751-8113/40/25/S05.

[85] P. Sikivie, Axion Cosmology, Lect. Notes Phys. 741 (2008) 19–50. arXiv:astro-ph/0610440, doi:10.1007/978-3-540-73518-2_2.

[86] J. E. Kim, G. Carosi, Axions and the Strong CP Problem, Rev. Mod. Phys. 82 (2010) 557–602, [Erratum: Rev.Mod.Phys. 91, 049902 (2019)]. arXiv:0807.3125, doi:10.1103/RevModPhys.82.557.

[87] O. Wantz, E. P. S. Shellard, Axion Cosmology Revisited, Phys. Rev. D 82 (2010) 123508. arXiv:0910.1066, doi:10.1103/PhysRevD.82.123508.

[88] M. Kawasaki, K. Nakayama, Axions: Theory and Cosmological Role, Ann. Rev. Nucl. Part. Sci. 63 (2013) 69–95. arXiv:1301.1123, doi:10.1146/annurev-nucl-102212-170536.

[89] D. J. E. Marsh, Axion Cosmology, Phys. Rept. 643 (2016) 1–79. arXiv:1510.07633, doi:10.1016/j.physrep.2016.06.005.

[90] I. G. Irastorza, J. Redondo, New experimental approaches in the search for axion-like particles, Prog. Part. Nucl. Phys. 102 (2018) 89–159. arXiv:1801.08127, doi:10.1016/j.ppnp.2018.05.003.

[91] Y. M. Cho, J. H. Kim, Dilatonic dark matter and its experimental detection, Phys. Rev. D 79 (2009) 023504. arXiv:0711.2858, doi:10.1103/PhysRevD.79.023504.

[92] K.-Y. Choi, D. K. Hong, S. Matsuzaki, Techni-dilaton as Dark Matter, Phys. Lett. B 706 (2011) 183–187. arXiv:1101.5326, doi:10.1016/j.physletb.2011.11.013.

[93] J. Khoury, A. Weltman, Chameleon fields: Awaiting surprises for tests of gravity in space, Phys. Rev. Lett. 93 (2004) 171104. arXiv:astro-ph/0309300, doi:10.1103/PhysRevLett.93.171104.

[94] P. Brax, C. van de Bruck, A.-C. Davis, J. Khoury, A. Weltman, Detecting dark energy in orbit: The cosmological chameleon, Phys. Rev. D 70 (2004) 123518. arXiv:astro-ph/0408415, doi:10.1103/PhysRevD.70.123518.

[95] J. Redondo, A. Ringwald, Light shining through walls, Contemp. Phys. 52 (2011) 211–236. arXiv:1011.3741, doi:10.1080/00107514.2011.563516.

[96] P. Arias, D. Cadamuro, M. Goodsell, J. Jaeckel, J. Redondo, A. Ringwald, WISPy Cold Dark Matter, JCAP 06 (2012) 013. arXiv:1201.5902, doi:10.1088/1475-7516/2012/06/013.

[97] P. W. Graham, J. Mardon, S. Rajendran, Vector Dark Matter from Inflationary Fluctuations, Phys. Rev. D 93 (10) (2016) 103520. arXiv:1504.02102, doi:10.1103/PhysRevD.93.103520.

[98] A. Caputo, A. J. Millar, C. A. J. O'Hare, E. Vitagliano, Dark photon limits: A handbook, Phys. Rev. D 104 (9) (2021) 095029. arXiv:2105.04565, doi:10.1103/PhysRevD.104.095029.

[99] N. Aggarwal, et al., Challenges and opportunities of gravitational-wave searches at MHz to GHz frequencies, Living Rev. Rel. 24 (1) (2021) 4. arXiv:2011.12414, doi:10.1007/s41114-021-00032-5.

[100] P. Astone, et al., Long term operation of the Rome 'Explorer' cryogenic gravitational wave detector, Phys. Rev. D 47 (1993) 362–375. doi:10.1103/PhysRevD.47.362.

[101] P. Astone, et al., The Gravitational wave detector NAUTILUS operating at T = 0.1-K, Astropart. Phys. 7 (1997) 231–243. doi:10.1016/S0927-6505(97)00023-6.

[102] D. Alesini, et al., The future search for low-frequency axions and new physics with the FLASH resonant cavity experiment at Frascati National Laboratories, Phys. Dark Univ. 42 (2023) 101370. arXiv:2309.00351, doi:10.1016/j.dark.2023.101370.

[103] M. Bertani, A. Cecchetti, B. Dulach, F. Fabbri, M. Giardoni, A. Lanaro, V. Lucherini, T. Bressani, A. Feliciello, A. Filippi, et al., The finuda superconducting magnet at daϕne, Nuclear Physics B-Proceedings Supplements 78 (1-3) (1999) 553–558. doi:10.1016/S0920-5632(99)00602-7.

[104] M. Modena, The DAPHNE cryogenic system (1997).

[105] R. H. Dicke, The Measurement of Thermal Radiation at Microwave Frequencies, Rev. Sci. Instrum. 17 (7) (1946) 268–275. doi:10.1063/1.1770483.

[106] I. Stern, A. A. Chisholm, J. Hoskins, P. Sikivie, N. S. Sullivan, D. B. Tanner, G. Carosi, K. van Bibber, Cavity design for high-frequency axion dark matter detectors, Rev. Sci. Instrum. 86 (12) (2015) 123305. arXiv:1603.06990, doi:10.1063/1.4938164.

[107] M. Mück, M. O. Andre, J. Clarke, J. Gail, C. Heiden, Niobium dc SQUID with microstrip input coupling as an amplifier for the axion detector, Nucl. Phys. B Proc. Suppl. 72 (1999) 145–151. doi:10.1016/S0920-5632(98)00517-9.

[108] M. Mück, R. McDermott, Radio-frequency amplifiers based on dc squids, Superconductor Science and Technology 23 (9) (2010) 093001. doi:10.1088/0953-2048/23/9/093001.
URL https://dx.doi.org/10.1088/0953-2048/23/9/093001

[109] P. Di Vecchia, G. Veneziano, Chiral Dynamics in the Large n Limit, Nucl. Phys. B 171 (1980) 253–272. doi:10.1016/0550-3213(80)90370-3.

[110] G. Grilli di Cortona, E. Hardy, J. Pardo Vega, G. Villadoro, The QCD axion, precisely, JHEP 01 (2016) 034. arXiv:1511.02867, doi:10.1007/JHEP01(2016)034.

[111] A. Vilenkin, A. E. Everett, Cosmic Strings and Domain Walls in Models with Goldstone and PseudoGoldstone Bosons, Phys. Rev. Lett. 48 (1982) 1867–1870. doi:10.1103/PhysRevLett.48.1867.

[112] P. Sikivie, Of Axions, Domain Walls and the Early Universe, Phys. Rev. Lett. 48 (1982) 1156–1159. doi:10.1103/PhysRevLett.48.1156.

[113] D. J. Gross, R. D. Pisarski, L. G. Yaffe, QCD and Instantons at Finite Temperature, Rev. Mod. Phys. 53 (1981) 43. doi:10.1103/RevModPhys.53.43.

[114] C. Bonati, M. D'Elia, M. Mariti, G. Martinelli, M. Mesiti, F. Negro, F. Sanfilippo, G. Villadoro, Axion phenomenology and θ-dependence from $N_f = 2 + 1$ lattice QCD, JHEP 03 (2016) 155. arXiv:1512.06746, doi:10.1007/JHEP03(2016)155.

[115] S. Borsanyi, M. Dierigl, Z. Fodor, S. D. Katz, S. W. Mages, D. Nogradi, J. Redondo, A. Ringwald, K. K. Szabo, Axion cosmology, lattice QCD and the dilute instanton gas, Phys. Lett. B 752 (2016) 175–181. arXiv:1508.06917, doi:10.1016/j.physletb.2015.11.020.

[116] S. Borsanyi, et al., Calculation of the axion mass based on high-temperature lattice quantum chromodynamics, Nature 539 (7627) (2016) 69–71. arXiv:1606.07494, doi:10.1038/nature20115.

[117] P. Petreczky, H.-P. Schadler, S. Sharma, The topological susceptibility in finite temperature QCD and axion cosmology, Phys. Lett. B 762 (2016) 498–505. arXiv:1606.03145, doi:10.1016/j.physletb.2016.09.063.

[118] H. Peng, et al., Cryogenic cavity detector for a large scale cold dark-matter axion search, Nucl. Instrum. Meth. A 444 (2000) 569–583. doi:10.1016/S0168-9002(99)00971-7.

[119] J. Buch, S. C. J. Leung, J. Fan, Using Gaia DR2 to Constrain Local Dark Matter Density and Thin Dark Disk, JCAP 04 (2019) 026. arXiv:1808.05603, doi:10.1088/1475-7516/2019/04/026.

[120] M. Benito, F. Iocco, A. Cuoco, Uncertainties in the Galactic Dark Matter distribution: An update, Phys. Dark Univ. 32 (2021) 100826. arXiv:2009.13523, doi:10.1016/j.dark.2021.100826.

[121] S. De Panfilis, A. C. Melissinos, B. E. Moskowitz, J. T. Rogers, Y. K. Semertzidis, W. Wuensch, H. J. Halama, A. G. Prodell, W. B. Fowler, F. A. Nezrick, Limits on the Abundance and Coupling of Cosmic Axions at 4.5-Microev $<$ m(a) $<$ 5.0-Microev, Phys. Rev. Lett. 59 (1987) 839. doi:10.1103/PhysRevLett.59.839.

[122] W. Wuensch, S. De Panfilis-Wuensch, Y. K. Semertzidis, J. T. Rogers, A. C. Melissinos, H. J. Halama, B. E. Moskowitz, A. G. Prodell, W. B. Fowler, F. A. Nezrick, Results of a Laboratory Search for Cosmic Axions and Other Weakly Coupled Light Particles, Phys. Rev. D 40 (1989) 3153. doi:10.1103/PhysRevD.40.3153.

[123] C. Hagmann, P. Sikivie, N. S. Sullivan, D. B. Tanner, Results from a search for cosmic axions, Phys. Rev. D 42 (1990) 1297–1300. doi:10.1103/PhysRevD.42.1297.

[124] C. O'Hare, cajohare/axionlimits: Axionlimits, https://cajohare.github.io/AxionLimits/ (2020). doi:10.5281/zenodo.3932430.

[125] G. Marconato, C. Pira, D. Alesini, D. D'Agostino, O. Azzolini, C. Braggio, R. Caforio, E. Chyhyrynets, A. D'Elia, M. Fracasso, U. Gambardella, V. Garcia, C. Gatti, G. Ghigo, D. D. Gioacchino, L. Gozzelino, G. Keppel, C. Ligi, G. Maccarrone, N. Pompeo, A. Rettaroli, A. Salmaso, E. Silva, F. Stivanello, S. Tocci, D. Torsello, Nbti thin film srf cavities for dark matter search, IEEE Transactions on Applied Superconductivity (2024) 1–6doi:10.1109/TASC.2024.3416541.

[126] L. F. Abbott, P. Sikivie, A Cosmological Bound on the Invisible Axion, Phys. Lett. B 120 (1983) 133–136. doi:10.1016/0370-2693(83)90638-X.

[127] M. Dine, W. Fischler, The Not So Harmless Axion, Phys. Lett. B 120 (1983) 137–141. doi:10.1016/0370-2693(83)90639-1.

[128] J. Preskill, M. B. Wise, F. Wilczek, Cosmology of the Invisible Axion, Phys. Lett. B 120 (1983) 127–132. doi:10.1016/0370-2693(83)90637-8.

[129] L. Visinelli, P. Gondolo, Dark Matter Axions Revisited, Phys. Rev. D 80 (2009) 035024. arXiv:0903.4377, doi:10.1103/PhysRevD.80.035024.

[130] M. S. Turner, Cosmic and Local Mass Density of Invisible Axions, Phys. Rev. D 33 (1986) 889–896. doi:10.1103/PhysRevD.33.889.

[131] V. B. Klaer, G. D. Moore, How to simulate global cosmic strings with large string tension, JCAP 10 (2017) 043. arXiv:1707.05566, doi:10.1088/1475-7516/2017/10/043.

[132] V. B. . Klaer, G. D. Moore, The dark-matter axion mass, JCAP 11 (2017) 049. arXiv:1708.07521, doi:10.1088/1475-7516/2017/11/049.

[133] M. Gorghetto, E. Hardy, G. Villadoro, Axions from Strings: the Attractive Solution, JHEP 07 (2018) 151. arXiv:1806.04677, doi:10.1007/JHEP07(2018)151.

[134] A. Vaquero, J. Redondo, J. Stadler, Early seeds of axion miniclusters, JCAP 04 (2019) 012. arXiv:1809.09241, doi:10.1088/1475-7516/2019/04/012.

[135] M. Buschmann, J. W. Foster, B. R. Safdi, Early-Universe Simulations of the Cosmological Axion, Phys. Rev. Lett. 124 (16) (2020) 161103. arXiv:1906.00967, doi:10.1103/PhysRevLett.124.161103.

[136] M. Gorghetto, E. Hardy, G. Villadoro, More axions from strings, SciPost Phys. 10 (2) (2021) 050. arXiv:2007.04990, doi:10.21468/SciPostPhys.10.2.050.

[137] M. Buschmann, J. W. Foster, A. Hook, A. Peterson, D. E. Willcox, W. Zhang, B. R. Safdi, Dark matter from axion strings with adaptive mesh refinement, Nature Commun. 13 (1) (2022) 1049. arXiv:2108.05368, doi:10.1038/s41467-022-28669-y.

[138] C. A. J. O'Hare, G. Pierobon, J. Redondo, Y. Y. Y. Wong, Simulations of axionlike particles in the postinflationary scenario, Phys. Rev. D 105 (5) (2022) 055025. arXiv:2112.05117, doi:10.1103/PhysRevD.105.055025.

[139] S. Hoof, J. Riess, D. J. E. Marsh, Statistical Uncertainties of the $N_{\rm DW} = 1$ QCD Axion Mass Window from Topological Defects (8 2021). arXiv:2108.09563, doi:10.21105/astro.2108.09563.

[140] B. Eggemeier, C. A. J. O'Hare, G. Pierobon, J. Redondo, Y. Y. Y. Wong, Axion minivoids and implications for direct detection, Phys. Rev. D 107 (8) (2023) 083510. arXiv:2212.00560, doi:10.1103/PhysRevD.107.083510.

[141] P. W. Graham, A. Scherlis, Stochastic axion scenario, Phys. Rev. D 98 (3) (2018) 035017. arXiv:1805.07362, doi:10.1103/PhysRevD.98.035017.

[142] F. Takahashi, W. Yin, A. H. Guth, QCD axion window and low-scale inflation, Phys. Rev. D 98 (1) (2018) 015042. arXiv:1805.08763, doi:10.1103/PhysRevD.98.015042.

[143] S. Hoof, F. Kahlhoefer, P. Scott, C. Weniger, M. White, Axion global fits with Peccei-Quinn symmetry breaking before inflation using GAMBIT, JHEP 03 (2019) 191, [Erratum: JHEP 11, 099 (2019)]. arXiv:1810.07192, doi:10.1007/JHEP03(2019)191.

[144] P. Athron, et al., GAMBIT: The Global and Modular Beyond-the-Standard-Model Inference Tool, Eur. Phys. J. C 77 (11) (2017) 784, [Addendum: Eur.Phys.J.C 78, 98 (2018)]. arXiv:1705.07908, doi:10.1140/epjc/s10052-017-5321-8.

[145] T. Bringmann, et al., DarkBit: A GAMBIT module for computing dark matter observables and likelihoods, Eur. Phys. J. C 77 (12) (2017) 831. arXiv:1705.07920, doi:10.1140/epjc/s10052-017-5155-4.

[146] G. R. Dvali, Removing the cosmological bound on the axion scale (1995). arXiv:hep-ph/9505253.

[147] P. J. Steinhardt, M. S. Turner, Saving the Invisible Axion, Phys. Lett. B 129 (1983) 51. doi:10.1016/0370-2693(83)90727-X.

[148] G. Lazarides, C. Panagiotakopoulos, Q. Shafi, Relaxing the Cosmological Bound on Axions, Phys. Lett. B 192 (1987) 323–326. doi:10.1016/0370-2693(87)90115-8.

[149] G. Lazarides, R. K. Schaefer, D. Seckel, Q. Shafi, Dilution of Cosmological Axions by Entropy Production, Nucl. Phys. B 346 (1990) 193–212. doi:10.1016/0550-3213(90)90244-8.

[150] M. Kawasaki, T. Moroi, T. Yanagida, Can decaying particles raise the upper bound on the Peccei-Quinn scale?, Phys. Lett. B 383 (1996) 313–316. arXiv:hep-ph/9510461, doi:10.1016/0370-2693(96)00743-5.

[151] L. Visinelli, P. Gondolo, Axion cold dark matter in non-standard cosmologies, Phys. Rev. D 81 (2010) 063508. arXiv:0912.0015, doi:10.1103/PhysRevD.81.063508.

[152] L. Visinelli, Light axion-like dark matter must be present during inflation, Phys. Rev. D 96 (2) (2017) 023013. arXiv:1703.08798, doi:10.1103/PhysRevD.96.023013.

[153] L. Visinelli, J. Redondo, Axion Miniclusters in Modified Cosmological Histories, Phys. Rev. D 101 (2) (2020) 023008. arXiv:1808.01879, doi:10.1103/PhysRevD.101.023008.

[154] P. Draper, J. Kozaczuk, J.-H. Yu, Theta in new QCD-like sectors, Phys. Rev. D 98 (1) (2018) 015028. arXiv:1803.00015, doi:10.1103/PhysRevD.98.015028.

[155] A. E. Nelson, H. Xiao, Axion Cosmology with Early Matter Domination, Phys. Rev. D 98 (6) (2018) 063516. arXiv:1807.07176, doi:10.1103/PhysRevD.98.063516.

[156] N. Ramberg, L. Visinelli, Probing the Early Universe with Axion Physics and Gravitational Waves, Phys. Rev. D 99 (12) (2019) 123513. arXiv:1904.05707, doi:10.1103/PhysRevD.99.123513.

[157] N. Blinov, M. J. Dolan, P. Draper, J. Kozaczuk, Dark matter targets for axionlike particle searches, Phys. Rev. D 100 (1) (2019) 015049. arXiv:1905.06952, doi:10.1103/PhysRevD.100.015049.

[158] N. Ramberg, L. Visinelli, QCD axion and gravitational waves in light of NANOGrav results, Phys. Rev. D 103 (6) (2021) 063031. arXiv:2012.06882, doi:10.1103/PhysRevD.103.063031.

[159] K. Mazde, L. Visinelli, The interplay between the dark matter axion and primordial black holes, JCAP 01 (2023) 021. arXiv:2209.14307, doi:10.1088/1475-7516/2023/01/021.

[160] A. Hook, Solving the Hierarchy Problem Discretely, Phys. Rev. Lett. 120 (26) (2018) 261802. arXiv:1802.10093, doi:10.1103/PhysRevLett.120.261802.

[161] L. Di Luzio, B. Gavela, P. Quilez, A. Ringwald, An even lighter QCD axion, JHEP 05 (2021) 184. arXiv:2102.00012, doi:10.1007/JHEP05(2021)184.

[162] L. Di Luzio, B. Gavela, P. Quilez, A. Ringwald, Dark matter from an even lighter QCD axion: trapped misalignment, JCAP 10 (2021) 001. arXiv:2102.01082, doi:10.1088/1475-7516/2021/10/001.

[163] R. Foot, H. Lew, R. R. Volkas, A Model with fundamental improper space-time symmetries, Phys. Lett. B 272 (1991) 67–70. doi:10.1016/0370-2693(91)91013-L.

[164] Z. Berezhiani, D. Comelli, F. L. Villante, The Early mirror universe: Inflation, baryogenesis, nucleosynthesis and dark matter, Phys. Lett. B 503 (2001) 362–375. arXiv:hep-ph/0008105, doi:10.1016/S0370-2693(01)00217-9.

[165] L. Gianfagna, M. Giannotti, F. Nesti, Mirror world, supersymmetric axion and gamma ray bursts, JHEP 10 (2004) 044. arXiv:hep-ph/0409185, doi:10.1088/1126-6708/2004/10/044.

[166] M. Giannotti, Mirror world and axion: Relaxing cosmological bounds, Int. J. Mod. Phys. A 20 (2005) 2454–2458. arXiv:astro-ph/0504636, doi:10.1142/S0217751X05024766.

[167] P. Svrcek, E. Witten, Axions In String Theory, JHEP 06 (2006) 051. arXiv:hep-th/0605206, doi:10.1088/1126-6708/2006/06/051.

[168] A. Arvanitaki, N. Craig, S. Dimopoulos, S. Dubovsky, J. March-Russell, String Photini at the LHC, Phys. Rev. D 81 (2010) 075018. arXiv:0909.5440, doi:10.1103/PhysRevD.81.075018.

[169] A. Arvanitaki, S. Dimopoulos, S. Dubovsky, N. Kaloper, J. March-Russell, String Axiverse, Phys. Rev. D 81 (2010) 123530. arXiv:0905.4720, doi:10.1103/PhysRevD.81.123530.

[170] E. Witten, Some Properties of O(32) Superstrings, Phys. Lett. B 149 (1984) 351–356. doi:10.1016/0370-2693(84)90422-2.

[171] J. P. Conlon, The QCD axion and moduli stabilisation, JHEP 05 (2006) 078. arXiv:hep-th/0602233, doi:10.1088/1126-6708/2006/05/078.

[172] M. Cicoli, M. Goodsell, A. Ringwald, The type IIB string axiverse and its low-energy phenomenology, JHEP 10 (2012) 146. arXiv:1206.0819, doi:10.1007/JHEP10(2012)146.

[173] M. Cicoli, V. Guidetti, N. Righi, A. Westphal, Fuzzy Dark Matter candidates from string theory, JHEP 05 (2022) 107. arXiv:2110.02964, doi:10.1007/JHEP05(2022)107.

[174] D. J. E. Marsh, D. Grin, R. Hlozek, P. G. Ferreira, Axiverse cosmology and the energy scale of inflation, Phys. Rev. D 87 (2013) 121701. arXiv:1303.3008, doi:10.1103/PhysRevD.87.121701.

[175] L. Visinelli, S. Vagnozzi, Cosmological window onto the string axiverse and the supersymmetry breaking scale, Phys. Rev. D 99 (6) (2019) 063517. arXiv:1809.06382, doi:10.1103/PhysRevD.99.063517.

[176] M. R. Baldeschi, R. Ruffini, G. B. Gelmini, On massive fermions and bosons in galactic halos, Phys. Lett. B 122 (1983) 221–224. doi:10.1016/0370-2693(83)90688-3.

[177] V. V. Flambaum, B. T. McAllister, I. B. Samsonov, M. E. Tobar, Searching for scalar field dark matter using cavity resonators and capacitors, Phys. Rev. D 106 (5) (2022) 055037. arXiv:2207.14437, doi:10.1103/PhysRevD.106.055037.

[178] T. Damour, A. M. Polyakov, The String dilaton and a least coupling principle, Nucl. Phys. B 423 (1994) 532–558. arXiv:hep-th/9401069, doi:10.1016/0550-3213(94)90143-0.

[179] T. Damour, J. F. Donoghue, Phenomenology of the Equivalence Principle with Light Scalars, Class. Quant. Grav. 27 (2010) 202001. arXiv:1007.2790, doi:10.1088/0264-9381/27/20/202001.

[180] J. Manley, D. Wilson, R. Stump, D. Grin, S. Singh, Searching for Scalar Dark Matter with Compact Mechanical Resonators, Phys. Rev. Lett. 124 (15) (2020) 151301. arXiv:1910.07574, doi:10.1103/PhysRevLett.124.151301.

[181] T. A. Wagner, S. Schlamminger, J. H. Gundlach, E. G. Adelberger, Torsion-balance tests of the weak equivalence principle, Class. Quant. Grav. 29 (2012) 184002. arXiv:1207.2442, doi:10.1088/0264-9381/29/18/184002.

[182] A. Hees, J. Guéna, M. Abgrall, S. Bize, P. Wolf, Searching for an oscillating massive scalar field as a dark matter candidate using atomic hyperfine frequency comparisons, Phys. Rev. Lett. 117 (6) (2016) 061301. arXiv:1604.08514, doi:10.1103/PhysRevLett.117.061301.

[183] J. Bergé, P. Brax, G. Métris, M. Pernot-Borràs, P. Touboul, J.-P. Uzan, MICROSCOPE Mission: First Constraints on the Violation of the Weak Equivalence Principle by a Light Scalar Dilaton, Phys. Rev. Lett. 120 (14) (2018) 141101. arXiv:1712.00483, doi:10.1103/PhysRevLett.120.141101.

[184] J. Wang, L. Hui, J. Khoury, No-Go Theorems for Generalized Chameleon Field Theories, Phys. Rev. Lett. 109 (2012) 241301. arXiv:1208.4612, doi:10.1103/PhysRevLett.109.241301.

[185] S. Vagnozzi, L. Visinelli, P. Brax, A.-C. Davis, J. Sakstein, Direct detection of dark energy: The XENON1T excess and future prospects, Phys. Rev. D 104 (6) (2021) 063023. arXiv:2103.15834, doi:10.1103/PhysRevD.104.063023.

[186] C. Burrage, J. Sakstein, A Compendium of Chameleon Constraints, JCAP 11 (2016) 045. arXiv:1609.01192, doi:10.1088/1475-7516/2016/11/045.

[187] C. Burrage, J. Sakstein, Tests of Chameleon Gravity, Living Rev. Rel. 21 (1) (2018) 1. arXiv:1709.09071, doi:10.1007/s41114-018-0011-x.

[188] J. Jaeckel, E. Masso, J. Redondo, A. Ringwald, F. Takahashi, The Need for purely laboratory-based axion-like particle searches, Phys. Rev. D 75 (2007) 013004. arXiv:hep-ph/0610203, doi:10.1103/PhysRevD.75.013004.

[189] P. Brax, C. van de Bruck, A.-C. Davis, D. F. Mota, D. J. Shaw, Testing Chameleon Theories with Light Propagating through a Magnetic Field, Phys. Rev. D 76 (2007) 085010. arXiv:0707.2801, doi:10.1103/PhysRevD.76.085010.

[190] M. Ahlers, A. Lindner, A. Ringwald, L. Schrempp, C. Weniger, Alpenglow - A Signature for Chameleons in Axion-Like Particle Search Experiments, Phys. Rev. D 77 (2008) 015018. arXiv:0710.1555, doi:10.1103/PhysRevD.77.015018.

[191] H. Gies, D. F. Mota, D. J. Shaw, Hidden in the Light: Magnetically Induced Afterglow from Trapped Chameleon Fields, Phys. Rev. D 77 (2008) 025016. arXiv:0710.1556, doi:10.1103/PhysRevD.77.025016.

[192] G. Rybka, et al., A Search for Scalar Chameleons with ADMX, Phys. Rev. Lett. 105 (2010) 051801. arXiv:1004.5160, doi:10.1103/PhysRevLett.105.051801.

[193] A. S. Chou, et al., A Search for chameleon particles using a photon regeneration technique, Phys. Rev. Lett. 102 (2009) 030402. arXiv:0806.2438, doi:10.1103/PhysRevLett.102.030402.

[194] J. H. Steffen, A. Upadhye, A. Baumbaugh, A. S. Chou, P. O. Mazur, R. Tomlin, A. Weltman, W. Wester, Laboratory Constraints on Chameleon Dark Energy and Power-Law Fields, Phys. Rev. Lett. 105 (2010) 261803. arXiv:1010.0988, doi:10.1103/PhysRevLett.105.261803.

[195] A. Upadhye, J. H. Steffen, A. S. Chou, Designing dark energy afterglow experiments, Phys. Rev. D 86 (2012) 035006. arXiv:1204.5476, doi:10.1103/PhysRevD.86.035006.

[196] V. Anastassopoulos, et al., Search for chameleons with CAST, Phys. Lett. B 749 (2015) 172–180. arXiv:1503.04561, doi:10.1016/j.physletb.2015.07.049.

[197] P. Brax, C. P. Burgess, F. Quevedo, Axio-Chameleons: a novel string-friendly multi-field screening mechanism, JCAP 03 (2024) 015. arXiv:2310.02092, doi:10.1088/1475-7516/2024/03/015.

[198] L. B. Okun, Limits of electrodynamics: paraphotons?, Sov. Phys. JETP 56 (1982) 502.

[199] B. Holdom, Two U(1)'s and Epsilon Charge Shifts, Phys. Lett. B 166 (1986) 196–198. doi:10.1016/0370-2693(86)91377-8.

[200] R. Foot, X.-G. He, Comment on Z Z-prime mixing in extended gauge theories, Phys. Lett. B 267 (1991) 509–512. doi:10.1016/0370-2693(91)90901-2.

[201] M. Pospelov, A. Ritz, M. B. Voloshin, Bosonic super-WIMPs as keV-scale dark matter, Phys. Rev. D 78 (2008) 115012. arXiv:0807.3279, doi:10.1103/PhysRevD.78.115012.

[202] S. Ghosh, E. P. Ruddy, M. J. Jewell, A. F. Leder, R. H. Maruyama, Searching for dark photons with existing haloscope data, Phys. Rev. D 104 (9) (2021) 092016. arXiv:2104.09334, doi:10.1103/PhysRevD.104.092016.

[203] A. Ringwald, J. Schütte-Engel, C. Tamarit, Gravitational Waves as a Big Bang Thermometer, JCAP 03 (2021) 054. arXiv:2011.04731, doi:10.1088/1475-7516/2021/03/054.

[204] S. Vagnozzi, A. Loeb, The Challenge of Ruling Out Inflation via the Primordial Graviton Background, Astrophys. J. Lett. 939 (2) (2022) L22. arXiv:2208.14088, doi:10.3847/2041-8213/ac9b0e.

[205] A. Addazi, Y.-F. Cai, A. Marciano, Testing Dark Matter Models with Radio Telescopes in light of Gravitational Wave Astronomy, Phys. Lett. B 782 (2018) 732–736. arXiv:1712.03798, doi:10.1016/j.physletb.2018.06.015.

[206] R. H. Cyburt, B. D. Fields, K. A. Olive, T.-H. Yeh, Big Bang Nucleosynthesis: 2015, Rev. Mod. Phys. 88 (2016) 015004. arXiv:1505.01076, doi:10.1103/RevModPhys.88.015004.

[207] V. Domcke, C. Garcia-Cely, N. L. Rodd, Novel Search for High-Frequency Gravitational Waves with Low-Mass Axion Haloscopes, Phys. Rev. Lett. 129 (4) (2022) 041101. arXiv:2202.00695, doi:10.1103/PhysRevLett.129.041101.

[208] V. Domcke, C. Garcia-Cely, S. M. Lee, N. L. Rodd, Symmetries and selection rules: optimising axion haloscopes for Gravitational Wave searches, JHEP 03 (2024) 128. arXiv:2306.03125, doi:10.1007/JHEP03(2024)128.

[209] A. Berlin, D. Blas, R. Tito D'Agnolo, S. A. R. Ellis, R. Harnik, Y. Kahn, J. Schütte-Engel, Detecting high-frequency gravitational waves with microwave cavities, Phys. Rev. D 105 (11) (2022) 116011. arXiv:2112.11465, doi:10.1103/PhysRevD.105.116011.

[210] A. Escrivà, F. Kuhnel, Y. Tada, Primordial Black Holes (2022). arXiv:2211.05767.

[211] S. Hawking, Gravitationally collapsed objects of very low mass, Mon. Not. Roy. Astron. Soc. 152 (1971) 75. doi:10.1093/mnras/152.1.75.

[212] Y. B. Zel'dovich, I. D. Novikov, The Hypothesis of Cores Retarded during Expansion and the Hot Cosmological Model, Soviet Astron. AJ (Engl. Transl.), 10 (1967) 602.

[213] B. J. Carr, S. W. Hawking, Black holes in the early Universe, Mon. Not. Roy. Astron. Soc. 168 (1974) 399–415. doi:10.1093/mnras/168.2.399.

[214] P. S. Cole, A. D. Gow, C. T. Byrnes, S. P. Patil, Primordial black holes from single-field inflation: a fine-tuning audit, JCAP 08 (2023) 031. arXiv:2304.01997, doi:10.1088/1475-7516/2023/08/031.

[215] J. Martin, T. Papanikolaou, V. Vennin, Primordial black holes from the preheating instability in single-field inflation, JCAP 01 (2020) 024. arXiv:1907.04236, doi:10.1088/1475-7516/2020/01/024.

[216] G. Dvali, F. Kühnel, M. Zantedeschi, Primordial black holes from confinement, Phys. Rev. D 104 (12) (2021) 123507. arXiv:2108.09471, doi:10.1103/PhysRevD.104.123507.

[217] B. Carr, K. Kohri, Y. Sendouda, J. Yokoyama, Constraints on primordial black holes, Rept. Prog. Phys. 84 (11) (2021) 116902. arXiv:2002.12778, doi:10.1088/1361-6633/ac1e31.

[218] G. F. Giudice, M. McCullough, A. Urbano, Hunting for Dark Particles with Gravitational Waves, JCAP 10 (2016) 001. arXiv:1605.01209, doi:10.1088/1475-7516/2016/10/001.

[219] M. Maggiore, Gravitational Waves. Vol. 1: Theory and Experiments, Oxford University Press, 2007. doi:10.1093/acprof:oso/9780198570745.001.0001.

[220] G. Franciolini, A. Maharana, F. Muia, Hunt for light primordial black hole dark matter with ultrahigh-frequency gravitational waves, Phys. Rev. D 106 (10) (2022) 103520. arXiv:2205.02153, doi:10.1103/PhysRevD.106.103520.

[221] M. Raidal, C. Spethmann, V. Vaskonen, H. Veermäe, Formation and Evolution of Primordial Black Hole Binaries in the Early Universe, JCAP 02 (2019) 018. arXiv:1812.01930, doi:10.1088/1475-7516/2019/02/018.

[222] K. Choi, J.-c. Hwang, K. W. Hwang, String theoretic axion coupling and the evolution of cosmic structures, Phys. Rev. D 61 (2000) 084026. arXiv:hep-ph/9907244, doi:10.1103/PhysRevD.61.084026.

[223] J. E. Kim, Gravity wave and model-independent axion, J. Korean Phys. Soc. 71 (3) (2017) 127–129. arXiv:1608.02540, doi:10.3938/jkps.71.127.

[224] N. Seto, A. Taruya, Measuring a Parity Violation Signature in the Early Universe via Ground-based Laser Interferometers, Phys. Rev. Lett. 99 (2007) 121101. arXiv:0707.0535, doi:10.1103/PhysRevLett.99.121101.

[225] Y. Ali-Haimoud, Y. Chen, Slowly-rotating stars and black holes in dynamical Chern-Simons gravity, Phys. Rev. D 84 (2011) 124033. arXiv:1110.5329, doi:10.1103/PhysRevD.84.124033.

[226] T. Tsutsui, A. Nishizawa, Observational constraint on axion dark matter with gravitational waves, Phys. Rev. D 106 (8) (2022) L081301. arXiv:2207.00667, doi:10.1103/PhysRevD.106.L081301.

[227] G. Lambiase, L. Mastrototaro, L. Visinelli, Gravitational waves and neutrino oscillations in Chern-Simons axion gravity, JCAP 01 (2023) 011. arXiv:2207.08067, doi:10.1088/1475-7516/2023/01/011.

[228] D. Yoshida, J. Soda, Exploring the string axiverse and parity violation in gravity with gravitational waves, Int. J. Mod. Phys. D 27 (09) (2018) 1850096. arXiv:1708.09592, doi:10.1142/S0218271818500967.

[229] S. Jung, T. Kim, J. Soda, Y. Urakawa, Constraining the gravitational coupling of axion dark matter at LIGO, Phys. Rev. D 102 (5) (2020) 055013. arXiv:2003.02853, doi:10.1103/PhysRevD.102.055013.

[230] M. E. Gertsenshtein, Wave resonance of light and gravitational waves, Sov. Phys. JETP 14 (1962) 84–85.

[231] Y. B. Zel'dovich, Electromagnetic and gravitational waves in a stationary magnetic field, Zh. Eksp. Teor. Fiz. 68 (1973) 1311–1315.

[232] A. Palessandro, T. Rothman, A simple derivation of the Gertsenshtein effect, Phys. Dark Univ. 40 (2023) 101187. arXiv:2301.02072, doi:10.1016/j.dark.2023.101187.

[233] J. Hong, J. E. Kim, S. Nam, Y. Semertzidis, Calculations of resonance enhancement factor in axion-search tube-experiments (2014). arXiv:1403.1576.

[234] C. A. J. O'Hare, A. M. Green, Axion astronomy with microwave cavity experiments, Phys. Rev. D 95 (6) (2017) 063017. arXiv:1701.03118, doi:10.1103/PhysRevD.95.063017.

[235] A. Berlin, et al., Searches for New Particles, Dark Matter, and Gravitational Waves with SRF Cavities (2022). arXiv:2203.12714.

[236] O. Pujolas, V. Vaskonen, H. Veermäe, Prospects for probing gravitational waves from primordial black hole binaries, Phys. Rev. D 104 (8) (2021) 083521. arXiv:2107.03379, doi:10.1103/PhysRevD.104.083521.

[237] C. Gatti, L. Visinelli, M. Zantedeschi, Cavity Detection of Gravitational Waves: Where Do We Stand? (3 2024). arXiv:2403.18610.

[238] K. Schmieden, M. Schott, A Global Network of Cavities to Search for Gravitational Waves (GravNet): A novel scheme to hunt gravitational waves signatures from the early universe, PoS EPS-HEP2023 (2024) 102. arXiv:2308.11497, doi:10.22323/1.449.0102.

[239] A. Arvanitaki, A. Madden, K. Van Tilburg, Piezoaxionic effect, Phys. Rev. D 109 (7) (2024) 072009. arXiv:2112.11466, doi:10.1103/PhysRevD.109.072009.

[240] A. Arvanitaki, S. Dimopoulos, K. Van Tilburg, Sound of Dark Matter: Searching for Light Scalars with Resonant-Mass Detectors, Phys. Rev. Lett. 116 (3) (2016) 031102. arXiv:1508.01798, doi:10.1103/PhysRevLett.116.031102.

[241] M. Goryachev, W. M. Campbell, I. S. Heng, S. Galliou, E. N. Ivanov, M. E. Tobar, Rare Events Detected with a Bulk Acoustic Wave High Frequency Gravitational Wave Antenna, Phys. Rev. Lett. 127 (7) (2021) 071102. arXiv:2102.05859, doi:10.1103/PhysRevLett.127.071102.

[242] K. Lakin, A review of thin-film resonator technology, IEEE Microwave Magazine 4 (4) (2003) 61–67. doi:10.1109/MMW.2003.1266067.

[243] M. Goryachev, M. E. Tobar, Gravitational Wave Detection with High Frequency Phonon Trapping Acoustic Cavities, Phys. Rev. D 90 (10) (2014) 102005, [Erratum: Phys.Rev.D 108, 129901 (2023)]. arXiv:1410.2334, doi:10.1103/PhysRevD.90.102005.

[244] P. D. Lasky, E. Thrane, Did Goryachev et al. detect megahertz gravitational waves?, Phys. Rev. D 104 (10) (2021) 103017. arXiv:2110.13319, doi:10.1103/PhysRevD.104.103017.

[245] W. M. Campbell, M. Goryachev, M. E. Tobar, Author Correction: The multi-mode acoustic gravitational wave experiment: MAGE [doi: 10.1038/s41598-023-35670-y], Sci. Rep. 13 (1) (2023) 10638. arXiv:2307.00715, doi:10.1038/s41598-024-55260-w.

[246] W. M. Campbell, S. Galliou, M. E. Tobar, M. Goryachev, Electro-mechanical tuning of high-Q bulk acoustic phonon modes at cryogenic temperatures, Appl. Phys. Lett. 122 (3) (2023) 032202. arXiv:2207.01176, doi:10.1063/5.0131361.

[247] Y. Chu, P. Kharel, T. Yoon, L. Frunzio, P. T. Rakich, R. J. Schoelkopf, Creation and control of multi-phonon Fock states in a bulk acoustic-wave resonator, Nature 563 (7733) (2018) 666–670. doi:10.1038/s41586-018-0717-7.

[248] U. von Lüpke, Y. Yang, M. Bild, L. Michaud, M. Fadel, Y. Chu, Parity measurement in the strong dispersive regime of circuit quantum acoustodynamics, Nature Phys. 18 (7) (2022) 794–799. arXiv:2110.00263, doi:10.1038/s41567-022-01591-2.

[249] M. Bild, M. Fadel, Y. Yang, U. von Lüpke, P. Martin, A. Bruno, Y. Chu, Schrödinger cat states of a 16-microgram mechanical oscillator, Science 380 (6642) (2023) adf7553. arXiv:2211.00449, doi:10.1126/science.adf7553.

[250] Y. Kahn, J. Schütte-Engel, T. Trickle, Searching for high-frequency gravitational waves with phonons, Phys. Rev. D 109 (9) (2024) 096023. arXiv:2311.17147, doi:10.1103/PhysRevD.109.096023.

[251] A. Berlin, R. T. D'Agnolo, S. A. R. Ellis, P. Schuster, N. Toro, Directly Deflecting Particle Dark Matter, Phys. Rev. Lett. 124 (1) (2020) 011801. arXiv:1908.06982, doi:10.1103/PhysRevLett.124.011801.

[252] Z. Bogorad, N. Toro, Ultralight millicharged dark matter via misalignment, JHEP 07 (2022) 035. arXiv:2112.11476, doi:10.1007/JHEP07(2022)035.

[253] A. Berlin, R. Tito D'Agnolo, S. A. R. Ellis, J. I. Radkovski, Signals of millicharged dark matter in light-shining-through-wall experiments, JHEP 08 (2023) 017. arXiv:2305.05684, doi:10.1007/JHEP08(2023)017.

[254] N. Blinov, C. Gao, R. Harnik, R. Janish, N. Sinclair, Dark Matter Searches on a Photonic Chip (1 2024). arXiv:2401.17260.

[255] J. Redondo, Solar axion flux from the axion-electron coupling, JCAP 12 (2013) 008. arXiv:1310.0823, doi:10.1088/1475-7516/2013/12/008.

[256] J. Eby, V. Takhistov, Diffuse Axion Background (1 2024). arXiv:2402.00100.

[257] D. Lee, W. Chung, Y. Semertzidis, Cylindrical Cavity Simulation for Searching Axions, in: 11th Patras Workshop on Axions, WIMPs and WISPs, 2015, pp. 210–213. doi:10.3204/DESY-PROC-2015-02/lee_doyu.

[258] D. Alesini, et al., KLASH Conceptual Design Report (2019). arXiv:1911.02427.

[259] G. Reuter, E. Sondheimer, Theory of the Anomalous Skin Effect in Metals, Nature 161 (1948) 394–395. doi:10.1038/161394a0.

[260] C. Ligi, G. Delle Monache, R. Ricci, C. Sanelli, Daϕne cryogenic coooling system: status and perspectives, EPAC 2002 Proceedings (2002) 2523–2525.

[261] M. Mück, M.-O. André, J. Clarke, J. Gail, C. Heiden, Radio-frequency amplifier based on a niobium dc superconducting quantum interference device with microstrip input coupling, Applied Physics Letters 72 (22) (1998) 2885–2887. doi:10.1063/1.121490.

[262] A. Vinante, P. Falferi, R. Mezzena, M. Mück, Hot-electron effect in palladium thin films, Phys. Rev. B 75 (2007) 104303. doi:10.1103/PhysRevB.75.104303.
URL https://link.aps.org/doi/10.1103/PhysRevB.75.104303

[263] D. Drung, C. Assmann, J. Beyer, M. Peters, F. Ruede, T. Schurig, dc squid readout electronics with up to 100 mhz closed-loop bandwidth, IEEE Transactions on Applied Superconductivity 15 (2) (2005) 777–780. doi:10.1109/TASC.2005.850057.

[264] M. Mück, C. Welzel, J. Clarke, Superconducting quantum interference device amplifiers at gigahertz frequencies, Applied Physics Letters 82 (19) (2003) 3266–3268. doi:10.1063/1.1572970.

[265] M. Mück, M.-O. André, J. Clarke, J. Gail, C. Heiden, Microstrip superconducting quantum interference device radio-frequency amplifier: Tuning and cascading, Applied Physics Letters 75 (22) (1999) 3545–3547. doi:10.1063/1.125383.

[266] M. Mück, J. B. Kycia, J. Clarke, Superconducting quantum interference device as a near-quantum-limited amplifier at 0.5 ghz, Applied Physics Letters 78 (7) (2001) 967–969. doi:10.1063/1.1347384.

[267] K. W. Rigby, D. Marek, T. C. P. Chui, Squid holder with high magnetic shielding, Review of Scientific Instruments 61 (2) (1990) 834–838. doi:10.1063/1.1141503.

[268] A. Savitzky, M. J. E. Golay, Smoothing and differentiation of data by simplified least squares procedures., Anal. Chem. 36 (8) (1964) 1627. doi:10.1021/ac60214a047.

[269] P. Navarro, B. Gimeno, J. Monzó-Cabrera, A. Díaz-Morcillo, D. Blas, Study of a cubic cavity resonator for gravitational waves detection in the microwave frequency range, Phys. Rev. D 109 (10) (2024) 104048. arXiv:2312.02270, doi:10.1103/PhysRevD.109.104048.

[270] A. J. Brady, C. Gao, R. Harnik, Z. Liu, Z. Zhang, Q. Zhuang, Entangled sensor-networks for dark-matter searches, PRX Quantum 3 (2022) 030333. doi:10.1103/PRXQuantum.3.030333.
URL https://link.aps.org/doi/10.1103/PRXQuantum.3.030333

[271] B. Allen, W. G. Anderson, P. R. Brady, D. A. Brown, J. D. E. Creighton, FINDCHIRP: An Algorithm for detection of gravitational waves from inspiraling compact binaries, Phys. Rev. D 85 (2012) 122006. arXiv:gr-qc/0509116, doi:10.1103/PhysRevD.85.122006.

[272] C. J. Moore, R. H. Cole, C. P. L. Berry, Gravitational-wave sensitivity curves, Class. Quant. Grav. 32 (1) (2015) 015014. arXiv:1408.0740, doi:10.1088/0264-9381/32/1/015014.

[273] A. Alimenti, K. Torokhtii, D. Di Gioacchino, C. Gatti, E. Silva, N. Pompeo, Impact of superconductors' properties on the measurement sensitivity of resonant-based axion detectors, Instruments 6 (1) (2022). doi:10.3390/instruments6010001.
URL https://www.mdpi.com/2410-390X/6/1/1

[274] A. Vinante, M. Bonaldi, P. Falferi, M. Cerdonio, R. Mezzena, G. A. Prodi, S. Vitale, Stabilization and optimization of a two-stage dc squid coupled to a high q resonator, Physica C: Superconductivity 368 (1) (2002) 176–180. doi:https://doi.org/10.1016/S0921-4534(01)01162-5.
URL https://www.sciencedirect.com/science/article/pii/S0921453401011625

[275] S. V. Uchaikin, et al., Josephson Parametric Amplifier based Quantum Noise Limited Amplifier Development for Axion Search Experiments in CAPP (2024). arXiv:2406.07899.

[276] Q. Liang, et al., Axion Detection Experiments Meet the Majoron (2024). arXiv:2406.19083.

[277] K. Schmieden, M. Schott, Supax: A new axion search experiment using superconductive cavities, PoS EPS-HEP2021 (2021) 141. doi:10.22323/1.398.0141.

[278] J. R. Navarro-Madrid, J. M. García-Barceló, A. Díaz-Morcillo, Microwave Technologies in Experiments for Detection of Dark Matter Axions (4 2024). arXiv:2404.15926.

[279] J. M. García-Barceló, A. Díaz-Morcillo, B. Gimeno, Enhancing resonant circular-section haloscopes for dark matter axion detection: approaches and limitations in volume expansion (9 2023). arXiv:2309.13199.

[280] A. Berlin, D. Blas, R. Tito D'Agnolo, S. A. R. Ellis, R. Harnik, Y. Kahn, J. Schütte-Engel, M. Wentzel, Electromagnetic cavities as mechanical bars for gravitational waves, Phys. Rev. D 108 (8) (2023) 084058. arXiv:2303.01518, doi:10.1103/PhysRevD.108.084058.

[281] J. M. García-Barceló, A. A. Melcón, A. Díaz-Morcillo, B. Gimeno, A. J. Lozano-Guerrero, J. Monzo-Cabrera, J. R. Navarro-Madrid, P. Navarro, Methods and restrictions to increase the volume of resonant rectangular-section haloscopes for detecting dark matter axions, JHEP 08 (2023) 098. arXiv:2302.10569, doi:10.1007/JHEP08(2023)098.

[282] J. M. García Barceló, et al., On the development of new tuning and inter-coupling techniques using ferroelectric materials in the detection of dark matter axions, IEEE Access 11 (2023) 30360.

[283] P. Navarro, et al., Wide-band full-wave electromagnetic modal analysis of the coupling between dark-matter axions and photons in microwave resonators, Phys. Dark Univ. 36 (2022) 101001. arXiv:2107.03137, doi:10.1016/j.dark.2022.101001.

[284] A. Díaz-Morcillo, et al., Design of New Resonant Haloscopes in the Search for the Dark Matter Axion: A Review of the First Steps in the RADES Collaboration, Universe 8 (1) (2021) 5. arXiv:2111.14510, doi:10.3390/universe8010005.

[285] S. Calatroni, Technology wg activities: status and plans, https://indico.cern.ch/event/1369776/ (2024).